FREE-SPACE DIFFRACTION EFFECTS IN AN ALL OPTICAL PASSIVE DRIVEN SYSTEM

By

DARLENA JOYCE JONES

Bachelor of Science

Southwest Missouri State University

Springfield, Missouri

1987

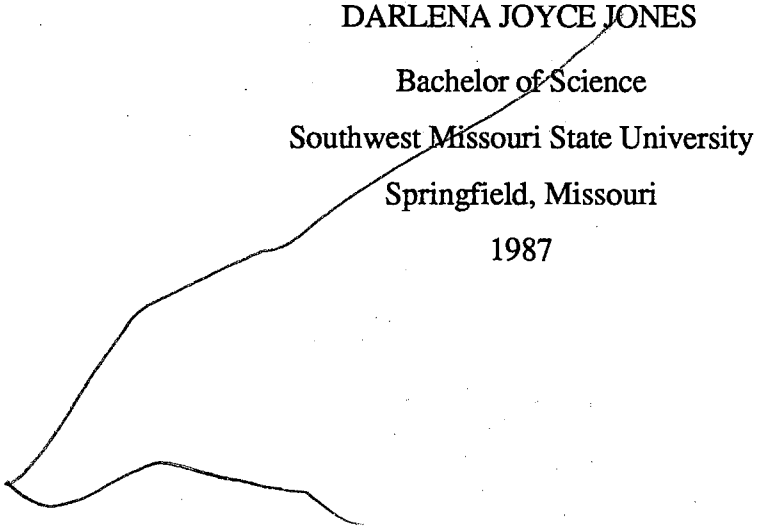

Submitted to the Faculty of the
Graduate College of the
Oklahoma State University
in partial fulfillment of
the requirements for
the Degree of
DOCTOR OF PHILOSOPHY
December, 1993

FREE-SPACE DIFFRACTION EFFECTS IN AN ALL OPTICAL PASSIVE DRIVEN SYSTEM

Thesis Approved:

Donna Kay Bandy

Thesis Advisor

Dean of the Graduate College

PREFACE

Transverse effects are known to play a central role in nonlinear-optical systems. Since experiments are generally performed with lasers with finite transverse dimensions, the transverse nature of the field must be considered. Experimental evidence, for example, indicates that mechanisms in the form of diffusive and diffractive coupling within the medium, free-space diffraction, or some combination of these, can create transverse structures which are important in optical bistability and self-focusing/defocusing. In particular, transverse coupling is attributed to such phenomena as radial dependence of the switch up times of bistable loops, spatial hysteresis, and the formation of solitary waves in passive systems.

The dynamical effects of free-space diffraction in a unidirectional ring cavity containing a thin resonant absorber driven by an external coherent signal is considered. Minimal focusing effects exist in this system by incorporating a thin medium whose width is small compared to the cavity length and Raleigh range. There is no restriction on the medium response time relative to the round trip time; i.e. the time-dependent polarization is not adiabatically eliminated from the equations of motion. Free-space diffraction effects are isolated and diffraction and diffusive coupling within the medium is negligible. In this model where free-space diffraction is the dominant mechanism for changing the field profile in the system, shifting, deformation, and radial variation of the bistable loop and spatial hysteresis is attributed to an inherent dispersion induced by the free-space diffraction.

I wish to express sincere appreciation to my thesis advisor, Dr. Donna Bandy, for her encouragement and thoughtful advice throughout my graduate program. I have learned much more than physics from you. Many thanks also go to Drs. Ray Zanoni, James Wicksted, Jerzy Krasinski, and Roger Reeves for serving on my graduate committee. Their suggestions and support were very helpful throughout the study.

Special thanks go to Gary Giedd, my undergraduate research advisor, for pushing,

nagging, and finally coercing me into physics. I hate to say it, but you were right after all.

I have a deep gratitude towards John Kohler who designed the network of workstations located in my lab that facilitated the computations found in this thesis. Thanks also to Jonathan Graham, our systems operator, who keeps our computers purring without fault.

To my friends Carol Bandy, Traci Morris, the entire crew of the "Dead Dinner Society", Bahman Taheri, my long-time office mate, Linda Hunter, and the rest of the graduate students too numerous to name, I will always remember you in my heart.

Love and appreciation goes to my parents, Wendell and Ernestine Jones, my brother, Michael Jones, and my sister and brother-in-law, Diana and Ray Prendes, for putting up with my extended stay in school. Thank you for believing in me.

But my deepest love goes to my closest friend, Michael Witt. Thank you for making me laugh.

TABLE OF CONTENTS

LIST OF FIGURES

CHAPTER I

INTRODUCTION

Optical bistability (OB) is an exciting field of research because of its potential application to all-optical logic and the interesting phenomena it encompasses. Since the first theoretical description of optical bistability in a passive medium in 1974 by McCall, [1] bistability has been observed in many different materials including tiny semiconductor etalons. Current applied research is focused on optimizing these devices by decreasing their size, switching times, operating power, and operating them at room temperature. Both improved nonlinear materials and more efficient device configurations are being sought. Current fundamental research centers on the interesting physical behavior of simple bistable systems. Many bistable devices consist of a nonlinear medium within an optical resonator, just as do lasers, except the passive bistable devices are excited only by the incident coherent light. The counterparts of many of the phenomena studied in lasers, such as fluctuations, regenerative pulsations, and optical turbulence, can be observed in passive bistable systems, often under better controlled conditions. Optical bistability in lasers, which was seen prior to passive bistability, is not considered in this thesis.

A system is said to be optically bistable if it has two stable output intensity states for the same value of the input intensity state over some range of input values. Such a system is clearly nonlinear. However, nonlinearity alone is not sufficient to assure bistability. It is feedback that permits the nonlinear transmission to be multivalued. This definition implies that the bistable system can be cycled completely and repeatedly by varying the input intensity. Systems that exhibit hysteresis as a function of some other parameter, like temperature, is not of interest here.

Seidel [2] in 1969 is apparently the first to understand the significance of optical bistability and to officially record the idea of a passive bistable optical device. He first proposed such a device as a natural extension of his work on similar effects in the

microwave region and filed a patent, which was granted in 1971, because of the potentially rich engineering possibilities, ranging from an all-optical computer to optical communications.

Equally pioneering and independent work on absorptive bistability was done by Szoke, Daneou, Glodhar, and Kurnit. [3] They analyzed a Fabry-Perot interferometer containing a saturable absorber and derived the condition for purely absorptive bistability. They mentioned several problems still under study today: standing-wave effects, residual or unsaturable absorption, production of an infinite pulse train from a cw input, and crosstalk between nearby beams that could lead to adding and memory operations performed in parallel. McCall [1] further analyzed absorptive bistability by studying the effects of inhomogeneous broadening, standing waves, and transverse modes.

The first experimental observation of passive optical bistability was reported by McCall, Gibbs, Churchill, and Venkatesan in 1975. [4] They used the D_2 line in Na-vapor between the mirrors of a plane Fabry-Perot interferometer. This first observation of OB was due to nonlinear refractive index effects, not the anticipated nonlinear absorptive effects. It was this work in which bistability was observed that created the avalanche of experimental, as well as theoretical studies that followed.

In 1976, Bonifacio and Lugiato [5] proposed an elegant first-principle treatment of plane wave absorptive OB which gave evidence for the existence of cooperative behavior and revealed deep analogies with first-order phase transitions. Two years later they also reported the first analytical theory of plane wave dispersive OB with propagation effects and saturation.[6] Using mean-field theory and the Maxwell-Bloch equations, they produced a number of predictions concerning the transient behavior and quantum statistical effects.

Ikeda, [7] in 1978, developed a mapping model for plane wave OB to capture the delay effects of the long round trip time in a cavity compared with the response time of the nonlinear medium. From this simple map, which discarded the time derivative in the delay-differential equations, instabilities were predicted. Later analyses cast doubt on some of these results, [8, 9] as it was shown that the bifurcation structure of the delay-differential equations departed from that of the maps beyond the first instability.

From 1979 to 1982 the plane wave mean-field model was used by researchers like

Meystre and Hopf, [10] Benza and Lugiato, [11] Hopf et al., [12] and Lugiato et al., [13] to investigate transient behavior. Others, such as Agrawal et al., [14] Carmichael and Walls, [15] and Casagrande and Lugiato, [16] used the mean-field model at the quantum statistical level to describe the spectrum of transmitted and fluorescent light. Much effort has gone into describing the bimodal character of the distribution function in the instability region, completing the analogy between OB and first-order phase transition. [17-20]

During the late 1970s to the early 1980s, many experiments in the field of optical bistability was performed. In 1977, Venkatesan and McCall [21] reported bistability, differential gain, and optical limiting in a Fabry-Perot (FP) cavity containing a ruby crystal. A year later, Grischkowski [22] reported optical switching using a nonlinear FP cavity with a fast response time. That same year, McCall and Gibbs [23] observed optical bistability arising from an intensity-dependent thermal change in optical pathlength. Experiments studying the transient behaviors of FP cavities filled with either absorptive or dispersive materials were demonstrated by Bishofberger and Shen, [24] Garmire et al., [25] and Grant and Kimble. [26] Other experiments in optical bistability were performed by Sandel and Gallagher, [27] Grant and Kimble, [28] Arimondo et al., [29] and Rosenberger et al. [30] For additional information on plane wave theoretical and experimental studies, see Refs. 31 and 32.

In the mid-1980s, higher-speed computers were available which allowed the advent of more complex theories. The natural evolution in the theoretical description of both absorptive and dispersive optical bistability includes transverse effects. Experiments performed by Kimble's group on absorptive OB in Na-vapor [33] required an analysis involving transverse effects and gave good agreement. Experiments studying optical bistability are generally performed with lasers of finite transverse dimensions, usually with a Gaussian radial intensity profile. Beam profiles and mechanisms that change the profile, namely diffraction and self-focusing or defocusing, can substantially alter the bistability. Clearly, transverse effects do not eliminate bistability in general, since intrinsic bistability is observed using Gaussian beams. However, in some cases bistability observed with a Gaussian beam is close to uniform-plane-wave predictions; this may be because diffusion of the excitation within the medium results in far less radial dependence in the phase shift than in the input beam. [31] Nevertheless, transverse effects do affect the optically bistable

system.

The study of transverse effects in optical bistability proved the most fruitful of all passive nonlinear-optical phenomena. Reasons for studying transverse effects in optical bistability included the possibility of parallel processing optical computers based on optically bistable devices, which raised questions of minimum device size, transverse coupling mechanisms, and information storage. Studies of these questions may be more beneficial in terms of theory than of application, e.g. leading to spontaneous pattern formation based on transverse solitary waves. [34] They also constitute interesting coupled matter-field systems, in which the space-time evolution of the material excitation plays an important role in the phenomena. Another feature of transverse effects in OB is the richness of the dynamical instabilities. This meant a cross-fertilization of studies of transverse effects in OB with new ideas and techniques in nonlinear dynamics and chaos and, in particular, with the parallel developments in studies of laser instabilities.

Self-focusing, a dispersive effect, was perhaps the first strongly nonlinear process in which transverse effects played a central role. [35-41] While the simplest intuitive result was the formation of local hot spots in a previously nearly uniform beam, in extended media new results were found like the formation of narrow intense channels of a beam, called filaments. Conical emission, [42] coherent on-resonance self-focusing, [43] and enhancement [44] arose from quantitative studies of self-focusing and related phenomena in single-pass systems using inhomogeneously broadened atomic vapors, where thermal and mechanical effects and/or damage, which complicate filamentation, were absent.

The new theoretical studies of transverse effects in optical bistability prompted many researchers to explore various limits to reduce the complexity of the system allowing for use of well known numerical routines. The vast majority of the models studied the diffraction of the field within the medium or diffusion of the excitation.

The high finesse of many optically bistable cavities encouraged the widely used approximation of longitudinal uniformity, which was termed early the "mean-field limit". Of course, when there is transverse variation of the field this term seems a little contradictory. Perhaps it is better to recognize that one is averaging the effects of mirror coupling and longitudinal variation in the beam intensity, properties that are not well described by terms like uniform-field approximation.

The high finesse of these optically bistable cavities also encouraged a Gauss-Laguerre mode-expansion approach to transverse effects for experimental comparisons, with early success for Ballagh et al. [45] and Drummond. [46] Likewise, an outstanding agreement between a bistability experiment and a single-Gaussian-mode model was reported by Kimble and co-workers. [33] A mode-expansion model [50] explained spatial hysteresis, in which the bistable loop occurred in the beam profile, with or without power hysteresis after a few experiments [47-49] indicated spatial hysteresis existed. However, with hindsight that model may have indicated a transverse modulational instability rather than a cavity-induced effect. [51]

Experiments in semiconductors such as GaAs [52] and InSb [53] in 1979 demanded attention because of the obvious device potential. Finesse was usually low, invalidating the mean-field limit and making mode-expansion techniques of doubtful value.[50] Fourier-transform (FT) techniques proved to be a good answer, as shown by Moloney et al. [54] and Rosanov et al. [55, 56] Most papers which used the FT technique adiabatically eliminated the atomic variables, polarization and population difference, to reduce the number of variables in the system thus making a FT technique applicable. This reduced system, where the medium response time was assumed to be much less than the round trip time, was within the so-called Ikeda approximation. [7]

In ring resonators, the fast-Fourier-transform or beam-propagation method described above gave a quasi-dynamical simulation of the long-term evolution of the cavity fields. These simulations showed that switching waves moved out from the beam center at switch on, thus giving a discontinuity in the power output at switch up, where a pointwise application of the plane-wave transmission formula gave only a change of slope. More importantly, the sharp field gradients at the switching edge were found in self-focusing media to destabilize the switched-on region, generating robust and often stable groups of solitary waves (spatial solitons, loosely speaking). [57, 58]

Modeling Gaussian-beam devices means taking advantage of cylindrical symmetry, for which the fast-Fourier-transform method is not so well adapted. There is a related fast-Hankel-transform method; [59] unfortunately, it roughly doubles the computing time and has been shown to be unstable. The problems with the fast-Hankel-transform method permitted other numerical techniques to compete and there was agreement between finite-

difference and fast-Hankel-transform models of the same system. [60, 61]

Including the photocarrier diffusion, which is necessary in bulk semiconductor devices, showed that the shape and sense of the bistable loop were strongly affected by diffusion. [62, 63] Grigor'yants and Dyuzhikhov [64] reported direct measurements of these effects. Taken together with earlier experiments of beam-width dependence of OB thresholds plus some profile measurements, [65] these results suggested the optical bistability properties of bulk semiconductors like InSb were as understood as the optically bistable properties of Na-vapor since diffusion dominated diffraction in semiconductor media. The diffusion property allowed for rather simple modeling, pioneered by Rosanov and co-workers [66] and developed by Firth and Galbraith [67] to model arrays of OB devices, which will be required in any practical optical memory. The diffusive coupling permitted simple modeling of the dynamics of such arrays, leading to estimates of the critical separation for independent memory action of the individual pixels. It was also shown that ideal optical memories necessarily possess spatially chaotic (but temporally stable) states. [68, 69] An alternative, perhaps equivalent approach was the demonstration that spatially modulated broad-beam pumping permits nonmonotonic static switching waves of complex structure. [70]

Mapping models which were known to have quick computation times were investigated with the inclusion of transverse coupling by Rosanov et al., [71] Moloney and co-workers [57, 72, 73] and Firth and Wright. [74] When multilongitudinal-mode effects are ignored, the dynamics are governed by diffraction and diffusion with characteristic times much longer than the delay time, and there were few concerns about mapping models for longitudinal instabilities. The main finding was that the intensities of the different pairs of the Gaussian input beam locally generated different plane wave pulsing frequencies which tended to frustrate the period-doubling route to chaos, leading instead to frequency locking. Instability thresholds tended to be lowered with transverse coupling due to modulational instabilities. [75]

Experimental studies of dynamic instabilities in optically bistable systems have been somewhat limited, especially with regard to transverse effects. When temporal pulsations predicted in both the plane wave temporal mapping theories and the continuous-temporal variable theories seemed not to be emerging in the experiments of Kimble's group on single

mode OB using Na-vapor, several authors [76-83] considered a modification in which they simply averaged over the transverse intensity profile, which was assumed to be Gaussian. After some disputed results it emerged that the coherent sideband instabilities induced by the Rabi oscillations could be suppressed or enhanced, depending on whether the system was passive and optically bistable, laser with an injected signal, or a free-running laser. However, transverse effects seemed to be somewhat less destructive of multimode instabilities, as was demonstrated in a set of waveguide experiments by Segard and co-workers. [84]

The theoretical and experimental results described above concentrate on diffraction of the field within the medium or the diffusion of the excitation. With few exceptions, the contribution of free-space diffraction to the overall system is neglected. Again, as a natural evolution to the full understanding of this dynamically rich system and the future hope for optical computing, we theoretically study the dynamical effects of free-space diffraction in a unidirectional ring cavity containing a thin resonant absorber driven by an external coherent signal. We minimize focusing effects by incorporating a medium whose width is much smaller than the cavity length and the Raleigh range. We place no restriction on the medium response time relative to the round trip time; the time-dependent polarization and population difference is not adiabatically eliminated from the equations of motion. We isolate free-space diffraction effects and argue that diffraction and diffusive coupling within the medium is negligible. In this model where free-space diffraction is the dominant mechanism for changing the field profile in the system, shifting and deformation of the bistable loop and spatial hysteresis occurs. We see a radial variation of the bistable loop, however, this effect is not strong; this is consistent with those who argue that radial variation of the bistable loop is an effect of diffusion.[64]

In Chapter II we review the origin of the basic equations of motion for both the medium and the free-space diffraction and establish numerical algorithms. In Chapters III and IV we describe some plane wave and transverse effects phenomena reported earlier and establish links between our studies of free-space diffraction to these earlier works. Our basic tools will comprise numerical methods for the solution of the differential equations and our own fast-Hankel-transform. In Chapter V, we conclude.

CHAPTER II

DESCRIPTION OF THE OPTICAL SYSTEM

We present a model that describes the dynamical behavior of the electromagnetic field in a passive medium. It is configured in a ring cavity and driven by a coherent external signal. The key elements in our model are as follows: (1) The medium polarization and population difference are not adiabatically eliminated from the equations of motion, i.e. these variables keep their time dependence. This allows the polarization and population difference to actively participate in the field dynamics. (2) There is no transverse coupling within the medium, i.e. no cross-talk between transverse modes within the medium. Small annular rings of plane-wave-like fields are allowed to propagate through the thin medium without coupling to other rings. The medium is considered to be a thin sample compared to the cavity length and Raleigh range. (3) At the exit of the medium boundary, the field is diffracted through free space using the Kirchoff diffraction integral. The free space is subdivided into equal cells in which the field is diffracted - cell by cell. Each cell has continuous memory of the current field conditions and earlier field conditions. This method of propagation eliminates any abrupt changes in the field dynamics at the medium entrance that might be an artifact of the programming. We argue that this method of field propagation (in space and through the medium), and the thin nature of the medium diminishes/eliminates diffusive and diffractive coupling within the medium as a possible transverse coupling mechanism of this system.

In this chapter we present the geometrical configuration of the ring cavity, detail the Maxwell-Bloch equations that describe the interaction of the field and atoms and Kirchoff's diffraction integral that simulates free-space diffraction, discuss the aperture on the injected signal, and present the appropriate system boundary conditions.

Geometrical Configuration

The geometrical configuration of an optical system plays a considerable role in the overall field dynamics. In general there are two types of configurations, single-pass and multi-pass. Only the multi-pass system allows feedback which is essential for optical bistability using a medium that is not intrinsically bistable. For the purpose of this thesis, we consider only a feedback system in the form of a cavity.

Cavities come in all sizes and shapes containing any number of reciprocal or nonreciprocal devices like mirrors, apertures, or isolators. Depending on the shape of the cavity and the devices within them, the field is either unidirectional or counterpropagating, stable or unstable. The cavities may contain either passive or active mediums, or a combination thereof.

We choose a unidirectional cavity because the inclusion of counterpropagating fields creates a serious complication in the field dynamics. In the absence of a medium, counterpropagating waves cause interference patterns on the scale of a wavelength. In the presence of a medium, the atoms exposed to different intensity levels acquire a modulated pattern of inversion which acts as a grating, and is capable of scattering the forward propagating wave in the backward direction, and vice versa; this effect is responsible for dynamical coupling of the two waves. In order to avoid this type of complication, we choose a cavity configuration that allows only one direction of propagation; in practice this can be accomplished with a ring resonator and a non-reciprocal device, such as a Faraday isolator, to suppress one of the two propagating waves.

The unidirectional cavity used in this model is shown in Fig. 1. Its total length is designated as Λ. We insert two fully reflecting spherical mirrors, M_1 and M_2, whose radii of curvature are R_1 and R_2, respectively, to insure that the majority of the radiation does not escape the cavity but will be refocused during each pass around the cavity. p_1 and p_2 represent the distances between the spherical mirrors and the medium and p_3 represents the round trip distance from M_2 to M_1. We insert a thin resonant two-level medium whose thickness, L, is $L = 0.005\Lambda$. We made this medium thin compared to the cavity length and Raleigh range so that diffraction effects inside the medium could be neglected which

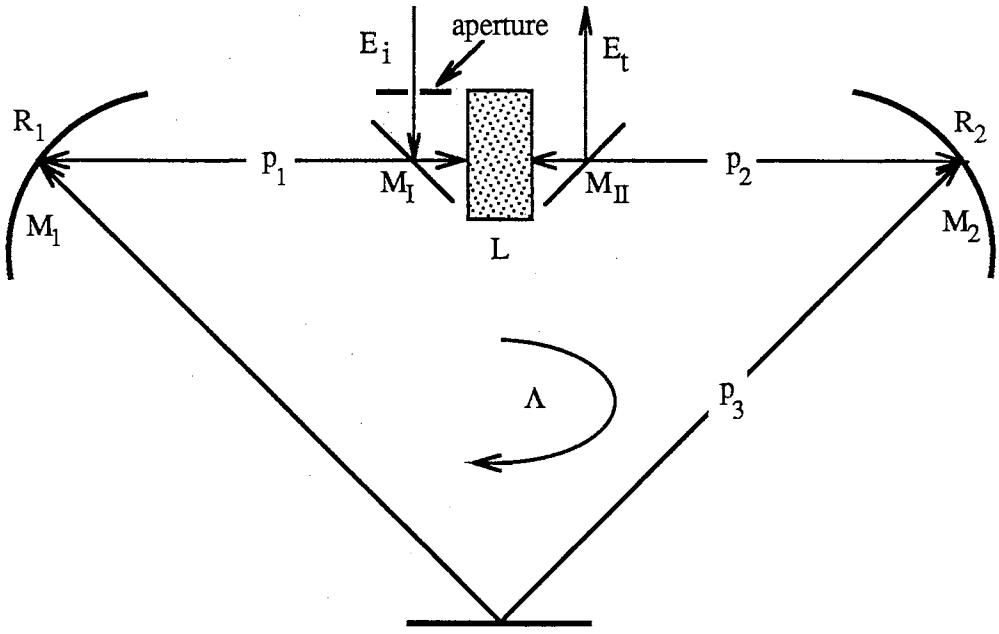

Figure 1. Ring Cavity Schematic

allows us to isolate free-space diffraction effects. The aperture of the injected signal will be discussed later. We finish the cavity design by adding two partially transmitting planar mirrors M_I and M_{II} with equal transmittivity amplitude T. M_I functions as an entrance for the external signal and M_{II} as the output coupler.

The stability of the cavity is an important issue. An empty ring cavity is always stable, provided that the mirrors are planar. However, when any other optical device is placed inside the cavity, the cavity may become unstable. For certain applications unstable resonators prove useful. They can create large mode volume and good discrimination against higher-order transverse modes. [85] However, for the purpose of this thesis we choose to operate in a stable cavity configuration since the vast majority of knowledge in theoretical optical bistability deals with a stable cavity configuration. For instance, a stable cavity allows for the paraxial approximation which assumes the field changes slowly over a wavelength. This approximation greatly reduces the complexity of the model and thus the computation time.

The empty cavity stability analysis which shows the range of cavity parameters which guarantee stability is given in Appendix A. The simplest case of the stable optical resonator, which is the one we choose, is the symmetrical system where $p_1 + p_2 + L = p_3 = \Lambda / 2$. Most experimental setups use symmetrical cavities with system parameters lying well within the stability confinement region along the $R_1 = R_2$ line. For that reason, we choose $R_1 = R_2 = \Lambda$.

Associated with any cavity is a set of axial-mode frequencies, [85]

$$\omega_c^m = 2\pi m \frac{c}{\Lambda} \qquad \text{(II.1)}$$

with a lifetime,

$$\gamma_c = \frac{c\,T}{\Lambda} \qquad \text{(II.2)}$$

provided that T -> 0. Here c represents the speed of light in a vacuum. Figure 2 shows the schematic of the relative cavity frequency.

We choose to use a passive medium for this thesis for several reasons: (1) Passive systems are more likely to be practical because they are simpler (they do not require an inverted medium) and hence are likely to be smaller and require less power; (2) an active

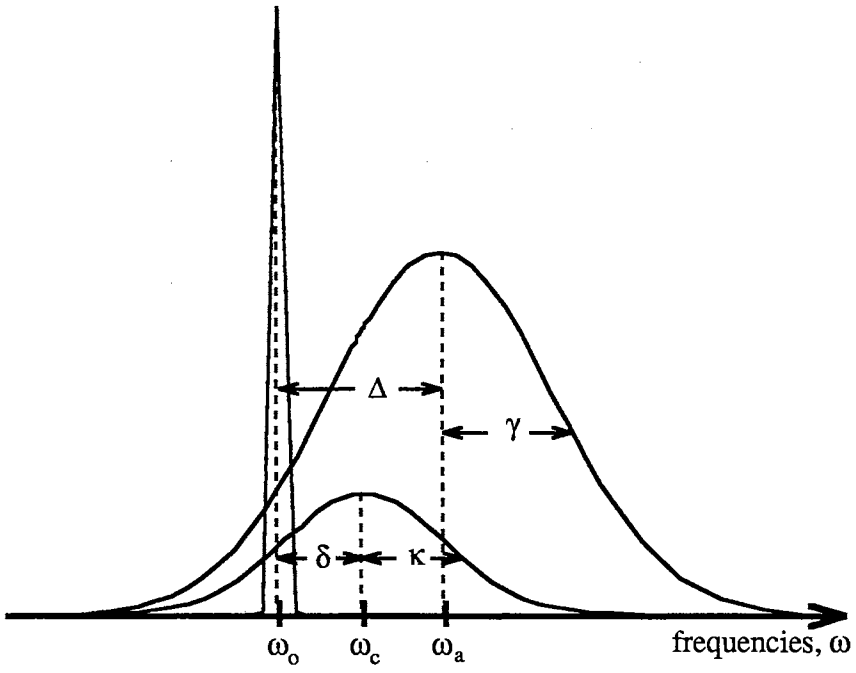

Figure 2. Schematic of Frequency Spectrum. The frequencies are the atomic (ω_a), cavity (ω_c), and signal (ω_o). We assume that the injected signal is monochromatic which makes its spectrum a delta-function. $\delta = \omega_c - \omega_o$ and $\Delta = \omega_a - \omega_o$. κ and γ are the decay rates of the cavity and the medium, respectively.

system is more complicated: the frequency of the laser may change or several modes may lase simultaneously, and the external excitation required to produce population inversion generally results in a complex environment; and (3) because there is a wealth of published information in the area of optical bistability.

Theoretical Description of the Atom-Field Interaction

Theoretical Development

In general, the interaction between an electromagnetic field and an atomic medium is a quantum process especially when significant energy exchanges take place between the medium and the field. However, since the intensity of the field is usually sufficiently large, laser fields in particular, a classical description is valid. Atoms, on the other hand, undergo transitions between pairs of stationary states whose description is entirely based on quantum mechanics. When the existing radiation is sufficiently removed from an atomic resonance, the behavior of an atom can be adequately described by the Lorenz oscillating dipole model, at least for the purpose of describing the susceptibility which includes the medium contribution to the index of refraction and the linear absorption coefficient. On or near resonance this description breaks down and a more accurate theoretical framework is needed. The traditional approach in the field of quantum optics is to describe the electromagnetic field in terms of the classical wave equation and the response of the atoms to the field in terms of the Schroedinger equation. The link between the classical macroscopic variables and the quantum mechanical microscopic variables is provided by the following argument.

The classical electromagnetic wave equation is driven by a macroscopic bulk polarization. On the other hand, an atomic wavefunction, that consists of a superposition of two stationary states of opposite parity, yields a nonzero expectation value for the dipole moment. By requiring that the bulk polarization be equal to the atomic density multiplied by the expectation value of the dipole operator, one has the required link between the Maxwell's classical wave equation and Schroedinger's quantum mechanical equation. In dealing with the atomic evolution, it is common to consider combinations of atomic probability amplitudes instead of the wavefunction itself. Because of the operational

meaning attached to these variables, the resulting atomic equations of motion can become formally identical to the Bloch equations of nuclear magnetic resonance. For this reason, the coupled equations of motion for the field and the atoms are commonly referred to as the Maxwell-Bloch equations.

Unfortunately, there is no mechanism by which an excited atom can be forced to decay (no spontaneous emission or collisions between atoms resulting in relaxation) in this semiclassical theory. For the purpose of this thesis, as well as for most problems in quantum optics, this problem is easily solved. We assume that the atoms are driven by an external field and are never left in a nonradiating excited state in the absence of radiation. Thus all relaxation processes can safely be described by phenomenological relaxation terms. This section is devoted to the derivation and numerical method of solution of the Maxwell-Bloch equations.

The passage of light through matter is accompanied by the simultaneous occurrence of absorption, dispersion, and diffraction. The classical electromagnetic wave equation is given by Maxwell's wave equation

$$\nabla_T^2 \vec{\mathcal{E}}(\vec{r},t) + \frac{\partial^2 \vec{\mathcal{E}}(\vec{r},t)}{\partial z^2} - \frac{n_o^2}{c^2}\frac{\partial^2 \vec{\mathcal{E}}(\vec{r},t)}{\partial t^2} = \mu_o \frac{\partial^2 \vec{\mathcal{P}}(\vec{r},t)}{\partial t^2} \qquad \text{(II.3)}$$

where $\vec{\mathcal{E}}$ is the electric field amplitude and $\vec{\mathcal{P}}$ is the macroscopic polarization per unit volume of the medium. ∇_T^2 represents the transverse Laplacian (written in either cylindrical or Cartesian coordinates) and describes the diffraction of the field within the medium. $\vec{r}$ is the direction vector; z and t represent space and time variables, respectively. The phase velocity of propagation of the wave in vacuum is $c = (\mu_o \varepsilon_o)^{-1/2}$ where μ_o is the permeability of free space and ε_o is the permittivity of free space. The background refractive index is n_o and is considered close to unity since our medium is assumed to have low density. We have also assumed that the atoms or molecules are identical which eliminates any inhomogeneous effects.

It is clear that Eq. (II.3) is not sufficient to describe the propagation of the field within a medium. The response of the medium, which is contained in the polarization, must be

determined. The simplest statement that we can make is to assume that $\mathcal{P}$ is proportional $\mathcal{E}$ according to a relation of the type

$$\vec{\mathcal{P}} = \varepsilon_o \chi \vec{\mathcal{E}} \tag{II.4}$$

where χ is the susceptibility. χ is a scaler if the medium is isotropic and can be represented by higher rank tensors if the medium is anisotropic. Unfortunately, Eq. (II.4) limits the behavior of the medium since its reaction is governed by a field-independent quantity, χ. In this thesis, we lift this restriction imposed on the atomic polarization and thus find equations to describe the medium behavior.

We assume that the cavity field is unidirectional and is linearly polarized in a direction (we specify the x-axis) perpendicular to the axis of the active medium (we specify the z-axis). The field and polarization become

$$\vec{\mathcal{E}}(\vec{r},t) = \hat{i}\,\mathcal{E}(r, z, t) = \frac{\hat{i}}{2}\left(\mathcal{E}_o(r, z,t)\, e^{i(k_o z - \omega_o t)} + \text{c.c.}\right) \tag{II.5a}$$

$$\vec{\mathcal{P}}(\vec{r},t) = \hat{i}\,\mathcal{P}(r, z, t) = \frac{\hat{i}}{2} N\mu i \left(\mathcal{P}_o(r, z,t)\, e^{i(k_o z - \omega_o t)} + \text{c.c.}\right) \tag{II.5b}$$

where N is the density of atoms in the medium and μ is the modulus of the atomic transition dipole moment. $k_o = n_o\, \omega_o / c$ is the wave vector in vacuum where we have chosen the frequency of the injected signal, ω_o, to be close to the atomic transition frequency and a cavity mode. $\mathcal{E}_o$ and $\mathcal{P}_o$ are slowly varying envelopes of the field and polarization, respectively.

Substituting Eqs. (II.5) into the wave equation, Eq. (II.3), and in the slowly varying envelope approximation (SVEA), i.e. under the assumption that

$$\left|\frac{\partial \mathcal{E}_o}{\partial z}\right| << k_o\, \mathcal{E}_o \quad \text{and} \quad \left|\frac{\partial \mathcal{E}_o}{\partial t}\right| << \omega_o\, \mathcal{E}_o \tag{II.6}$$

the equation for the field envelope in the form of the transport equation is

$$-\frac{i}{2k_o} \nabla_T^2\, \mathcal{E}_o + \frac{\partial \mathcal{E}_o}{\partial z} + \frac{1}{c}\frac{\partial \mathcal{E}_o}{\partial t} = \frac{iN\mu\omega_o}{2c\varepsilon_o}\, \mathcal{P}_o \tag{II.7}$$

A similar result holds for the complex conjugate variable

$\mathcal{E}_o$*. The SVEA demands that the growth of the field envelope is on the order of the wavelength and the time variation is slow compared to the optical carrier frequency.

The resonant or near resonant interaction of a collection of atoms with the electromagnetic field can be described to good approximation by neglecting all atomic levels, except for the pair of states which are resonant or nearly resonant with the radiation. The evolution of the atomic variables is governed by Schroedinger's equation

$$i\bar{h}\frac{\partial}{\partial t}\,|\Psi(t)> = H\,|\Psi(t)> \tag{II.8}$$

where $\bar{h}$ is Planck's constant divided by 2π. The Hamiltonian operator, H, is the sum of an unperturbed part, H_o, which sets the atomic energy spectrum, and a perturbed part, H_1, which describes the interaction of the atoms with their common radiation field to first order. If we model the atom as a two level system with unperturbed eigenstates $|1>$ and $|2>$ corresponding to the unperturbed energies $\mathcal{E}_1 < \mathcal{E}_2$, the time-dependent state vector $|\Psi(t)>$ is given by

$$|\Psi(t)> = a_1(t)\,|1> + a_2(t)\,|2> \tag{II.9}$$

where $a_1(t)$ and $a_2(t)$ are the time-dependent complex probability amplitudes. $|\Psi(t)>$ is a normalized vector, i.e. $|a_1(t)|^2 + |a_2(t)|^2 = 1$. The unperturbed Hamiltonian satisfies the relation

$$H_o\,|i> = \mathcal{E}_i\,|i> \quad \text{where } i = 1, 2 \tag{II.10}$$

and the interaction Hamiltonian, H_1, is given by

$$H_1 = -\vec{p}\cdot\vec{\mathcal{E}} = -p_x\,\mathcal{E} \tag{II.11}$$

where $p_x = ex$ is the projection of the dipole moment operator along the direction of polarization of the field, e is the charge of the electron, and $\mathcal{E}$ is given by Eq. (II.5a).

Using Eqs. (II.8 - 11), Schroedinger's equation becomes

$$i\bar{h}\,\frac{da_1}{dt}\,|1> + i\bar{h}\,\frac{da_2}{dt}\,|2> = \left(\mathcal{E}_1 - p_x\mathcal{E}\right)a_1\,|1> + \left(\mathcal{E}_2 - p_x\mathcal{E}\right)a_2\,|2> \tag{II.12}$$

Forming the inner product of Eq. (II.11) with the bras $<1|$ and $<2|$, we construct the equations of motion for the amplitudes a_1 and a_2

$$i\bar{h}\frac{da_1}{dt} = \mathcal{E}_1 a_1 - \mu\mathcal{E} a_2 \qquad \text{(II.13a)}$$

$$i\bar{h}\frac{da_2}{dt} = \mathcal{E}_2 a_2 - \mu\mathcal{E} a_1 \qquad \text{(II.13b)}$$

where $\mu = <1 \mid p_x \mid 2> = <2 \mid p_x \mid 1>$ are the dipole matrix elements and are assumed to be real without loss of generality. (If μ happens to be a complex number, we can let $\mu = |\mu| \exp(i\phi)$ and associate the phase factor $\exp(i\phi)$ with the electric field. The result is a trivial change in the phase of the carrier wave, which has no physical significance.)

Next we identify that if there are N contributing atoms per unit volume, then the macroscopic polarization , $\mathcal{P} = N < p_x >$, becomes a bilinear combination of the probability amplitudes

$$\mathcal{P} = N <\Psi(t) \mid p_x \mid \Psi(t)> = N\mu \left(a_1^*(t)\, a_2(t) + a_1(t)\, a_2^*(t)\right) \qquad \text{(II.14)}$$

Comparing Eq. (II.14) with our original assumption for the polarization, Eq. (II.5b), gives

$$\mathcal{P}_o = -2i\, a_1^*\, a_2\, e^{-i(k_o z - \omega_o t)} \qquad \text{(II.15)}$$

Taking the time derivative of Eq. (II.15) and using the relations given in Eqs. (II.13) and (II.5a) we find

$$\frac{d\mathcal{P}_o}{dt} = i\left(\omega_a - \omega_o\right)\mathcal{P}_o - \frac{i\mu}{\bar{h}}\mathcal{E}_o\mathcal{D} \qquad \text{(II.16)}$$

where $\omega_a = (\mathcal{E}_2 - \mathcal{E}_1)/\bar{h}$ is the resonant frequency of the two-level atom and $\mathcal{D} \equiv a_2^* a_2 - a_1^* a_1$ is identified as the population difference per atom. Refer to Fig. 2 for the frequency schematic.

Identifying the population difference, $\mathcal{D}$, leads us to develop its equation of motion similar to the development of Eq. (II.16). The equation describing the population difference is

$$\frac{d\mathcal{D}}{dt} = \frac{\mu}{2\bar{h}}\left(\mathcal{E}_o^*\,\mathcal{P}_o + \mathcal{E}_o\,\mathcal{P}_o^*\right) \qquad \text{(II.17)}$$

where higher order terms like $\exp(\pm i\, 2\omega_o t)$ were neglected in this first order

approximation.

An additional item is needed before Eqs. (II.7, 16, 17) can be used as an operating model. We must simulate the irreversible processes like spontaneous emission and atomic collisions that cause the decay of the population difference and polarization. The incoherent decay can be included easily by subtracting the term $\gamma_\perp \mathcal{P}_o$ from Eq. (II.16) and the term $\gamma_{//}(\mathcal{D}+1)$ from Eq. (II.17) where $\gamma_\perp = 1/T_2$ is the decay rate of the polarization and $\gamma_{//} = 1/T_1$ is the decay rate of the population difference. T_2 and T_1 are identified as the decay times of the polarization and population difference, respectively. When the cavity field is turned off, the system relaxes to the ground state, i.e. $\mathcal{D} = -1$ or $|a_1|^2 = 1$ and $|a_2|^2 = 0$. With these phenomenologically added terms, the two atomic equations that result are called the Bloch equations.

It is often convenient to scale our working equations to dimensionless values. Let us define a new set of dimensionless variables

$$E(r, z, t) = \frac{\mu}{\hbar \sqrt{\gamma_\perp \gamma_{//}}} \mathcal{E}_o(r, z, t) \tag{II.18a}$$

$$P(r, z, t) = \sqrt{\frac{\gamma_\perp}{\gamma_{//}}} \mathcal{P}_o(r, z, t) \tag{II.18b}$$

$$D(r, z, t) = \mathcal{D}(r, z, t) \tag{II.18c}$$

It is also convenient to rescale the time to the polarization decay rate, $\tau = \gamma_\perp t$. At this point the full set of Maxwell-Bloch equations take the form

$$-\frac{i}{2k_o} \nabla_T^2 E + \frac{\partial E}{\partial z} + \frac{1}{\beta} \frac{\partial E}{\partial \tau} = -\alpha P \tag{II.19a}$$

$$\frac{\partial P}{\partial \tau} = -(1 + i\Delta) P - ED \tag{II.19b}$$

$$\frac{\partial D}{\partial \tau} = \frac{\gamma}{2}(E^*P + EP^*) - \gamma(D + 1) \tag{II.19c}$$

where $\beta \equiv c / \gamma_\perp$ is the speed of light scaled to the polarization decay rate and $\gamma \equiv \gamma_{//} / \gamma_\perp$ is the ratio of the population difference decay rate to the polarization decay rate; for the

purpose of this thesis, $\beta = 2.0$ and $\gamma = 0.01$. With this choice for β and γ, $\gamma_{//}$ and $\gamma_{\perp}$ become 1.5×10^6 /s and 1.5×10^8 /s, respectively, which are consistent with atomic or molecular gases. [85] The choice for $\gamma = 0.01$ sets the system in the adiabatic polarization regime, i.e. the medium relaxation time is greater than the round trip time, which allows us to compare to transverse effects systems which work in this limit. $\Delta = (\omega_a - \omega_o) / \gamma_{\perp}$ is the detuning of the injected signal carrier away from the atomic transition frequency, and

$$\alpha = \frac{N \mu^2 \omega_o}{2 \varepsilon_o \bar{h} \gamma_{\perp} c} \tag{II.20}$$

is the linear absorption coefficient per unit length of the atomic medium. We must also scale the cavity lifetime given in Eq. (II.2) by the polarization decay rate to give $\kappa = \gamma_c / \gamma_{\perp}$.

We are interested in studying the effects that free-space diffraction have on a system with a thin atomic medium. This is in contrast to those who study the effects of diffraction within the medium (for instance, Ref. 50). For this system we assume the diffraction term in Eq. (II.19a) is negligible allowing the field to act as a set of plane waves through the medium each corresponding to a particular annular ring. The transverse coupling of the field in this system resides in the diffraction integral which is analyzed in the next chapter. Remember that the systems that we compare to assume that the diffraction term in Eq. (II.19a) is appreciable. Therefore, the equations of motion for the medium become,

$$\frac{\partial E}{\partial z} + \frac{1}{\beta} \frac{\partial E}{\partial \tau} = - \alpha P \tag{II.21a}$$

$$\frac{\partial P}{\partial \tau} = - (1 + i\Delta) P - ED \tag{II.21b}$$

$$\frac{\partial D}{\partial \tau} = \frac{\gamma}{2} (E^* P + E P^*) - \gamma (D + 1) \tag{II.21c}$$

The initial conditions for Eqs. (II.21) are

$$\left.\begin{aligned} E(z, 0) &= \text{noise} \\ P(z, 0) &= \text{noise} \\ D(z, 0) &= -1 \end{aligned}\right\} \quad 0 \le z \le L \tag{II.22}$$

which state that the field and polarization in the medium are initially set by background noise and the initial condition for the population difference demands that the system be in the ground state.

Equations (II.21, 22) coupled with appropriate boundary conditions are the basis for the plane wave optical bistability systems which were studied extensively by researchers like Narducci et al. [87] and Lugiato and co-workers. [88 - 90] These plane wave systems are discussed in more detail in Chapter III.

Absorptive and Dispersive Optical Bistability Equations (II.21) describe mixed absorptive and dispersive optical bistability. However, bistability is demonstrated by the two extreme cases, purely absorptive and purely dispersive bistability. The mechanisms that cause the two systems to undergo bistability are different. For purely absorptive bistability, the absorption coefficient α depends nonlinearly on the optical intensity and the wave vector, $k_o = n_o\, \omega_o / c$, is constant where n_o is the index of refraction. In the case of purely dispersive optical bistability $\Delta >> 1$ ($\alpha = 0$), the index of refraction depends nonlinearly on the optical intensity. In this case, the cavity phase shift becomes intensity dependent.

Numerical Method

We numerically solve Eqs. (II.21) by a Taylor expansion method introduced by Risken and Nummedal [86]. Their method uses a discretization process, similar to the familiar finite-difference routines.

First, we divide the space-time domain into a grid as shown in Fig. 3 and introduce the following Taylor series expansions for all the variables in the problem

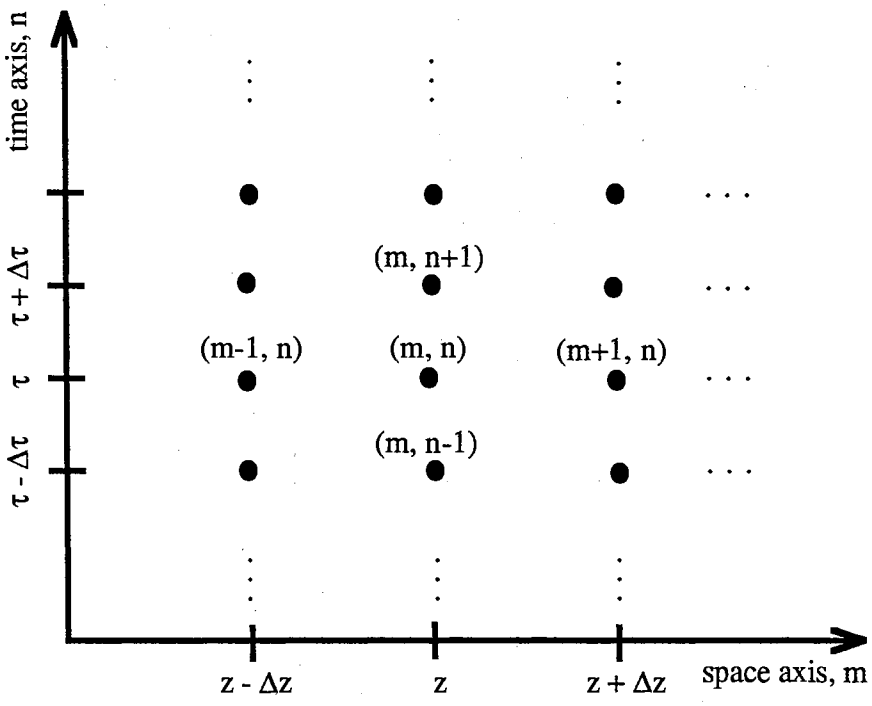

Figure 3. Schematic of the Descritized Time and Space Plane.

$$A_{m-1,\,n} = A_{m,\,n} - \Delta z \frac{\partial A_{m,\,n}}{\partial z} + \frac{1}{2}\Delta z^2 \frac{\partial^2 A_{m,\,n}}{\partial z^2} \tag{II.23a}$$

$$A_{m,\,n+1} = A_{m,\,n} + \Delta\tau \frac{\partial A_{m,\,n}}{\partial \tau} + \frac{1}{2}\Delta\tau^2 \frac{\partial^2 A_{m,\,n}}{\partial \tau^2} \tag{II.23b}$$

where A is a general representation of E, P, or D of Eqs. (II.21) and m and n denote indices of the discretized space and time, respectively. Notice that the rest of the Taylor series is truncated since we assume that the space and time steps are small, Δz and $\Delta\tau$ << 1. From the Taylor expansions, Eqs. (II.23), we have the basic formulas for the discretization process

$$\frac{\partial A_{m,\,n}}{\partial z} = \frac{A_{m,\,n} - A_{m-1,\,n}}{\Delta z} + \frac{1}{2}\Delta z \frac{\partial^2 A_{m,\,n}}{\partial z^2} \tag{II.24a}$$

$$\frac{\partial A_{m,n}}{\partial \tau} = \frac{A_{m,\,n+1} - A_{m,n}}{\Delta \tau} + \frac{1}{2}\Delta\tau \frac{\partial^2 A_{m,\,n}}{\partial \tau^2} \tag{II.24b}$$

By requiring that $\Delta z = \beta\,\Delta\tau$, the solutions of Eq. (II.21) are assured to propagate to the right.

The objective is to substitute Eqs. (II.24) into the left hand sides of Eqs. (II.21). Of course, to do this we must first calculate explicitly the second space and time derivatives. Taking the second time derivative of Eq. (II.21a) gives

$$\frac{\partial^2 E}{\partial \tau^2} = -\beta \frac{\partial^2 E}{\partial \tau\, \partial z} - \alpha\beta \frac{\partial P}{\partial \tau}$$

$$= -\beta \frac{\partial^2 E}{\partial \tau\, \partial z} + \alpha\beta \left((1 - i\Delta)\,P + ED\right) \tag{II.25}$$

where we have substituted in Eq. (II.21b). Taking the second space derivative of Eq. (II.21b) gives

$$\frac{\partial^2 E}{\partial z^2} = -\frac{1}{\beta} \frac{\partial^2 E}{\partial z\, \partial \tau} - \alpha \frac{\partial P}{\partial z}$$

$$= -\frac{1}{\beta}\frac{\partial^2 E}{\partial z\,\partial \tau} - \alpha\frac{P_{m,n} - P_{m-1,n}}{\Delta z} \qquad \text{(II.26)}$$

Notice that whenever a first space derivative appears (like $\partial P/\partial z$), we replace it by its first difference approximation since $\partial^2 P/\partial z^2$ is already proportional to the first power of Δz.

Substituting Eqs. (II.25) and (II.26) into Eqs. (II.24) and substituting Eqs. (II.24) into Eq. (II.21a) gives

$$E_{m,n+1} = E_{m-1,n} + \alpha\frac{\Delta\tau}{2}\left[\left(\Delta\tau\,(1\text{-}i\Delta) - 1\right)P_{m,n} - P_{m-1,n} + \Delta\tau\,E_{m,n}\,D_{m,n}\right] \qquad \text{(II.27)}$$

Breaking Eq. (II.27) into its real and imaginary parts gives

$$E^r_{m,n+1} = E^r_{m-1,n} + a^r_1 P^r_{m,n} - a^i_1 P^i_{m,n} + a_2 P^r_{m-1,n} + a_3 E^r_{m,n} D_{m,n} \qquad \text{(II.28a)}$$

$$E^i_{m,n+1} = E^i_{m-1,n} + a^i_1 P^r_{m,n} + a^r_1 P^i_{m,n} + a_2 P^i_{m-1,n} + a_3 E^i_{m,n} D_{m,n} \qquad \text{(II.28b)}$$

where the superscripts r and i denote real and imaginary, respectively. The coefficients of Eqs. (II.28) are given in Appendix B. The corresponding equations for the polarizations (real and imaginary) and the population difference are

$$\begin{aligned} P^r_{m,n+1} = {} & b^r_1 P^r_{m,n} - b^i_1 P^i_{m,n} + 2b_2 E^r_{m,n}\left(E^r_{m,n} P^r_{m,n} - E^i_{m,n} P^i_{m,n}\right) \\ & + D_{m,n}\left(b^r_3 E^r_{m,n} - b^i_3 E^i_{m,n} + b_4 E^r_{m-1,n} + b_5 P^r_{m,n}\right) + b_6 E^r_{m,n} \end{aligned} \qquad \text{(II.29a)}$$

$$\begin{aligned} P^i_{m,n+1} = {} & b^r_1 P^i_{m,n} + b^i_1 P^r_{m,n} + 2b_2 E^r_{m,n}\left(E^r_{m,n} P^i_{m,n} + E^i_{m,n} P^r_{m,n}\right) \\ & + D_{m,n}\left(b^r_3 E^i_{m,n} + b^i_3 E^r_{m,n} + b_4 E^i_{m-1,n} + b_5 P^i_{m,n}\right) + b_6 E^i_{m,n} \end{aligned} \qquad \text{(II.29b)}$$

$$\begin{aligned} D_{m,n+1} = {} & c^r_1\left(E^r_{m,n} P^r_{m,n} + E^i_{m,n} P^i_{m,n}\right) + c^i_1\left(E^i_{m,n} P^r_{m,n} - E^r_{m,n} P^i_{m,n}\right) \\ & + c_2\left(E^r_{m-1,n} P^r_{m,n} + E^i_{m-1,n} P^i_{m,n}\right) + c_3 \left| P_{m,n} \right|^2 \\ & + c_4 D_{m,n} \left| E_{m,n} \right|^2 + c_5 D_{m,n} + c_6 \end{aligned} \qquad \text{(II.29c)}$$

where the coefficients are also given in Appendix B.

Free-Space Diffraction Representation

Theoretical Development

A more accurate treatment of optical beams in cavity resonators must take into account diffraction and the wave nature of the light. Few optical bistability models take into account free-space diffraction because most choose to study diffraction of the field within the medium relying on well developed Fast Fourier Transform algorithms. We choose to study the effect of free-space diffraction on a system which includes a passive optically bistable medium. Practical laser beams are almost always well enough collimated even under worst conditions that we can describe their diffraction properties using a scaler wave theory and working in the paraxial wave approximation. This section gives the history and theoretical development of the Kirchoff diffraction integral.

The first reference to diffraction phenomena appears in the work of Leonardo da Vinci in the 15th century. Such phenomena was, however, first described by Grimaldi in 1665. The corpuscular theory which, at the time, was widely believed to correctly describe the propagation of light, could not explain diffraction. Huygen, the first proponent of the wave theory, was unaware of Grimaldi's discoveries which supported his own views. The possibility of explaining diffraction effects on the basis of a wave theory was not noticed until about 1818. In that year, Fresnel's work appeared in which he showed that diffraction can be explained by the application of Huygen's construction together with the principle of interference. Fresnel's analysis was later put on a sound mathematical basis by Kirchoff in 1882 and the subject has since been extensively discussed by many authors. [91]

Diffraction problems are among the most difficult ones encountered in optics since analytical solutions are rare. The first such analytical solution was given in 1896 by Sommerfeld when he discussed the diffraction of a plane wave by a perfectly conducting semi-infinite plane screen. Since then rigorous solutions of a small number of other diffraction problems (mainly two-dimensional) have also been found, but, because of mathematical difficulties, approximate methods must be used in most cases of practical interest. Of these the theory of Huygen and Fresnel is by far the most powerful and is adequate for the treatment of the majority of problems encountered in instrumental optics.

According to Huygen's construction, every point of a wave-front may be considered as a center of a secondary disturbance which gives rise to spherical wavelets, and the wave-front at any later instant may be regarded as the envelope of these wavelets. Fresnel was able to account for diffraction by supplementing Huygen's construction with the postulate that the secondary wavelets mutually interfere. This combination of Huygen's construction with the principle of interference is called the Huygen-Fresnel Principle.

The basic idea of the Huygen-Fresnel theory is that the light disturbance at a point P_2 arises from the superposition of secondary waves that proceed from a surface situated between this point and the light source. This idea was put on a sounder mathematical basis by Kirchoff, who showed that the Huygen-Fresnel principle may be regarded as an approximate form of an integral theorem which expresses the solution of the homogeneous wave equation, at an arbitrary point in the field, in terms of the values of the solution and its first derivatives at all points on an arbitrary closed surface surrounding the point P_2.[87]

We consider first a strictly monochromatic scaler wave

$$V(r, z, t) = E(r, z)\, e^{-i\omega t} \tag{II.30}$$

where r represents the transverse coordinate and z represents the longitudinal coordinate. In vacuum the space-dependent part then satisfies the time-independent wave equation

$$\left(\nabla^2 + k^2\right) E(r, z) = 0 \tag{II.31}$$

where $k = \omega / c$. Equation (II.31) is known as Helmholtz's equation. Let $\vee$ be a volume bounded by a closed surface $\mathbb{S}$, and let P_2 be any point within $\vee$ (see Fig. 4); we assume that E possesses continuous first- and second-order partial derivatives within and on this surface. If E' is any other function which satisfies the same continuity requirements as E, we have by Green's theorem

$$\iiint_{V} \left(E\, \nabla^2 E' - E'\, \nabla^2 E\right) dV = - \iint_{S} \left(E \frac{\partial E'}{\partial n} - E' \frac{\partial E}{\partial n}\right) dS \tag{II.32}$$

where $\partial/\partial n$ denotes the differentiation along the inward normal to $\mathbb{S}$. In particular, if E' also satisfies Helmholtz's equation then it follows at once from Eq. (II.31) that the integrand on the left of Eq. (II.32) vanishes at every point of $\vee$, and consequently

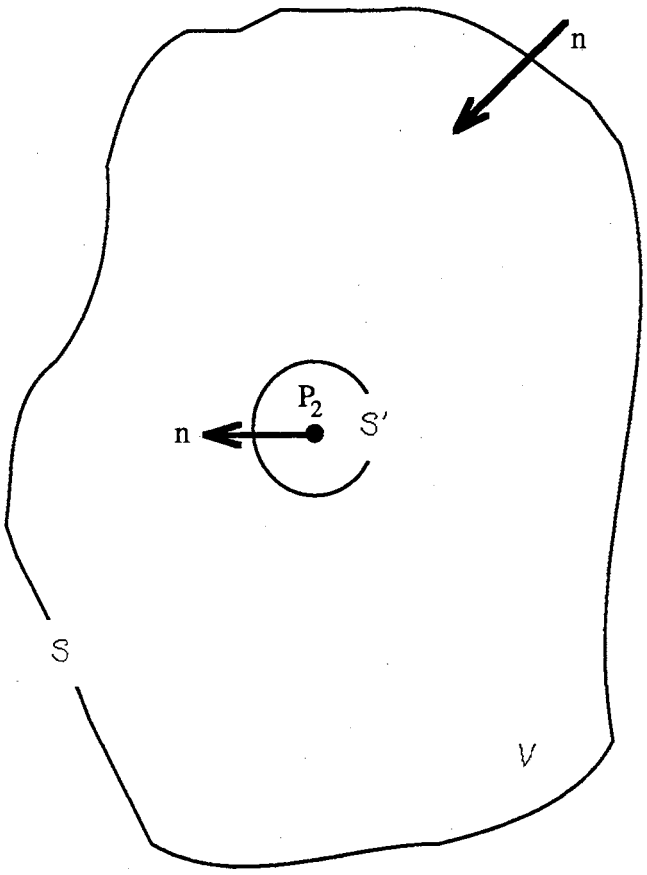

Figure 4. Region of Integration in the Derivation of the Diffraction Integral. n is the normal vector of the surfaces $\mathbb{S}$ and $\mathbb{S}'$ and P_2 is the point of interest.

$$\iint_S \left(E \frac{\partial E'}{\partial n} - E' \frac{\partial E}{\partial n}\right) dS = 0 \tag{II.33}$$

Suppose we take $E'(r,z) = \exp(iks) / s$ where s denotes the distance from P_2 to some point (r,z). This function has a singularity for $s = 0$, and since E' was assumed to be continuous and differentiable, P_2 must be excluded from the domain of integration. We shall therefore surround P_2 by a small sphere of radius ε and extend the integration throughout the volume between S and the surface S' of this sphere. In place of Eq. (II.33), we then have

$$\iint_S + \iint_{S'} \left(E \frac{\partial}{\partial n}\left(\frac{e^{iks}}{s}\right) - \frac{e^{iks}}{s}\frac{\partial E}{\partial n}\right) dS = 0 \tag{II.34}$$

which becomes

$$\iint_S \left(E \frac{\partial}{\partial n}\left(\frac{e^{iks}}{s}\right) - \frac{e^{iks}}{s}\frac{\partial E}{\partial n}\right) dS = - \iint_{S'} \left(E \frac{e^{iks}}{s}\left(ik - \frac{1}{s}\right) - \frac{e^{iks}}{s}\frac{\partial E}{\partial n}\right) dS'$$

$$= - \iint_{\Omega} \left(E \frac{e^{ik\varepsilon}}{\varepsilon}\left(ik - \frac{1}{\varepsilon}\right) - \frac{e^{ik\varepsilon}}{\varepsilon}\frac{\partial E}{\partial n}\right) \varepsilon^2 \, d\Omega \tag{II.35}$$

where $d\Omega$ denotes an element of the solid angle. Since the integral over S is independent of ε, we may replace the integral on the right-hand side by its limiting value as $\varepsilon \to 0$; the first and third terms in this integral give no contribution in the limit, and the total contribution of the second term is $4\pi E(P_2)$. Therefore, Eq. (II.35) becomes

$$E(P_2) = \frac{1}{4\pi} \iint_S \left(E \frac{\partial}{\partial n}\left(\frac{e^{iks}}{s}\right) - \frac{e^{iks}}{s}\frac{\partial E}{\partial n}\right) dS \tag{II.36}$$

This is one form of the integral theorem of Helmholtz and Kirchoff.

Although the integral theorem of Kirchoff embodies the basic idea of the Huygen-Fresnel principle, the laws governing the contributions from different elements of the surface are more complicated than Fresnel assumed. Kirchoff showed, however, that in many cases the theorem may be reduced to an approximate but much simpler form, which

is essentially equivalent to the formulation of Fresnel, but which in addition gives an explicit formula for the inclination factor that remained undetermined in Fresnel's theory.

Consider a monochromatic wave, from a point source, P_1, propagated through an opening in a plane opaque screen, and let P_2 as before be the point at which the light disturbance is to be determined, see Fig. 5. We assume that the linear dimensions of the opening in the screen, although large compared to the wavelength, are small compared to the distances of both P_1 and P_2 from the screen.

To find the disturbance at P_2 we take Kirchoff's integral over a surface $\mathcal{S}$ formed by: (1) the opening $\mathcal{A}$ in the screen, (2) a portion $\mathcal{B}$ of the non-illuminated side of the screen, and (3) a portion C of a large sphere of radius, R, centered at P_2 which, together with $\mathcal{A}$ and $\mathcal{B}$, forms a closed surface.

Kirchoff's theorem, expressed by Eq. (II.36) then gives

$$E(P_2) = \frac{1}{4\pi}\left[\iint_{\mathcal{A}} + \iint_{\mathcal{B}} + \iint_{C}\right]\left(E\frac{\partial}{\partial n}\left(\frac{e^{iks}}{s}\right) - \frac{e^{iks}}{s}\frac{\partial E}{\partial n}\right) d\mathcal{S} \tag{II.37}$$

The difficulty encountered in solving Eq. (II.37) is that the values of E and $\partial E/\partial n$ on $\mathcal{A}$, $\mathcal{B}$, and C which should be substituted in Eq. (II.37) are never known exactly. However, it is reasonable to suppose that everywhere on $\mathcal{A}$, except in the immediate neighborhood of the rim of the opening, E and $\partial E/\partial n$ will not appreciably differ from the values obtained in the absence of the screen, and that on $\mathcal{B}$ these quantities will be approximately zero. Kirchoff accordingly set

$$E = E_o\frac{e^{ikR}}{R} \text{ and } \frac{\partial E}{\partial n} = E_o\frac{e^{ikR}}{R}\left(ik - \frac{1}{R}\right)\cos\psi \text{ on } \mathcal{A} \tag{II.38a}$$

$$E = 0 \text{ on } \mathcal{B} \tag{II.38b}$$

as the values relating to the incident field (see Fig. 5) and E_o is a constant. R represents the distance from the source to the opening $\mathcal{A}$ and ψ represents the angle between the vector R and the normal vector. Eqs. (II.38) are called the Kirchoff's boundary conditions and are the basis of Kirchoff's diffraction theory.

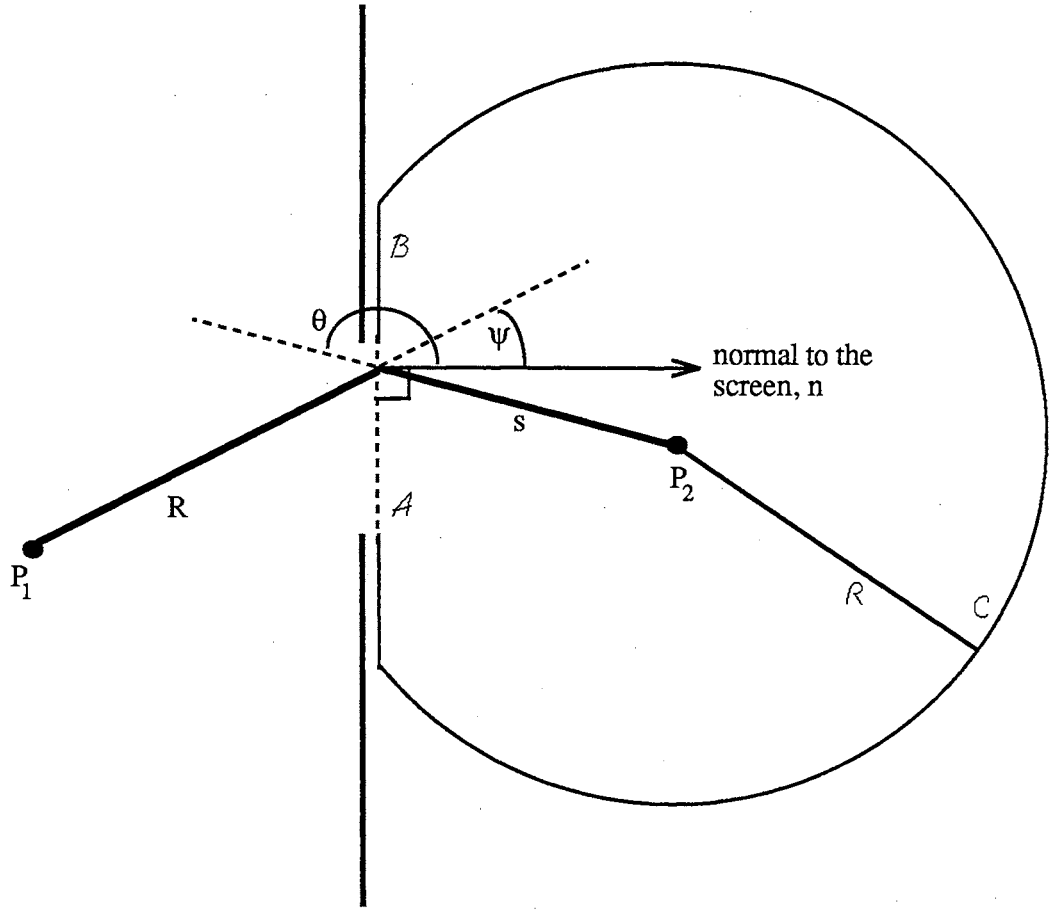

Figure 5. Illustration of the Derivation of the Fresnel-Kirchoff Diffraction Forumla.

Next we consider the contribution from the spherical portion, C. For our purposes it is sufficient to make the physically obvious assumption that the radiation field does not exist at all times but that it is produced by a source that begins to radiate at some particular instant of time $t = t_o$. Then at some time $t > t_o$, the field fills a region of space where the outer boundary is at distance less than $c(t - t_o)$ from P_1, c being the speed of light. If the radius R is chosen so large that at the time when the disturbance at P_2 is considered, no contributions from C could have reached P_2 because at the appropriate earlier time the field has not reached these distant regions, the integral over C will vanish.

Substituting Eqs. (II.38) into Eq. (II.37) and assuming that $k >> 1/R$ and $1/s$ (since R and s are both assumed much greater than the wavelength, λ) then we obtain

$$E(P_2) = -\frac{i}{2\lambda} \iint_A E_o \frac{e^{ikR}}{R} \frac{e^{iks}}{s} (\cos\psi - \cos\theta)\, dS \tag{II.39}$$

where θ represents the angle between $\vec{s}$ and the normal vector, $\vec{n}$. Equation (II.39) is known as the Fresnel-Kirchoff diffraction formula. The paraxial approximation, $\psi \to 0$ and $\theta \to \pi$, gives

$$E(P_2) = -\frac{i}{\lambda} \iint_A E(P_1) \frac{e^{iks}}{s} dS$$

$$\equiv \iint_A E(P_1)\, K(s)\, dS \tag{II.40}$$

where $K(s) \equiv e^{iks} / s$ is the kernel of the Fresnel-Kirchoff integral.

Next we follow the development of Fox and Li [92] who study diffraction problems under the scalar approximation, which is often used in optics, in a resonator cavity. We assume that the field is uniformly polarized and nearly transverse and with width a, see Fig. 6. Here, Λ represents the distance between planes 1 and 2 and the points P_1 and P_2 are analogous to the points discussed earlier. w_a is the width of the aperture and we demand that $\Lambda >> w_a$.

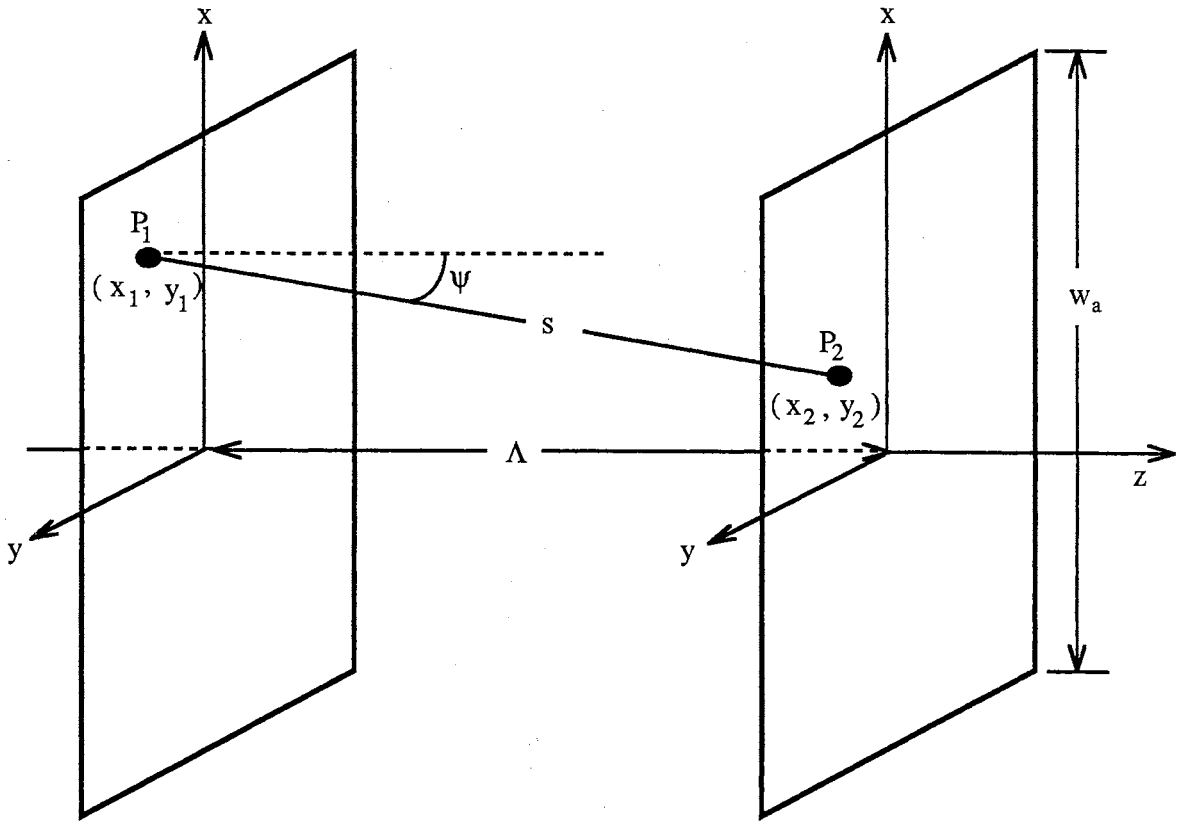

Figure 6. Diffraction Between Two Planes.

We can write s, the distance between points P_1 and P_2, as

$$s = \sqrt{\Lambda^2 + (x_1 - x_2)^2 + (y_1 - y_2)^2}$$

$$= \Lambda \sqrt{1 + \left(\frac{x_1 - x_2}{\Lambda}\right)^2 + \left(\frac{y_1 - y_2}{\Lambda}\right)^2} \qquad \text{(II.41)}$$

since we are dealing with a system whose cavity length is much greater than its transverse dimensions ($\Lambda >> w_a$) then $(x_1 - x_2)$, $(y_1 - y_2) \sim w_a$. This allows us to expand Eq. (II.41) into a binomial series

$$s = \Lambda \left(1 + \frac{1}{2}\left(\frac{x_1 - x_2}{\Lambda}\right)^2 + \frac{1}{2}\left(\frac{y_1 - y_2}{\Lambda}\right)^2 + \varepsilon'\right) \qquad \text{(II.42)}$$

where ε' represents all higher order terms in the expansion. Rewriting s we find

$$s = \Lambda + \frac{1}{2\Lambda}\left((x_1 - x_2)^2 + (y_1 - y_2)^2\right) + \varepsilon \qquad \text{(II.43)}$$

where $\varepsilon = \varepsilon' \Lambda$. Since $\Lambda >> w_a$ then $\Lambda >> (x_1 - x_2)$ and $(y_1 - y_2)$ and we can assume that s $\cong \Lambda$ in the denominator of the kernel, K(s). However, in the argument of the exponential term in K(s), s must contain more terms in the binomial expansion. Substituting Eq. (II.43) into the kernel we find the term $\exp(ik\varepsilon)$. We can only neglect this term if $k\varepsilon << 2\pi$. We note that ε is a converging series with alternating signs. By looking at the next term to find out its size

$$|\varepsilon| = \frac{1}{8\Lambda^3}\left((x_1 - x_2)^2 + (y_1 - y_2)^2\right)^2 + \ldots \qquad \text{(II.44)}$$

we find that

$$|\varepsilon| < \frac{1}{8\Lambda^3}\left(8w_a^2\right)^2 \cong \frac{w_a^4}{\Lambda^3} \qquad \text{(II.45)}$$

where $(x_1 - x_2)$ and $(y_1 - y_2)$ can each be no larger than $2\,w_a$. If $k\varepsilon << 2\pi$ then

$$\frac{k\, w_a^4}{\Lambda^3} = \frac{2\pi\, w_a^2}{\Lambda^2} F << 2\pi \tag{II.46}$$

where

$$F \equiv \frac{w_a^2}{\lambda\Lambda} \tag{II.47}$$

This means that $F << \Lambda^2 / w_a^2$ for Eq. (II.46) to hold. F is referred to as the Fresnel number. This leads us to the two criteria needed in order to expand s in a binomial series: (1) the distance over which diffraction takes place must be much greater than the aperture width, $\Lambda >> w_a$, and (2) the Fresnel number must be small compared to the square of the ratio of the diffraction distance to the aperture width, $F << \Lambda^2 / w_a^2$.

Using these criteria, we find for the kernel of the Fresnel-Kirchoff integral

$$K(x_1, x_2 ; y_1, y_2) = - \frac{i}{\lambda\Lambda} \exp\left(\frac{ik}{2\Lambda}\left[(x_1 - x_2)^2 + (y_1 - y_2)^2\right]\right) \tag{II.48}$$

where we have neglected the term $\exp(ik\Lambda)$ assuming that we can choose a distance Λ which is an integer multiple of the wavelength λ.

A very useful generalized form of paraxial optics has been developed in recent years. This generalized form can handle paraxial wave propagation not only in free space but also in multi-element optical systems. This more general type of paraxial wave theory can be expressed in several mathematically equivalent forms. The approach that seems most convenient describes paraxial wave propagation entirely in terms of ray (ABCD) matrices.

We can write the total path length through a set of optical elements as [85]

$$s = \Lambda + \frac{1}{2B}\left(Ax_1^2 - 2x_1x_2 + Dx_2^2\right) + \frac{1}{2B}\left(Ay_1^2 - 2y_1y_2 + Dy_2^2\right) \tag{II.49}$$

Using Eq. (II.49) we can write the kernel of the Fresnel-Kirchoff integral as

$$K(x_1, x_2; y_1, y_2) = \frac{-i}{\lambda B} \exp\left(\frac{ik}{2B}\left[A(x_1^2 + y_1^2) - 2(x_1x_2 + y_1y_2) + D(x_2^2 + y_2^2)\right]\right) \tag{II.50}$$

where the elements of the ray matrix, A, B, D for the system in this study is given by Eqs. (A.4) in Appendix A. For the system parameters ($R_1 = R_2 = \Lambda$, $p_1 + p_2 + L = p_3 = \Lambda/2$),

we find $A = D \cong -1/2$ and $B \cong 3\Lambda/8$.

Switching to cylindrical coordinates where $x = r\cos\phi$ and $y = r\sin\phi$ we find for the kernel

$$K(r_1, \phi_1 ; r_2, \phi_2) = -\frac{i}{\lambda B}\exp\left(\frac{ik}{2B}\left[Ar_1^2 - 2r_1r_2\cos(\phi_1 - \phi_2) + Dr_2^2\right]\right) \tag{II.51}$$

Substituting Eq. (II.51) into Eq. (II.40) gives

$$E(P_2) = -\frac{i}{\lambda B}e^{\frac{ik}{2B}Dr_2^2}\int_0^{\infty}E(P_1)\,e^{\frac{ik}{2B}Ar_1^2}\,r_1\,dr_1\int_0^{2\pi}e^{\frac{-ik}{B}r_1r_2\cos\Phi}\,d\Phi \tag{II.52}$$

where $\Phi = \phi_1 - \phi_2$. Strictly speaking, the limits on the angular integral should be from $-\phi_2$ to $2\pi - \phi_2$ but without loss of generality we can set $\phi_2 = 0$.

The integral representation of the zeroth order Bessel's function is [93]

$$2\pi\,J_o\left(\frac{k}{B}r_1r_2\right) = \int_0^{2\pi}e^{\frac{-ik}{B}r_1r_2\cos\Phi}\,d\Phi \tag{II.53}$$

Substituting Eq. (II.53) into Eq. (II.52) gives

$$E(P_2, t) = -\frac{ik}{B}e^{\frac{ik}{2B}Dr_2^2}\int_0^{\infty}E(P_1, t - \Delta t)\,e^{\frac{ik}{2B}Ar_1^2}\,J_o\left(\frac{k}{B}r_2r_1\right)\,r_1dr_1 \tag{II.54}$$

Note that we have added in the inherent time delay, $\Delta t = B/c$, caused by the travel of the field from P_1 to P_2.

At this point it becomes convenient to scale the radial coordinates to the beam width, w_o, $\rho = r_2 / w_o$ and $\zeta = r_1 / w_o$. This gives

$$E(\rho, P_2, \tau) = -2i\xi\,e^{i\xi D\rho^2}\int_0^{\infty}E(\zeta, P_1, \tau - \Delta\tau)\,e^{i\xi A\zeta^2}\,J_o(2\xi\rho\zeta)\,\zeta\,d\zeta \tag{II.55}$$

where $\xi = Z_r / B$ and Z_r is the Raleigh range given by $kw_o^2 / 2$. This equation is only valid

in far-field where $Z_r < \Lambda$. For that reason, we set $Z_r = \Lambda/4$ in this study. For a cavity length of 1m and $\lambda = 589.6$ nm for the D_2 line in sodium, this gives the input beam waist as $w_o \cong$ 220 μm. We scale the time in Eq. (II.55) by the polarization decay rate, $\tau = \gamma_\perp t$, to be consistent with the field within the medium.

Equation (II.55) is the Kirchoff's diffraction integral in cylindrical coordinates. It is this equation that will be used to calculate the diffracted field. The diffracted field is used as field memory for the spatial cell of the passive medium. The Kirchoff diffraction integral is a Hankel transform if the exponential term in the integrand is absorbed into the field. Currently, the Hankel transform has no set numerical method like the Fast Fourier Transform. In the next section we create an algorithm for solving this integral.

Numerical Method

The Hankel transform of order zero is defined here as

$$E(\rho) = \int_0^\infty J_o(2\xi\rho\zeta)\, E(\zeta)\, \zeta\, d\zeta \tag{II.56}$$

where $E(\rho)$ denotes the Hankel transformed function of $E(\zeta)$. The zeroth order Bessel function can be expanded exactly in terms of Laguerre generating functions as [89]

$$J_o(2\sqrt{xz}) = e^{-z} \sum_{n=0}^{\infty} \frac{z^n}{n!} L_n(x) \ . \tag{II.57}$$

These $L_n(x)$ functions are the normalized Laguerre functions whose recursion relation is

$$L_n(x) = \left(2 - \frac{x+1}{n}\right) L_{n-1}(x) - \left(1 - \frac{1}{n}\right) L_{n-2}(x) \tag{II.58}$$

where $L_o(x) = 1$ and $L_1(x) = 1 - x$. By defining $x = \xi\rho^2$ and $z = \xi\zeta^2$ we can write the Bessel function expansion as

$$J_o(2\xi\rho\zeta) = e^{-\xi\zeta^2} \sum_{n=0}^{\infty} \frac{\xi^n \zeta^{2n}}{n!} L_n(\xi\rho^2) \ . \tag{II.59}$$

Substituting Eq. (II.59) into the Hankel transform, Eq. (II.56), and making the change of variables $x = \zeta^2$ and $y = \rho^2$ we find

$$E(\sqrt{y}) = \int_0^\infty \frac{1}{2}\left(e^{(1-\xi)x} \sum_{n=0}^{\infty} \frac{\xi^n x^n}{n!} L_n(\xi y)\, E(\sqrt{x})\right) e^{-x}\, dx \ . \tag{II.60}$$

Equation (II.60) can be written as

$$E(\sqrt{y}) \equiv \int_0^\infty E(\sqrt{x}, y)\, e^{-x}\, dx \tag{II.61}$$

where

$$E(\sqrt{x}, y) \equiv \frac{1}{2}\left(e^{(1-\xi)x} \sum_{n=0}^{\infty} \frac{\xi^n x^n}{n!} L_n(\xi y)\, E(\sqrt{x})\right) \ . \tag{II.62}$$

Equation (II.61) is the familiar Gaussian quadrature which can be approximated by

$$E(\sqrt{y_i}) \cong \sum_{j=1}^{M} E(\sqrt{x_j}, y_i)\, w(x_j) \tag{II.63}$$

where the y_i and x_j are the abscissae of the Laguerre polynomial of order M and the $w(x_j)$ are the weights. This integration formula is exact for all polynomials of order $< 2M + 2$. Substituting Eq. (II.62) into Eq. (II.63) gives

$$E(\sqrt{y_i}) \cong \sum_{j=1}^{M} B_{ij}\, E(\sqrt{x_j}) \tag{II.64}$$

where the two-dimensional matrix B_{ij} is defined as

$$B_{ij} \equiv \frac{1}{2} w(x_j)\, e^{(1-\xi)x_j} \sum_{n=0}^{M-1} \frac{\xi^n x_j^n}{n!} L_n(\xi y_i) \ . \tag{II.65}$$

We replaced the infinite summation limit in the Bessel function expansion by M-1 for numerical evaluation. The B_{ij} matrix can be calculated accurately once and stored for later use. By taking advantage of this quadrature formula, we are able to write our Hankel transform as a real matrix / complex vector product.

As in any numerical formulation, we are concerned with roundoff error. This error

manifests itself in the Hankel transformed field at large radii, where the field should fall off exponentially. As the number of roundtrip passes increases, the error becomes amplified. Physically over the atomic and geometric parameters we use, the field should remain Gaussian in the transverse dimension at large radii. We demand this Gaussian structure by choosing a radial coordinate where the field still has appreciable magnitude and extrapolate the field

$$E(\sqrt{y_i}) = E(\sqrt{y_{i-1}})\, e^{-C(x_i - x_{i-1})} \tag{II.66}$$

where C controls the strength of the Gaussian smoothing.

The FORTRAN code used to numerically simulate both the medium and the free-space diffraction is given in Appendix C. The computations ran on a DECstation 3100 and DECstation 5000 workstations. We test the code against three known results. The first test, a Gaussian input field, gives the percent difference between the numerical and analytic results for small radii as less than 10^{-9} and rises to a few percent difference at large radii. The second test, a tightly apertured Gaussian input field, displays the well-known Airy function. The third test is the intercomparison between this model and the model based on the Gauss-Laguerre modal expansion of the field in the active counterpart, the free-running laser model given by the authors in Ref. 94. We show that for small focal lengths ($f = \Lambda/2$) in the free-space diffraction model and correspondingly large transverse mode spacing in the modal expansion model, excellent agreement in the radial profiles and the gain ramps.

Aperture on the Injected Signal

We place an aperture of width w_a on the injected signal to simulate diffraction effects in the system, see Fig. 1. In the discussion of the Kirchoff's diffraction integral we introduced the Fresnel number parameter, Eq. (II.47). We rewrite the Fresnel number to include the value of the Raleigh range and find

$$F = \frac{1}{4\pi}\left(\frac{w_a}{w_o}\right)^2 \tag{II.67}$$

For the purpose of this thesis, we consider the limiting conditions of large and small Fresnel numbers, $F >> 1$ and $F < 1$ simulating a plane wave limit and increased free-space

diffraction.

Boundary Conditions

To complete the optical bistability free-space diffraction model, we must consider the boundary conditions for this system. The boundary conditions at the input and output couplers, M_I and M_{II}, imposed on this system are

$$E(\rho, 0, \tau) = \sqrt{T}\, E_i(\rho) + R\, e^{i\delta} E_{FB}(\rho, \Lambda, \tau) \tag{II.68a}$$

$$E_t(\rho, L, \tau) = \sqrt{T}\, E(\rho, L, \tau) \tag{II.68b}$$

Here we place the origin of the space axis at the M_I mirror and we map the longitudinal distance relative to that point. At $z = L$ we have exited the medium and at $z = \Lambda$ we complete a roundtrip and arrive at the origin of the axis.

Equation (II.68a) establishes two essential features of this work, an injected signal which couples coherently with the internal cavity field and feedback. This equation is the superposition of the Gaussian injected signal with a planar phase front,

$$E_i(\rho) = E_{in}\, e^{-\rho^2} \tag{II.69}$$

attenuated by a factor $T^{1/2}$ and the feedback field, E_{FB}, given by Eq. (II.55). In that equation, $E(\rho, P_2, \tau) \rightarrow E_{FB}(\rho, \Lambda, \tau)$ and $E(\zeta, P_1, \tau - \Delta\tau) \rightarrow E(\zeta, L, \tau - \Delta\tau)$. T is the transmittivity of mirror M_I and $R = 1 - T$. The cavity / injected signal phase detuning is given by

$$\delta = (\omega_c - \omega_o)\, \tau_R \tag{II.70}$$

where $\tau_R = \Lambda\gamma_\perp/c$ is the scaled round trip time. For this thesis, we set $\delta = 0$ to reduce the number of system parameters which simplifies the system. We find similar behavior of the system if $\delta \neq 0$. This condition minimizes known cavity effects which allows a concentration on diffraction effects.

Equation (II.68b) represents the output field, E_t, at mirror M_{II} created from the field as it leaves the medium at position L.

An essential part of boundary conditions is periodicity. Because of the continuous

propagation of the field, we have the necessary isochronous boundary conditions through the feedback mechanism provided by the Kirchoff diffraction integral.

CHAPTER III

COMPARISON TO PLANE WAVE MODELS

Much theoretical work has been done in the area of plane wave effects in optical bistability since it was first predicted in 1974 [1] and experimentally verified a year later. [4] The early- to mid-1980s showed considerable research reporting phenomena like period-doubling bifurcations, [87] and self-pulsing and chaos. [88] For the purpose of this thesis, we will be mainly concerned with hysteresis and the effects of atomic and cavity detuning. For a good discussion on plane wave effects in optical bistability, see Ref. 31.

To begin our analysis of the effects that free-space diffraction has on an optically bistable system, we select the limiting case of a large Fresnel number, where the ratio of the aperture radius to the injected signal radius is large, and compare the dynamics of the on-axis intensity in the free-space diffraction (FSD) system to the intensity in systems modeled in the plane wave (PW) limit. This is justified since we treat the field through the medium as a series of plane waves each corresponding to a particular annular ring and since large Fresnel numbers approach the plane-wave limit of this model.

In this chapter, we briefly describe the well known plane wave model and compare the results displayed in the FSD system to the PW system.

Plane Wave Models

The Maxwell-Bloch equations coupled with boundary conditions are widely used to describe plane wave optical bistability. As a reminder, this system is a collection of homogeneously broadened two-level atoms whose central frequency ω_a is detuned from the injected signal frequency ω_o by Δ. The nearest cavity frequency ω_c is detuned from ω_o by the amount δ. The atomic line has a width $\gamma_\perp$ which is usually affected not only by the

spontaneous decay of the excited state but also by collision processes. The cavity linewidth κ is controlled by the mirror reflectivity and by the optical quality as known from the theory of optical interferometers. The coupled field-atom equations of motion are controlled by the atomic and cavity detuning parameters Δ and δ, respectively.

Most of the theoretical literature on the subject of plane wave OB concentrates on the physically relevant mean-field limit, a situation that is defined simultaneously by the effect of $\alpha L \rightarrow 0$ and $T \rightarrow 0$ while at the same time the ratio $\alpha L / T$ remains constant and arbitrary. The intention is to simulate a situation where the cavity field is nearly uniform over the length of the medium. The limit $\alpha L \rightarrow 0$ by itself leads to a trivial situation because it implies the disappearance of the passive medium and the loss of any significant interaction and feedback between the atoms and the radiation. On the other hand, by requiring $T \rightarrow 0$ by itself, the cavity field is made to interact weakly with the medium in a single pass. However, this also requires the cavity field to circulate many times before escaping. Thus the accumulated effect of the dilute medium on the radiation can be maintained sufficiently high. The single mode equations in the mean-field limit for the plane wave model are

$$\frac{dE}{d\tau} = -\kappa\left((1 + i\theta)\, E - E_i + 2CP\right) \tag{III.1a}$$

$$\frac{dP}{d\tau} = -(1 + i\Delta)\, P - ED \tag{III.1b}$$

$$\frac{dD}{d\tau} = \frac{\gamma}{2}\left(E^*P + EP^*\right) - \gamma\left(D + 1\right) \tag{III.1c}$$

where E_i represents the planar injected signal, $\kappa = cT/\gamma_\perp \Lambda$ is the cavity decay rate, $\theta = \delta/T$ is the cavity detuning scaled to the transmittivity, $C = \alpha L/2T = \alpha L/\kappa\Lambda$ is the bistability parameter, and $\gamma = \gamma_{//} / \gamma_\perp$ is the ratio of the population decay to the polarization decay rate. These equations utilize the Lugiato time and space transformation and dynamical variable transformations. [93] With these transformations, the boundary conditions of the cavity resonator are now incorporated within Eqs. (III.1) and need not be imposed separately.

The steady state equation, derived from Eqs. (III.1) by letting the time $\tau \rightarrow \infty$, is given by

$$E_i = E_t^{ss}\left(\left(1 + \frac{2C}{1 + \Delta^2 + |E_t^{ss}|^2}\right) + i\left(\theta - \frac{2C\Delta}{1 + \Delta^2 + |E_t^{ss}|^2}\right)\right) \tag{III.2}$$

where E_t^{ss} represents the steady state transmitted field. Equation (III.2) was first derived for absorptive bistability ($\theta = \Delta = 0$) by Bonifacio and Lugiato, [5] and later extended to the dispersive case by Lugiato. [90] The nature of this relation for different values of the control parameters C, Δ, and θ has been discussed extensively in the literature. Here, we only mention that Eq. (III.2) may be S-shaped under suitable conditions, a fact that suggests the possibility of hysteretic behavior. In particular, for the case of absorptive bistability ($\Delta = \theta = 0$), the steady state equation becomes

$$E_i = E_t^{ss}\left(1 + \frac{2C}{1 + |E_t^{ss}|^2}\right) \tag{III.3}$$

If we set $dE_i / dE_t^{ss} = 0$ in Eq. (III.3), we analytically find expressions for the switch up, $E_{i\uparrow}$, and switch down, $E_{i\downarrow}$, amplitudes

$$E_{i\uparrow} = \sqrt{C - 1 - \sqrt{C(C-4)}}\left(1 + \frac{2C}{C - \sqrt{C(C-4)}}\right) \tag{III.4a}$$

$$E_{i\downarrow} = \sqrt{C - 1 + \sqrt{C(C-4)}}\left(1 + \frac{2C}{C + \sqrt{C(C-4)}}\right) \tag{III.4b}$$

and the width of the bistability region, ΔE_i, as

$$\Delta E_i = E_{i\uparrow} - E_{i\downarrow} \tag{III.5}$$

all as a function of the bistability parameter, C. In the limit $C >> 1$,

$$E_{i\uparrow} \cong C \quad \text{and} \quad E_{i\downarrow} \cong \sqrt{8C} \tag{III.6}$$

Comparison of the FSD System to the PW Systems

If we compare the axial field modulus in the FSD system in the plane wave limit (large Fresnel number) to the planar field modulus of the PW models, we find there are similarities and differences between these two systems.

Figure 7 shows the steady state S-curve, Eq. (III.2), for the absorptive plane wave case when the atomic and cavity detunings $\Delta = \theta = 0$ and the bistability parameter $C = 37.5$. As the input field strength, E_i, is increased from 0, the field inside the cavity also increases, lowering the absorption that the field experiences and thus increasing the field intensity still further. The system first occupies the low transmission branch, then abruptly switches to the high transmission branch when $E_i = E_{i\uparrow}$, the switch up amplitude. Increasing the field strength further saturates the medium. If the field strength is subsequently lowered, the field inside the cavity tends to remain large because the absorption of the material system has already been reduced. One finds the switch down threshold occurring for smaller values of the incident field amplitude, namely when $E_i = E_{i\downarrow}$, the switch down amplitude. The system now follows the lower transmission branch. The bistable range, ΔE_i, is defined as the range of the injected signal amplitude during bistable operation. Hysteresis may occur within this bistable range. Due to the inherent time dependence of the diffraction integral, a steady state analysis of the free-space diffraction system is unavailable. However, we compare the results from the dynamics of stable operation of the FSD system to the steady state results of the plane wave system.

To compare these two systems we choose to analyze the switch up, switch down, and bistable range of both systems in resonance and with detuning. Figure 8 shows the behavior of the switch up, $E_{i\uparrow}$, switch down, $E_{i\downarrow}$, and bistable range, ΔE_i, of the resonant PW system as a function of the bistability parameter, C. From this figure we see that bistability occurs if $C > C_{min} = 4$ as predicted by theory. [31] For the range of C chosen, $E_{i\uparrow}$ appears linear while $E_{i\downarrow}$ has a square root dependence on C as predicted in Eq. (III.6).

Figures 9 show the behavior of the on-axis $E_{i\uparrow}$, $E_{i\downarrow}$, and ΔE_i, of the resonant FSD system as a function of C for different values of the absorption

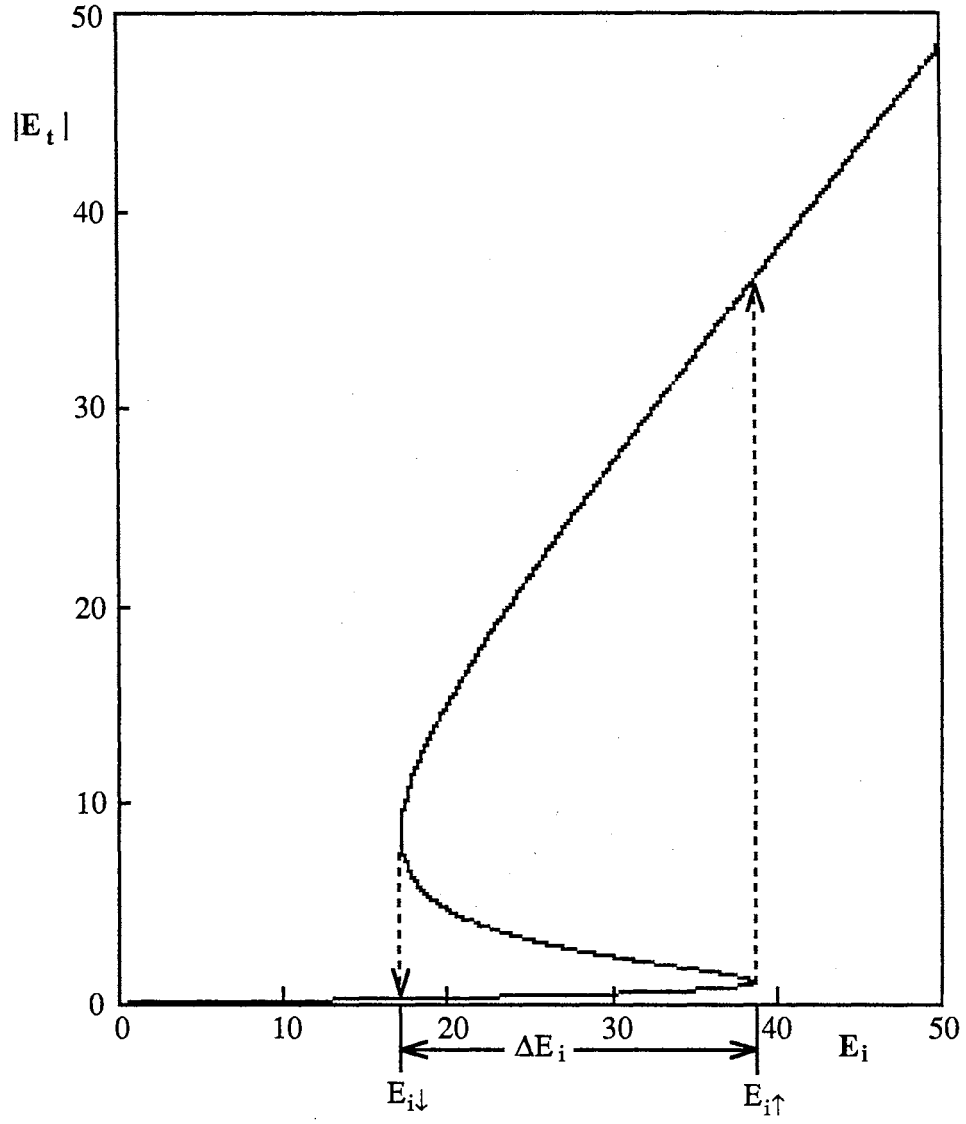

Figure 7. An Example of the Plane Wave Steady State Curve. C = 37.5, $\Delta = \theta = 0$

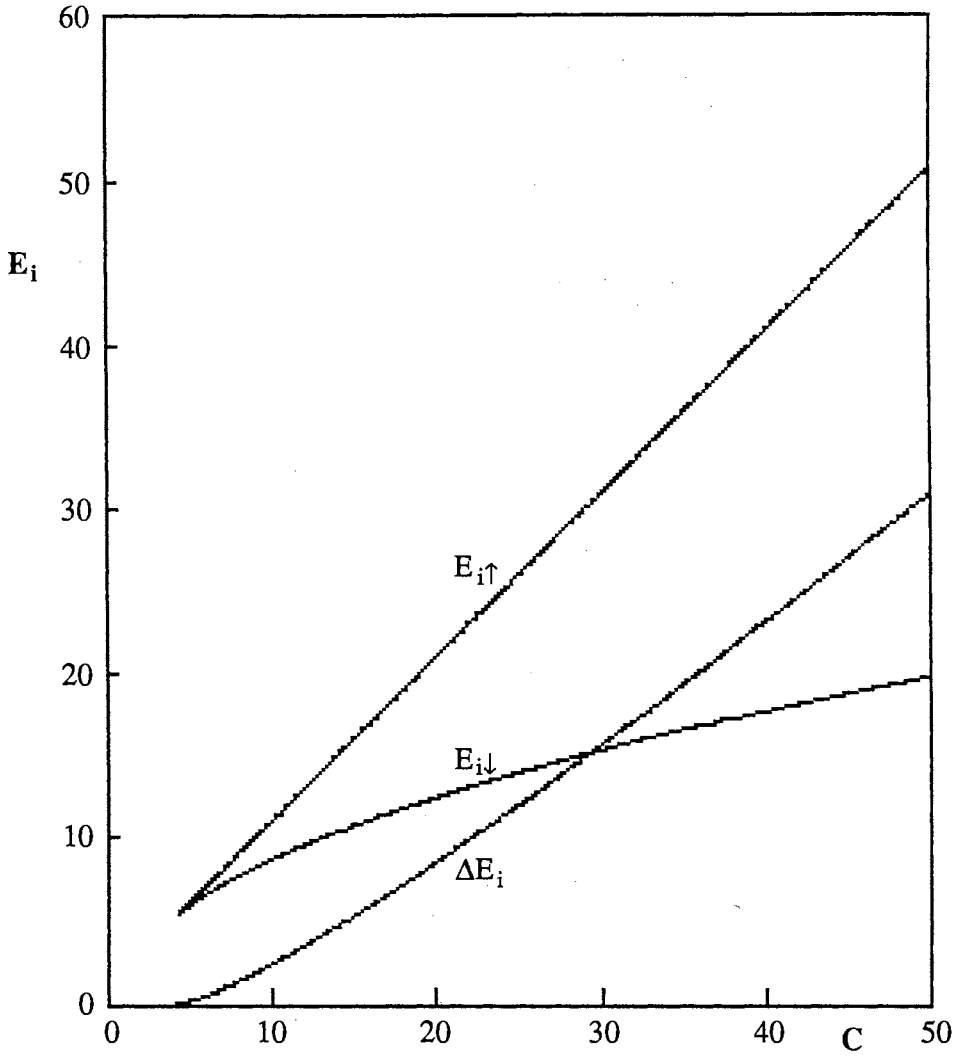

Figure 8. Plane Wave Switch Up and Switch Down Amplitudes and Bistable Range as a Function of the Bistability Parameter. $\Delta = 0$.

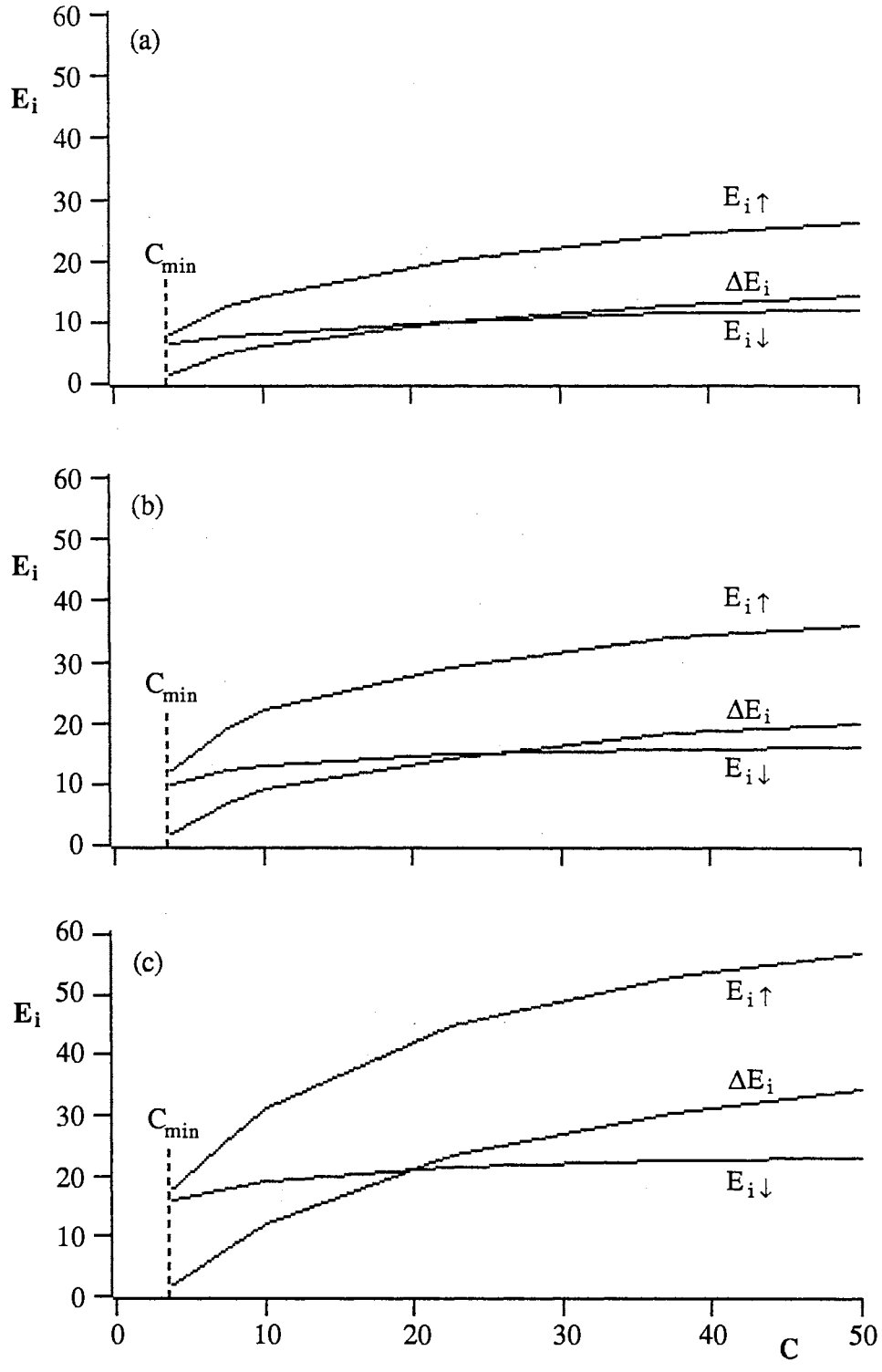

Figure 9. Switch Up and Switch Down Amplitudes and the Bistable Range as a Function of the Bistability Parameter for the FSD System. The parameters are: $\Delta = 0$, and $\kappa = \alpha L/2C\Lambda$. (a) $\alpha L = 0.375$; (b) $\alpha L = 0.75$; (c) $\alpha L = 1.25$. The dotted line marks C_{min} for the plane wave case.

αL ($\kappa = \alpha L/C\Lambda$). It is apparent that the FSD system is dependent on the independent values of the absorption and cavity detuning and not just the ratio of the two as found in the PW case. This may be due to the strong cavity dependence of the free-space diffraction. At the absorption value $\alpha L = 0.375$ in Fig. 9a we see that $E_{i\uparrow}^{FSD} < E_{i\uparrow}^{PW}$ for all values of C where the superscripts indicate FSD or PW systems. But, at the absorption $\alpha L = 1.25$ in Fig. 9c, $E_{i\uparrow}^{FSD} > E_{i\uparrow}^{PW}$. The dotted lines mark where the minimum value of the bistability parameter C_{min} may occur even though $\Delta E_i \neq 0$. At values of C below $C_{min} \sim 4$ it is difficult to determine whether there is bistability in the system due to the deformity of the bistable loop.

As we noted earlier, $E_{i\uparrow}^{PW} \sim C$ for large C, i.e. as the value of the bistability parameter increases the value of the switch up amplitude linearly increases for the plane wave system to switch to the upper branch. In the FSD system, $E_{i\uparrow}^{FSD}$, $E_{i\downarrow}^{FSD}$, and ΔE_i all approach a limiting value. For $\alpha L = 0.375$, $E_{i\uparrow}^{FSD} \rightarrow \sim 30$ while for $\alpha L = 1.25$, $E_{i\uparrow}^{FSD} \rightarrow \sim 60$.

To compare the effects that detuning have on both systems, we plot the switch up, $E_{i\uparrow}$, and switch down, $E_{i\downarrow}$, amplitudes and the bistable range, ΔE_i, as a function of atomic detuning for both systems in Figs. 10. The FSD system parameters, $\alpha L = 0.75$ and $\kappa = 0.02$ gives the bistable parameter value of $C = 37.5$ which is used for the plane wave system. From Fig. 10a we see that the PW system is symmetrical about the $\Delta = 0$ line because the system is unchanged if $\Delta \rightarrow -\Delta$ in the modulus of the steady state equation, Eq. (III.2), if the cavity detuning $\theta = 0$. We also find that the bistable range ΔE_i is a maximum if $\Delta = 0$ and decreases as $\Delta \rightarrow \pm 10$. From this we see that atomic detuning in a plane wave, homogeneously broadened system is a destructive effect.

When free-space diffraction is added, the system no longer has the symmetric behavior in the absence of implicit cavity detuning as shown in Fig. 10b. This asymmetry may be caused by a free-space diffraction induced cavity detuning due to an inherent phase shift in

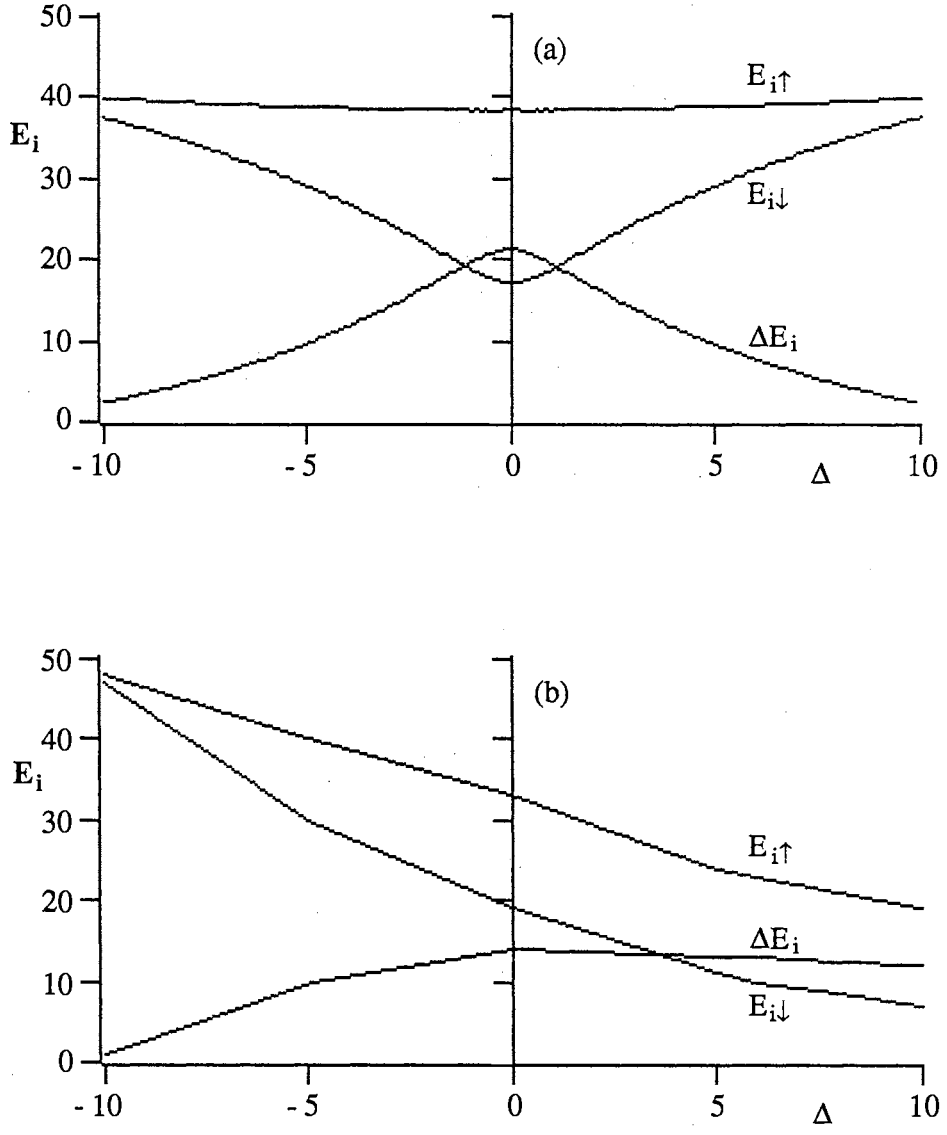

Figure 10. Switch Up and Switch Down Amplitudes and Bistable Range as a Function of Detuning. (a) The PW System with C = 37.5 and $\theta = 0$; (b) The FSD System with $\alpha L = 0.75$ and $\kappa = 0.02$.

the diffracted field. We also find that positive atomic detuning is not destructive in this system since the bistable range remains large for large values of positive detuning, however, larage negative detuning destroys bistability.

For comparison if we detune the cavity frequency away from the injected signal carrier frequency for the PW system, we find a situation similar to the FSD system. Figures 11 show the plane wave system for increasing values of positive cavity detuning ($\omega_c > \omega_o$). The PW system is no longer symmetrical about the $\Delta = 0$ line similar to the FSD system. However for large detunings, bistability is destroyed for large negative atomic detuning. If the cavity detuning is negative ($\omega_c < \omega_o$), the PW system no longer resembles the FSD system. The asymmetry displayed in the PW system caused by cavity detuning leads us to predict that free-space diffraction does indeed induce a positive cavity detuning but not enough to eliminate bistability.

The physical appearance of the bistable loop is compared for the FSD and the PW systems. Figures 12 show a ramp up and a ramp down for both the plane wave and the free-space diffraction systems. Ramps are performed by slowly increasing (decreasing) the injected signal amplitude according to the following relation $E_i = E_i^o + v*\tau_R$ where E_i^o is the initial injected signal amplitude; $E_i^o = 0$ for the ramp up and $E_i^o > E_{i\uparrow}$ for the ramp down. The velocity parameter $v = \pm 10^{-4}$ (the positive sign denotes a ramp up and the negative sign denotes a ramp down) and τ_R is the round trip time. These ramps were created by solving Eqs. (II.21) with (II.55), and (III.1). The system parameters used for this comparison are $C = 37.5$ ($\alpha L = 0.75$), $\Delta = \theta = 0$, $\kappa = 0.02$, and $\gamma = 0.01$. These parameters describe a resonant and good cavity system. There are four clear behavioral departures: (1) The PW system, Fig. 12a, has short switch up and switch down times, i.e. there is no deformation of the bistable loop. The bistable loop for the FSD system, Fig. 12b, is deformed compared to the PW bistable loop, i.e. the switch up/down is much slower than in the PW system. (2) The transmitted field, $|E_t|$, for the PW system is much larger (for these parameters, a factor of 10) than the transmitted field of the FSD system. This is due to the high cavity losses associated with diffraction effects. (3) The bistable

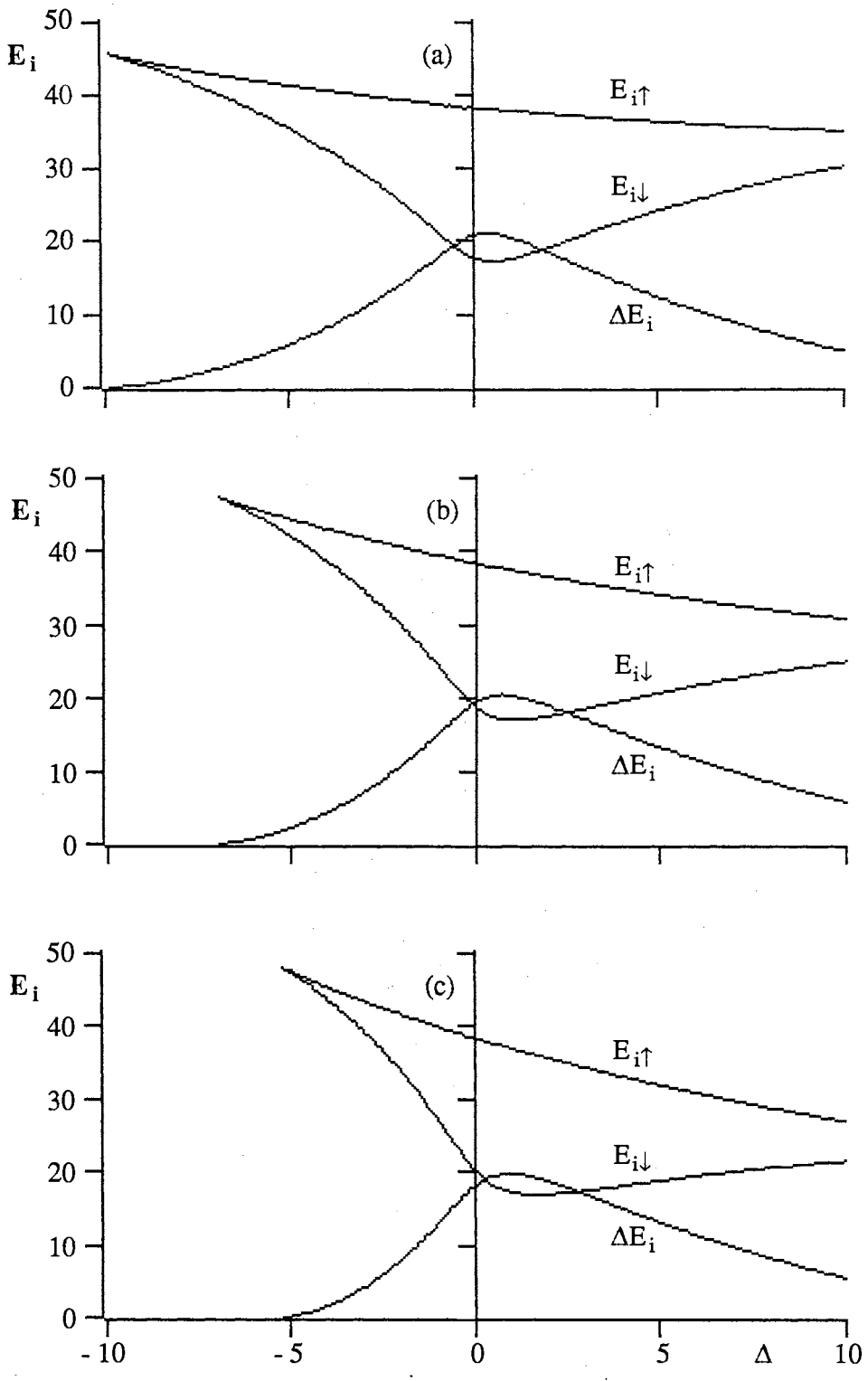

Figure 11. Plane Wave Switch Up and Switch Down Amplitudes and Bistable Range as a Function of Detuning. C = 37.5. (a) θ = 0.5; (b) θ = 1.0; (c) θ = 1.5.

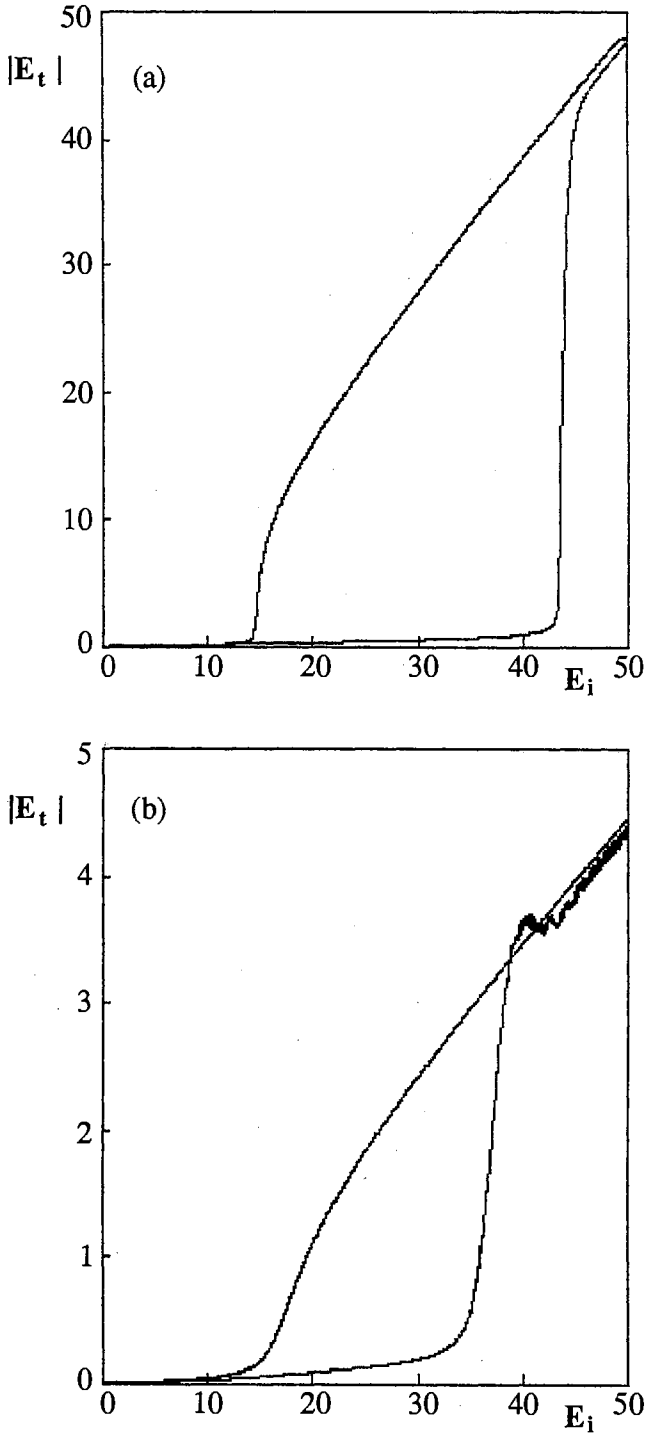

Figure 12. The Transmitted Field as a Function of the Injected Field. (a) PW System with C = 37.5, $\Delta = \theta = 0$; (b) FSD System with $\alpha L = 0.75$, $\kappa = 0.02$, and $\Delta = 0$.

range (width of the bistable loop) of the PW system is larger than the bistable range of the FSD system as previously shown. (4) In the PW model, the hysteresis loop does not change significantly as long as the cavity quality κ is in the good cavity limit or high-Q condition. In the FSD model, we see a strong dependence on κ, i.e. a strong dependence on cavity quality due to the cavity dependence of the diffraction integral.

The stability of the plane wave steady state is studied according to conventional linear stability methods. [95] The main idea of the method is to explore the behavior of the system in the neighborhood of a steady state. If small deviations from steady state should grow exponentially, the system will be said to be unstable. One result of the linear stability analysis for the PW system shows that the segment of negative slope of the steady state curve (see Fig. 7) will always be unstable. Along the negative slope region of the state equation, an increase of E_i yields a decrease in the output intensity. This is an unphysical situation. Another result shows that the lower transmission branch of the state equation is stable while the high transmission branch can undergo undamped periodic oscillations and chaos. [93] Although we do not perform a linear stability analysis on the FSD system due to the inherent time dependence of the diffraction integral, we find dynamically that the FSD model exhibits the unstable behavior of the negative slope branch and a stable lower branch like the PW system, but there is unstable behavior in the upper branch for a wider range of parameter space than the PW system.

Discussion

In this chapter we compared the on-axis intensity of the free-space diffraction system in the regime of large Fresnel numbers to the intensities displayed in the plane wave system and found similarities and differences. (1) The minimum value of the bistability parameter for both system to undergo bistability is approximately the same. (2) The FSD system is strongly affected by the individual values of the absorption loss and the cavity loss while the PW system is dependent only on the ratio of the absorption loss to the cavity loss provided that the cavity quality is good. (3) The switch on/off amplitudes and the bistable range of the PW system in the absence of cavity detuning is symmetrical about the $\Delta = 0$

line, i.e. the system is unchanged if $\Delta \rightarrow - \Delta$. Under the influence of cavity detuning the switch on/off amplitudes and the bistable range are no longer symmetrical which is the effect reported in the FSD system without explicit cavity detuning. (4) The PW bistable loops have a sharp turn on/off while the FSD bistable loops are deformed. (5) The FSD model exhibits the unstable behavior of the negative slope branch and a stable lower branch like the PW system, but there is unstable behavior in the upper branch for a wider range of parameter space than the PW system.

The similarities displayed between these two systems are due to the plane wave like nature of the field through the medium in the FSD system. The differences between these two systems may be attributed to the Gaussian nature of the injected signal, the added complexity of free-space diffraction, and the cavity induced phase shift calculated in the diffraction integral.

CHAPTER IV

TRANSVERSE EFFECTS IN OPTICAL BISTABILITY

Transverse effects are known to play a central role in nonlinear-optical systems. Since experiments are generally performed with lasers with finite transverse dimensions, the transverse nature of the field must be considered. In some such systems pattern formation is dependent sensitively on the particular physical mechanism(s) that may be active. [96] Experimental evidence, for example, indicates that these mechanisms which can create transverse structures are important in optical bistability and focusing/defocusing. [31] Mechanisms that influence transverse field profiles can take the form of diffusive and diffractive coupling within the medium, free-space diffraction, or some combination of these. In particular, transverse coupling is attributed to such phenomena as radial dependence of the switch up times of bistable loops, [31] spatial hysteresis, [66] and the formation of solitary waves in passive systems. [57] For current studies and a good historical review of transverse effects in both active and passive systems see Ref. 97.

Understanding the mechanisms behind transverse coupling of the field is important. The change in the field profile may be due, for example, to the response of the medium in the form of diffusive or diffractive coupling within the medium or to free-space propagation through the optics of the physical setup. New technology in high speed, low cost computers provides opportunities for newer, sophisticated numerical models that can explore these mechanisms. Of these models both high and low finesse cavities are considered. For high finesse cavities, the widely used mean-field limit encourages a Gauss-Laguerre mode-expansion approach. [45] In low finesse cavities where the mean-field limit no longer applies, a Fourier-transform (FT) technique is frequently used to propagate the field through the medium. [54] Most papers which use the FT technique adiabatically eliminate the polarization and population difference to reduce the complexity of

the system thus making a FT technique applicable. This reduced system, where the medium response time is assumed to be much less than the round trip time, is within the so-called Ikeda approximation. [7] Free-space diffraction is incorporated in models by Le Berre, Ressayre, Tallet, and Zondy [44, 98, 99] who study single-pass systems.

We consider the dynamical effects of free-space diffraction in a unidirectional ring cavity containing a thin resonant absorber driven by an external coherent signal. We have minimized focusing effects by incorporating a thin medium whose width is small compared to the cavity length and Raleigh range. We place no restriction on the medium response time relative to the round trip time; i.e. the time-dependent polarization is not adiabatically eliminated from the equations of motion. We isolate free-space diffraction effects and argue that diffraction and diffusive coupling within the medium is negligible. In this model where free-space diffraction is the dominant mechanism for changing the field profile in the system, shifting and deformation of the bistable loop and spatial hysteresis occurs. Radial variation of the bistable loop is found, however, it is not a strong effect. We conclude that radial variation of the bistable loop is largely an effect of diffusion as suggested by Ref. 64. In this chapter, we briefly describe the most popular models that study diffractive or diffusive coupling within the medium and compare effects seen in the FSD system with effects reported in these other transverse effects models.

Other Transverse Effects Models

We compare the system that studies free-space diffraction to transverse effects systems that study diffractive coupling of the field within the medium and diffusive coupling of the excitation. From this point on we refer to these systems as DCM, transverse coupling within the medium and DCE, diffusive coupling of the excitation. This is not to imply that we compare the FSD system to all systems that include transverse effects, just the models that are described in this thesis.

In general, there are two types of transverse coupling mechanisms. (1) Diffractive coupling of the field is important when the input pump beam spot area, $A < \lambda L$ where λ is the optical wavelength and L is the length of the medium. (2) Diffusive coupling is significant when the spot area has a size $A < L_D^2$, where L_D is the diffusion length of the

excitation responsible for the nonlinearity. In this section we briefly define the models associated with diffractive coupling within the medium and diffusive coupling of the excitation.

Diffractive Coupling Within the Medium

The Maxwell-Bloch equations coupled with boundary conditions are used to describe the optically bistable system which includes transverse coupling of the field within the medium. Most of the theoretical literature on the subject of transverse effects in OB concentrates on the diffraction effects within the medium by including the Laplacian term in the field equation. The full set of Maxwell-Bloch equations take the form

$$-\frac{i}{2k_o}\nabla_T^2 E + \frac{\partial E}{\partial z} + \frac{1}{\beta}\frac{\partial E}{\partial \tau} = -\alpha P \tag{IV.1a}$$

$$\frac{\partial P}{\partial \tau} = -(1 + i\Delta) P - ED \tag{IV.1b}$$

$$\frac{\partial D}{\partial \tau} = \frac{\gamma}{2}(E^*P + EP^*) - \gamma(D + 1) \tag{IV.1c}$$

where $\beta \equiv c / \gamma_\perp$ is the speed of light scaled to the polarization decay rate, $\gamma \equiv \gamma_{//} / \gamma_\perp$ is the ratio of the population difference decay rate to the polarization decay rate, $\Delta = (\omega_a - \omega_o) / \gamma_\perp$ is the detuning of the injected signal carrier away from the atomic transition frequency, and α is the absorption per unit length of the atomic medium. To complete this model, appropriate cavity boundary conditions must be imposed.

Much of the work in this area has been done in the limit that the medium response time is much faster than both the cavity round-trip time and changes in the input field amplitude or phase, the so-called Ikeda limit. In this limit we find the steady state polarization and population difference of Eqs. (IV.1b, c)

$$P_{ss} = \frac{(1 - i\Delta) E}{1 + \Delta^2 + |E|^2} \tag{IV.2a}$$

$$D_{ss} = -\frac{1+\Delta^2}{1+\Delta^2+|E|^2} \qquad \text{(IV.2b)}$$

and the equation of motion becomes

$$-\frac{i}{2k_o}\nabla_T^2 E + \frac{\partial E}{\partial Z} = \alpha\frac{1-i\Delta}{1+\Delta^2+|E|^2}E \qquad \text{(IV.3)}$$

where $Z = z$ and $\tau \rightarrow \tau - z/\beta$ are the new retarded variables. Rewriting this equation to include the Fresnel number, F, gives

$$-\frac{i}{4\pi\Lambda F}\nabla_T^2 E + \frac{\partial E}{\partial Z} = \alpha\frac{1-i\Delta}{1+\Delta^2+|E|^2}E \qquad \text{(IV.4)}$$

where the transverse coordinate has been scaled to the pulse width, ω_o.

This quasi-dynamical equation, Eq. (IV.4), represents the governing equation used in most systems that study diffraction effects within the medium.[45, 50, 57] The first term in Eq. (IV.4) describes diffraction effects while the last term is the product of the nonlinear saturable absorption/dispersion with the field. Once again, note that a steady-state Bloch equation has been used to describe absorptive and dispersive effects and that diffraction effects due to free-space propagation are ignored.

Diffusion of the Excitation

In this model, diffusion of the excitation is the primary mechanism for transverse coupling of the nonlinear medium. This is a significant effect in materials like InSb. [64] Theoretical research in this area has been done by, for instance, Firth et al. [67, 100] who showed that diffraction and diffusion give rise to qualitatively similar effects and by Koch et al. [101] who solved the transport equation and discovered a "kink" or a discontinuity in the excitation density in the direction of the beam propagation.

We consider a plane parallel etalon composed of a material (like InSb) characterized by a diffusive Kerr-type nonlinearity, pumped by an input beam of scaled transverse profile $E_i(\rho)$. The round trip nonlinear phase shift Φ can, if diffraction within the medium is negligible, be obtained by solving the partial differential equation [100]

$$\tau_e \frac{\partial \Phi}{\partial t} - L_D^2 \frac{\partial^2 \Phi}{\partial \rho^2} = \frac{I_i(\rho)}{1 + F_{ff} \sin^2(\Phi - \delta)} - \Phi \qquad \text{(IV.5)}$$

where τ_e is the decay time of the excitation (recombination time in InSb), $L_D = (D \tau_e)^{1/2}$ where D is the diffusion coefficient, δ is the cavity detuning, and $I_i(\rho)$ is the scaled input intensity. The medium contribution resides within the finesse factor, F_{ff}, given by

$$F_{ff} = \frac{4R e^{-\alpha L}}{\left(1 - R e^{-\alpha L}\right)^2} \qquad \text{(IV.6)}$$

where R is the reflectivity and α is the absorption coefficient.

Comparisons With Other Transverse Systems

We compare known phenomena displayed in systems that consider diffractive coupling within the medium and systems that consider diffusive coupling of the excitation to the free-space diffraction system. We show that the FSD system is inherently dispersive and behaves similar to systems which display self-lensing. Self-lensing is a consequence of a thick medium, transverse effects, and a nonlinear refractive index which is positive for self-focusing (negative for self-defocusing). As a result of this nonlinear response, the refractive index of the material is larger (smaller) at the center of the laser beam than at its periphery, with the result that the medium is in effect turned into a positive (negative) lens. Due to the thin nature of the medium in the FSD system and the lack of transverse coupling within the medium, we argue that self-focusing/defocusing, in the known definition, is negligible.

There are six different phenomena, bistability threshold, switch on powers, spatial hysteresis, shifting, deformation, and radial variation of the bistable loop that is displayed in the FSD system. We compare these effects to similar effects reported in either the DCM or the DCE systems.

Bistability Threshold and Switch On Power

Independent papers by Ballagh et al. [45] and Drummond [46] that compare diffractive

coupling in an optically thin medium in the absorptive case to the plane wave absorptive case suggest that: 1) The critical threshold for the bistability parameter increases when diffractive coupling is included, and 2) the injected signal for the switch on power is an order of magnitude greater compared to the plane-wave systems. For the limiting condition of large Fresnel numbers (plane-wave approximation), the FSD model in the absorptive limit ($\Delta = 0$) shows that the critical threshold for the bistability parameter remains about the same as the plane wave system and that the switch on power of the injected signal is approximately the same as the plane wave systems (see Figs. 7 and 8) - never an order of magnitude difference as in Refs.45 and 46.

By contrast, Refs. 45 and 46 report that the switch on power in the limit of dispersive bistability does not differ greatly from the plane wave system. As mentioned earlier, this is also seen in the FSD system in the limit of explicit absorptive bistability ($\Delta = 0$). The FSD system has an inherent dispersive property due to the phase shift acquired during free-space propagation.

Shifting and Deformation of the Bistable Loop

In general when transverse effects are considered in a dispersive passive bistable system, shifting and deformation of the bistability loop can occur. We say that the bistable loop has shifted, either for increasing or decreasing switch on amplitudes, compared to either the absorptive case ($\Delta = 0$) or the large Fresnel number case ($F >> 1$). We define deformation to mean a slow switch on or switch off. Shifting of the bistable loop is known to occur, for instance, in the study by Marburger and Felber [102] who show that self-focusing due to an effective refractive index change (positive detuning) reduces substantially the powers for bistable operation relative to the plane mirror geometry. In other words, they found that the effect of self-focusing shifts the bistable loop towards decreasing injected signal strengths.

In the limit of absorptive bistability, DCM systems report sharp switch on/off while deformation of the bistable loop is reported in the limit of dispersive bistability. [31] In particular, Moloney and Gibbs [57] show that for a dispersive system in the large Fresnel

number regime where diffractive coupling within the medium is dominant, deformation of the bistable loop is due to the rate at which the radial annular rings turn-on/off. The discontinuity between the "on" inner spot (residing on the upper branch) and the "off" outer spot (residing on the lower branch) results in a very slow expansion of the "on" spot, thus causing a deformed bistable loop. For small Fresnel numbers, there is less deformation allowing for whole-beam switching.

We consider the limiting conditions of large and small Fresnel numbers, $F >> 1$ and $F < 1$ to study the shifting and deformation of the bistable loop in the FSD system.

Large Fresnel Numbers For large Fresnel numbers where the ratio of the aperture radius to the injected signal radius is large, the FSD system displays a shift in the bistable loop similar to systems that include diffraction within the medium under the influence of self-focusing and self-defocusing. For a positive detuning, $\Delta > 0$, we see in the FSD model a shift in the first turning point of the bistable loop towards decreasing injected signal and a corresponding increase in axial intensity; conversely for negative detuning, $\Delta < 0$, there is a shift in the first turning point towards increasing injected signal and a corresponding decrease in axial intensity. This effect is shown in Figs. 13 - 15 which are a plot of the axial intensity as a function of the injected signal for three values of the atomic detuning parameter, $\Delta = 5, 0, -5$. Figures 13 have parameters of $\alpha L = 0.375$ and $\kappa = 0.01$. Figures 14 have $\alpha L = 0.75$ and $\kappa = 0.02$, and Figs. 15 have $\alpha L = 1.25$ and $\kappa = 0.033$. We choose these parameters to compare since the absorption to cavity loss ratio is constant, i.e. $C \propto \alpha L/\kappa = 37.5$ for each figure.

The low absorption system displayed in Figs. 13 is extremely affected by free-space diffraction effects since the bistable loop for $\Delta = \pm 5$ is greatly deformed. We find that the bistable loop for $\Delta = 5$ (Fig. 13a) is shifted towards decreasing injected signal and for $\Delta = -5$ (Fig. 13c) it is shifted towards increasing injected signal. However, as we increase both the absorption and cavity losses (see Figs. 14 and 15), the bistable loops are better developed, i.e. the increased absorption within the medium overcomes the effects due to

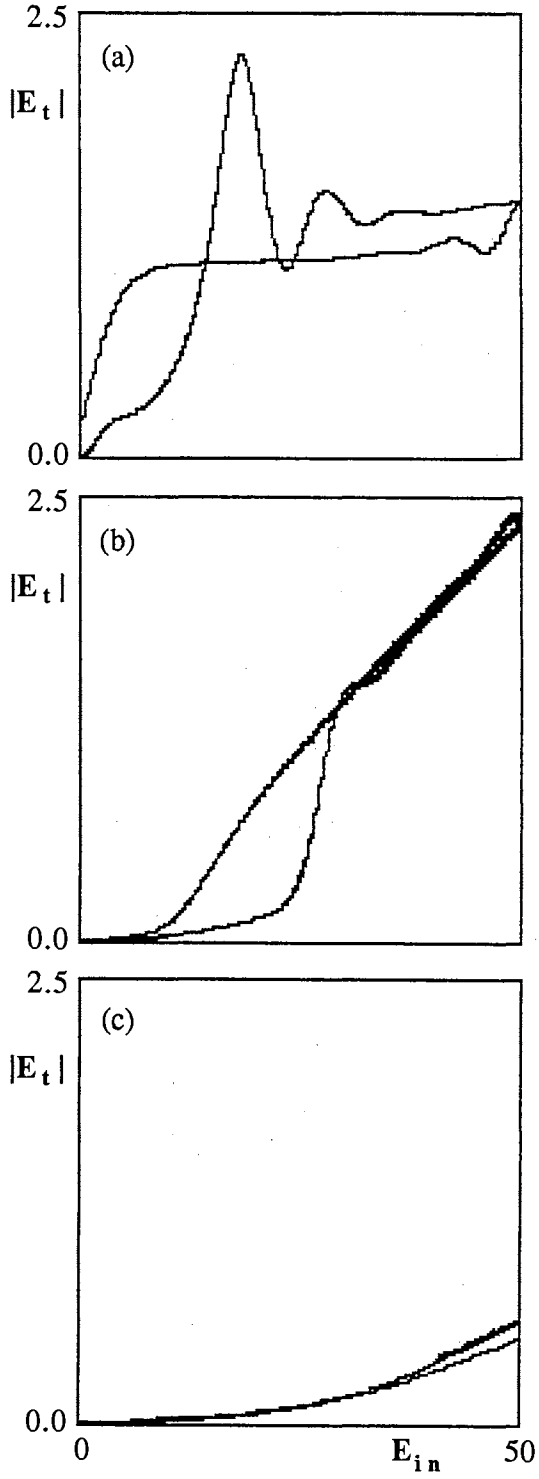

Figure 13. Shifting and Deformation Effects in the FSD System for Small Absorptions. $\alpha L = 0.375$, $\kappa = 0.01$ and $F >> 1$. (a) $\Delta = +5$; (b) $\Delta = 0$; (c) $\Delta = -5$.

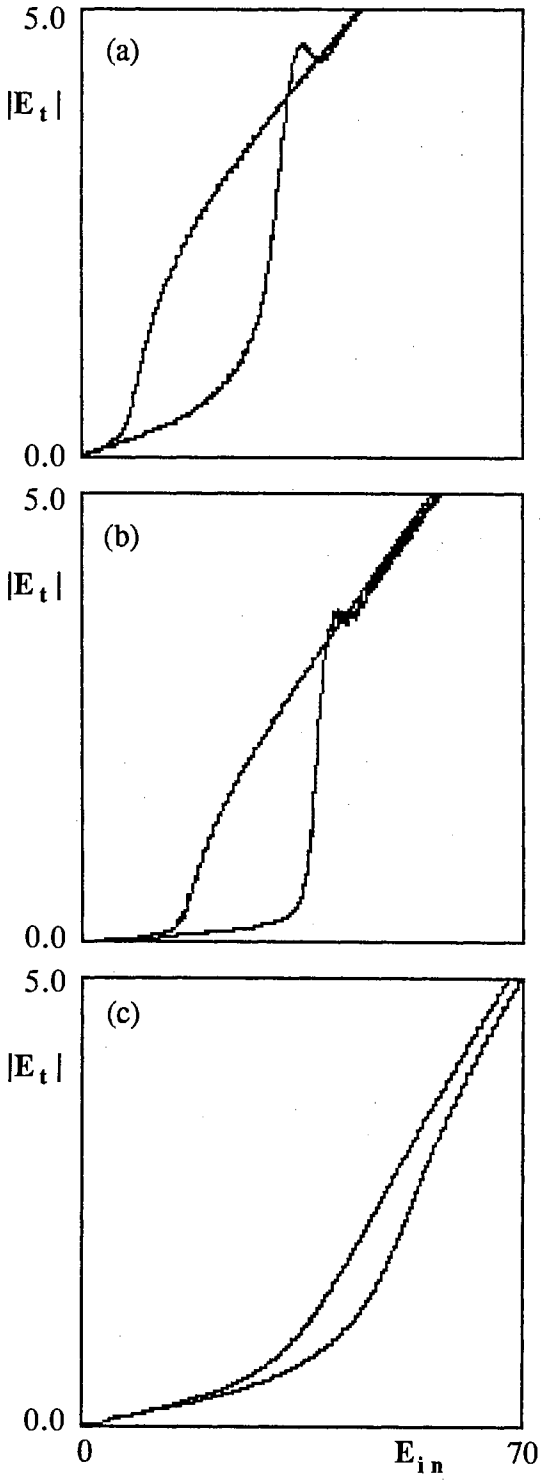

Figure 14. Shifting and Deformation Effects in the FSD System for Medium Absorptions. $\alpha L = 0.75$, $\kappa = 0.02$, and $F >> 1$. (a) $\Delta = +5$; (b) $\Delta = 0$; and (c) $\Delta = -5$

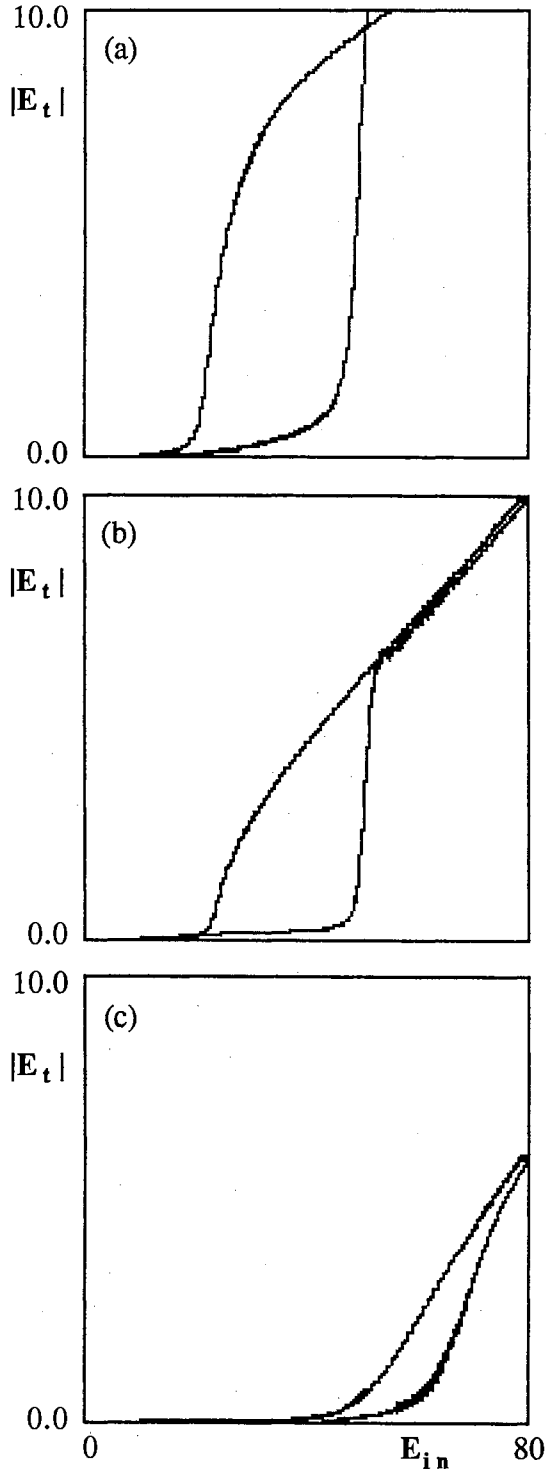

Figure 15. Shifting and Deformation Effects for Large Absorption in the FSD System. $\alpha L = 1.25$, $\kappa = 0.033$, and $F >> 1$. (a) $\Delta = 5$; (b) $\Delta = 0$; (c) $\Delta = -5$.

free-space diffraction. For negative detuning, there is a shift towards increasing injected signal and a decrease in axial intensity, and a shift towards decreasing injected signal and an increase in axial intensity is displayed for positive detuning. This is similar to DCM systems under the influence of self-focusing. [102]

Also shown in Figs. 13 - 15, the FSD system displays a strong deformation of the bistable loop as a function of the detuning. For positive detuning the deformation is minimal while negative detuning washes out the hysteresis. Positive detuning, associated with focusing effects, appears to be less destructive than negative detuning which is associated with defocusing effects. Here, free-space diffraction couples with atomic detuning causing an effect similar to self-focusing and self-defocusing.

In the good cavity condition where the cavity losses are small, $\kappa = 0.02$, we find that the FSD system behaves in an intuitive and physical way. Figures 16 shows for resonance, the bistable loops for three different absorptions. For small absorption (Fig. 16a), the system switches and saturates quickly. As the absorption increases, it takes a larger amplitude of the injected signal to switch the system. As the input field strength is slowly increased, the field inside the cavity also increases, lowering the absorption that the field experiences and thus increasing the field intensity still further. The system first occupies the low transmission branch then abruptly switches to the high transmission branch at the switch up amplitude. Increasing the field strength further saturates the medium. If the system has a small absorption coefficient then the switch up field amplitude will be smaller than the system with a larger absorption coefficient.

At a bad cavity condition where the cavity loss is an order of magnitude greater, $\kappa = 0.2$, a curious behavior is seen that is not reported in other transverse effects systems, to the knowledge of the author. Figure 17 shows the resonant FSD system for two different values of the cavity loss, κ. Here we find that an increased cavity loss causes the bistable loop to shift towards decreasing injected field strengths, noticeably deforms the loop, and increases the output intensity over the entire range of the injected signal parameter compared to the system with lower cavity loss $\kappa = 0.02$. Initially, this is counter-intuitive, but it may be explained as follows. If we effectively eliminate the medium, setting $\alpha L = 0$,

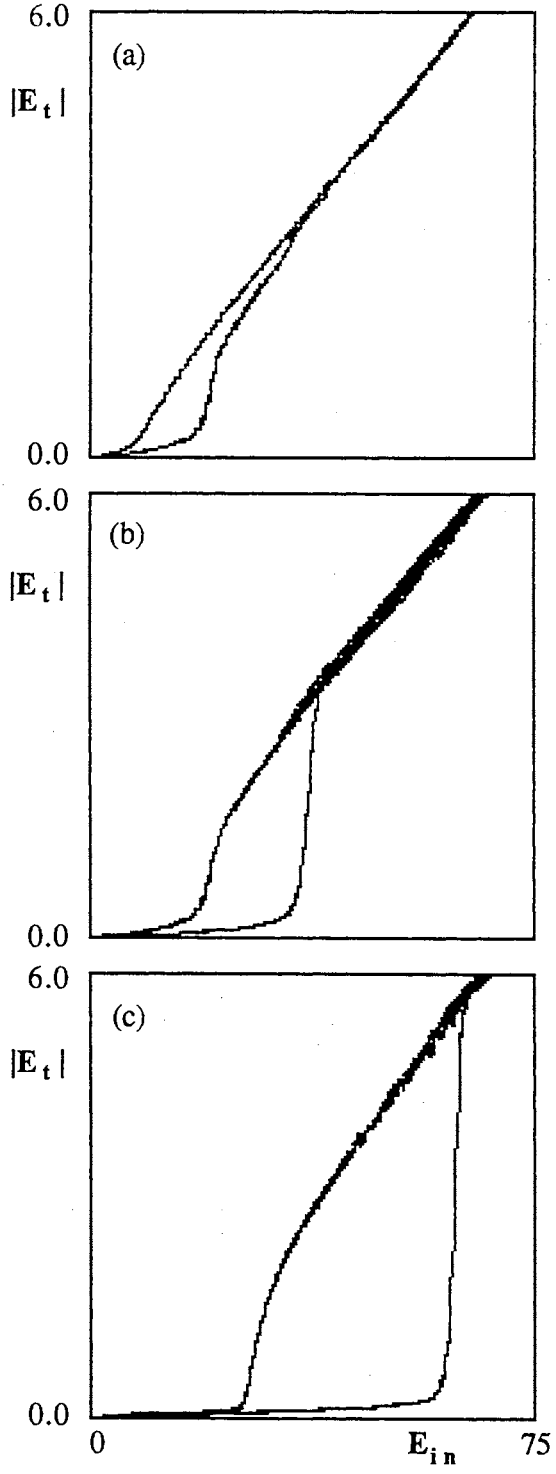

Figure 16. The Effect of Absorption and Large Fresnel Number of the FSD System. $\kappa = 0.02$, $\Delta = 0$, and $F >> 1$.

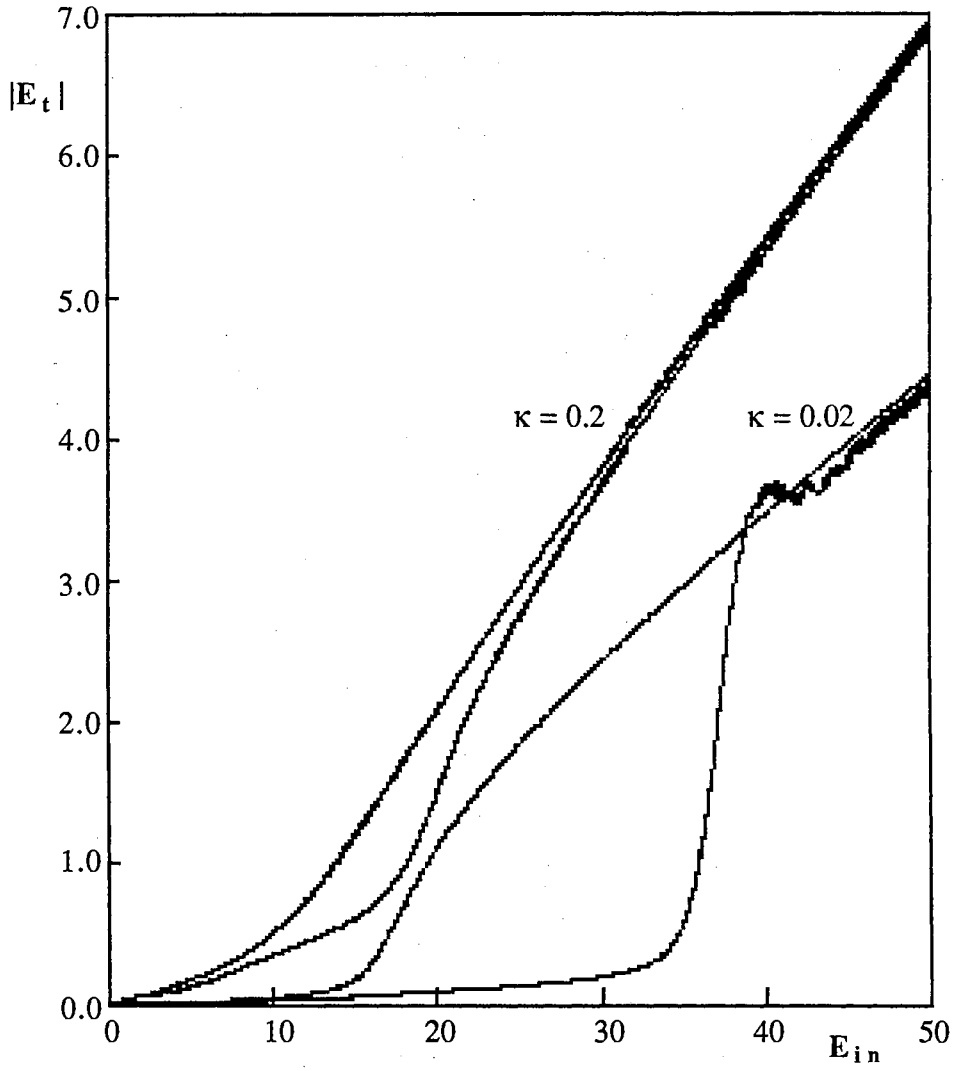

Figure 17. Dynamical Ramps Showing the Dependence of the FSD System on Cavity Quality. $\alpha L = 0.75$, $\Delta = 0$, and $F >> 1$.

and calculate the transmission from the cavity, we find that a cavity loss of $\kappa = 0.2$ is larger than the rate at which the intracavity field is lost through diffraction. This results in a larger output field compared to the cavity with low loss. In other words, in a good cavity (low mirror loss) the field remains in the cavity longer allowing free-space diffraction to leak the field out at a faster rate. As the injected field strength, E_{in}, is increased from 0 the field builds up quicker in the higher κ-cavity compared to the lower κ-cavity which results in a lower effective absorption of the medium. The medium quickly saturates and thus the bistable loop is shifted to the left.

Small Fresnel Numbers For decreasing Fresnel numbers where the ratio of the aperture radius to the injected signal radius is small, less deformation of the bistable loop exists in the FSD system. Figure 18 shows the behavior of the axial output field modulus as a function of the injected signal for three representative Fresnel numbers. We observe as $F \rightarrow 0$, three characteristics: 1) The bistability is not destroyed by strong diffractive coupling in free space - a result also noted by Moloney et al., [54] Scalora and Haus, [103] and Reinisch and Vitrant [104] whose systems include diffractive coupling within the medium. 2) There is a shift in the bistable loop towards decreasing injected signal strength. 3) There is a measurable increase in the axial output intensity. These last two results are merely an artifact of the type of cavity chosen and should not be considered physical. They can be explained by considering the following argument. As we decrease the Fresnel number, the low intensity wings of the injected signal are eliminated leaving only the high intensity central ring. The feedback field, which has broadened considerably due to diffraction, recombines with the injected signal to create a high intensity central ring with low intensity outer rings, similar to a field profile created by self-focusing. This type of field profile coupled with the nonlinear phase shift during free-space propagation induces the medium to response like a weak lens which, for very short distances, gives a larger axial field. Since the output coupler is a short distance from the input coupler, very little of the high intensity central ring has diffracted giving a false impression of a larger axial intensity compared to the large Fresnel number system. This increased intensity shifts the loop to the left. If the output coupler had been placed much further away from the medium

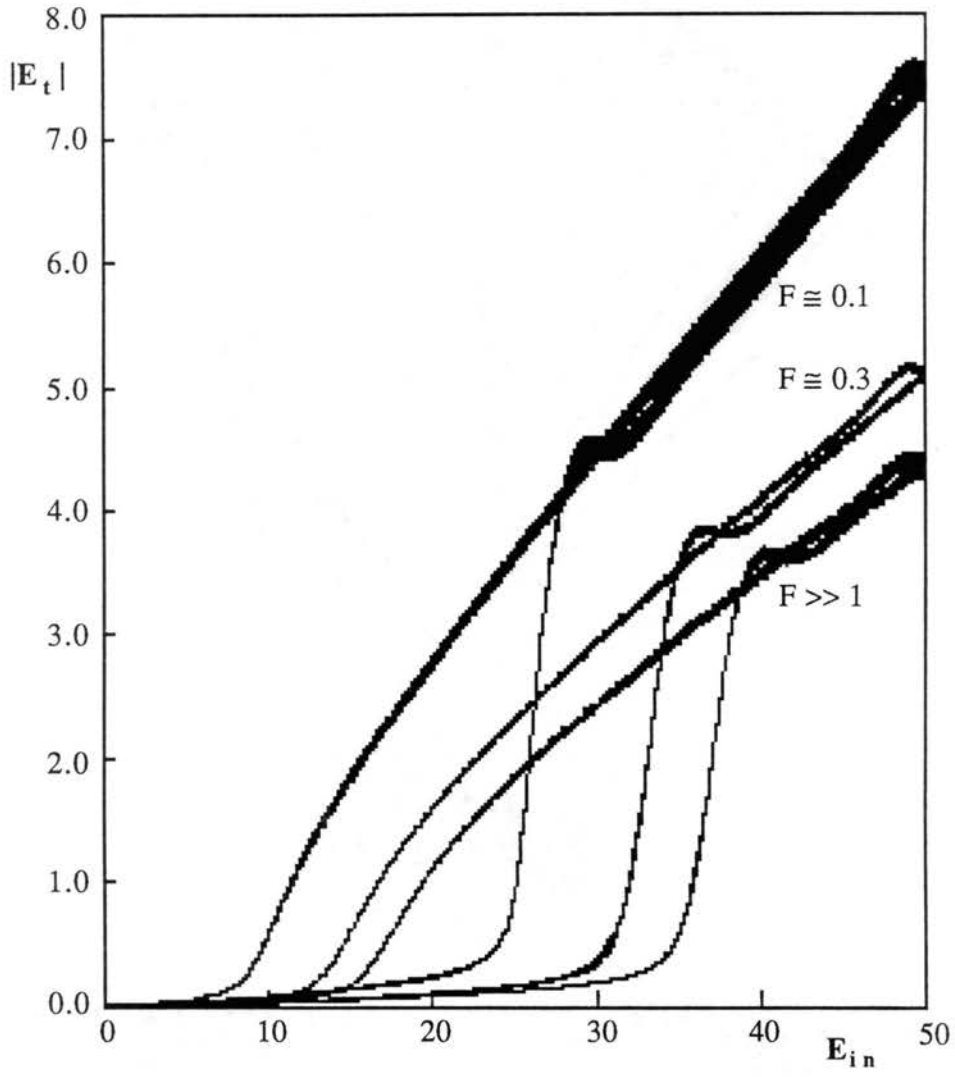

Figure 18. Dynamical Ramps Showing the System Dependence on the Fresnel Number. $\alpha L = 0.75$, $\kappa = 0.02$, and $\Delta = 0$.

allowing the free-space diffraction to broaden the profile, the expected result (a decrease in axial intensity and a shift to the right) would be given.

In Figs. 19 for a low Fresnel number, F ~ 0.1, with three different values of the atomic detuning, it can be seen that the system follows similarly to the behavior of the system with large Fresnel numbers except that the overall axial intensities are larger.

In Fig. 20, we compare the switch on amplitude for the large and small Fresnel cases for three values of the absorption and cavity loss (the ratio of absorption to cavity loss is constant, C = 37.5 in each case) as a function of detuning. There are four behavioral characteristics. (1) In general, the switch on power is smaller for the small Fresnel number system compared to the large Fresnel number system as mentioned earlier for the entire range of atomic detunings. However, at certain detunings (for $\alpha L = 0.375$, $\Delta = 5$ and for $\alpha L = 0.75$, $\Delta = 10$) the switch on amplitudes for both cases are the same. (2) For both the large and small Fresnel number systems for atomic detunings $|\Delta| > 5$ and $\alpha L = 0.375$, bistability no longer exists. (3) For $\Delta > 10$ in Fig. 20b, both the large and small Fresnel number systems have the same switch on amplitude. (4) We also see that as the detuning is increased, the injected signal switch on amplitude limits at particular values of $E_{i\uparrow}$, i.e. in Fig. 20a $E_{i\uparrow} \rightarrow \cong 10$ and in Fig. 20b $E_{i\uparrow} \rightarrow \cong 20$. For larger detunings, the bistable loop remains stationary, i.e. the loop will not continue to shift.

Spatial Hysteresis and Radial Variation of the Bistable Loop

Important transverse effects in optical bistability include the spatial hysteresis of the ouput-beam profile and radial variations of the bistable loop. Several papers study this phenomena which was first predicted by Rozanov and Semenov [66] and later considered theoretically by groups like Firth and Wright. [50] The subject is given experimental foundation by Grigor'yants and Dyuzhikhov [64] who study an InSb Fabry-Perot system. Diffusion within the medium is the assumed, dominant mechanism of transverse coupling in their system. Studies by Khoo et al. [105] report bistability in the transverse profile in the transmission through a nonlinear thin film.

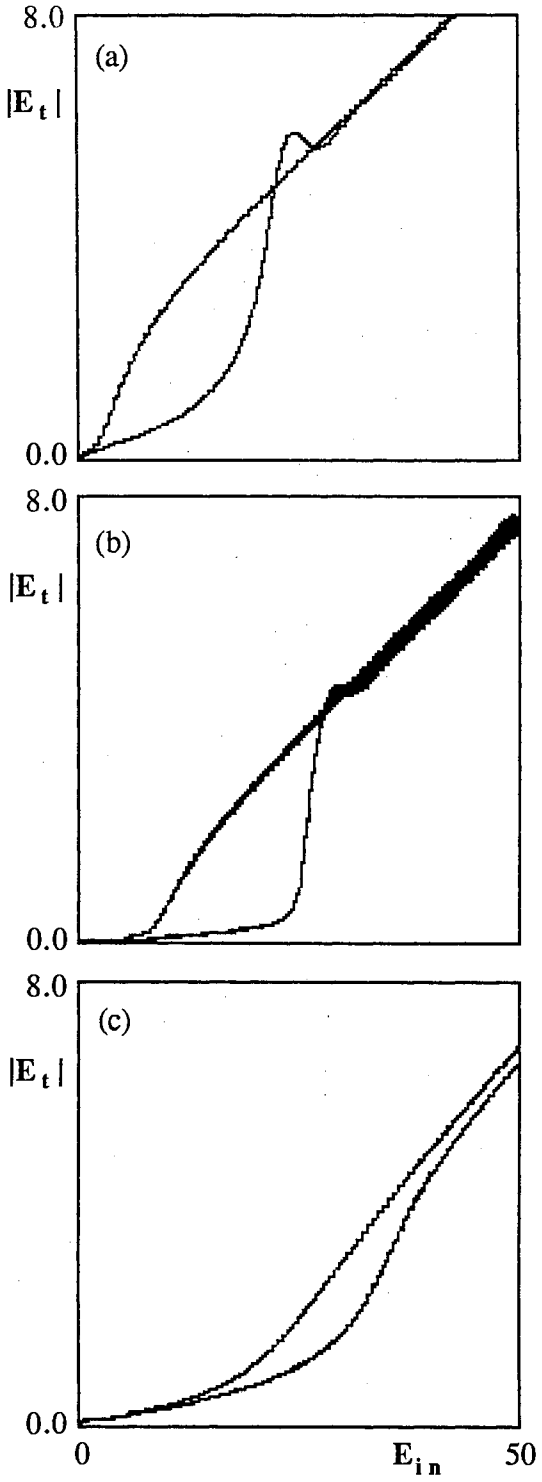

Figure 19. Dynamical Ramps Showing the Effect of Atomic Detuning and Small Fresnel Number. αL = 0.75, κ = 0.02, and F ≅ 0.1. (a) $\Delta = 5$; (b) $\Delta = 0$; and (c) $\Delta = -5$.

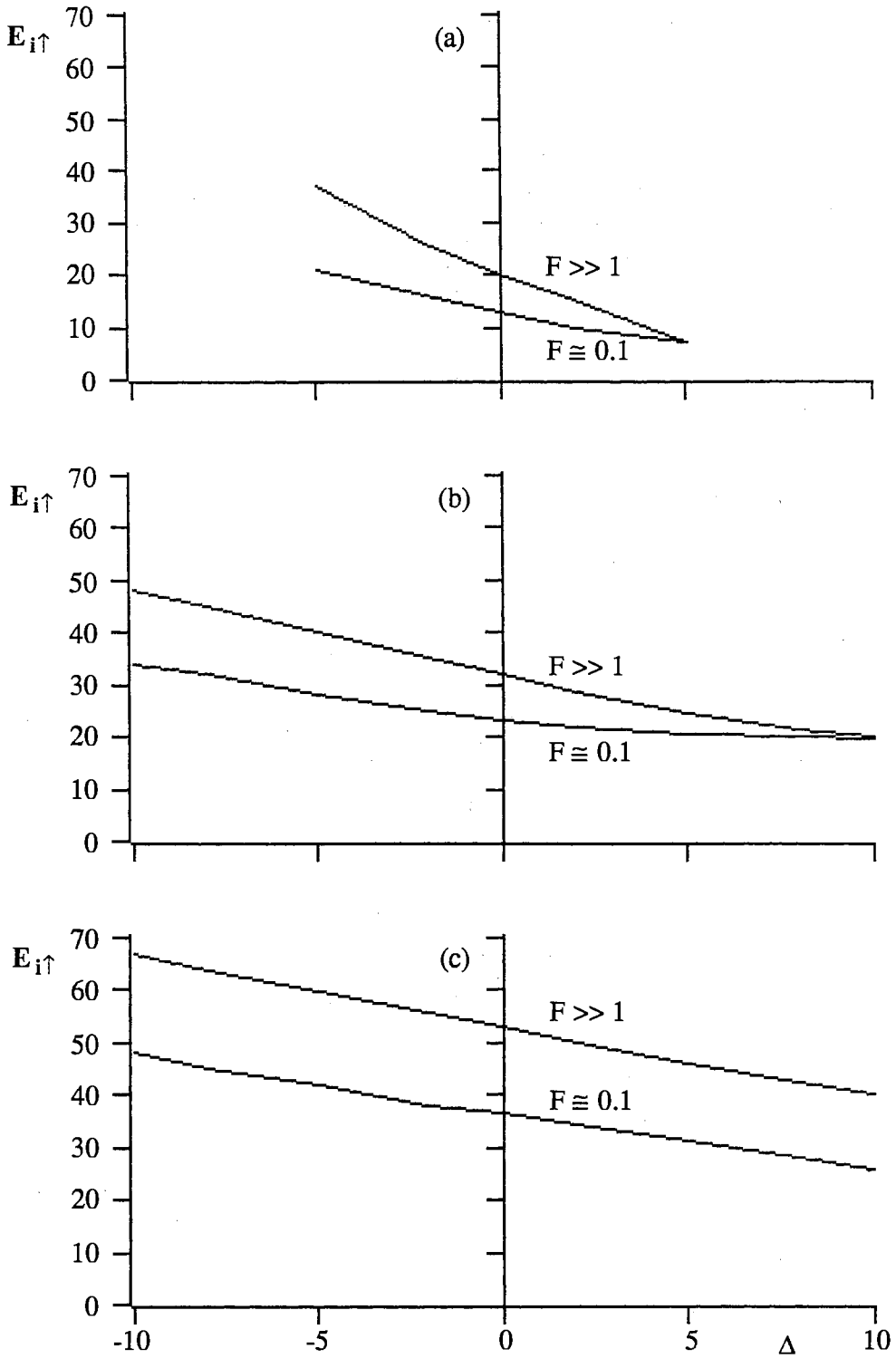

Figure 20. The Switch Up Amplitude as a Function of Atomic Detuning for the Two Cases, $F >> 1$ and $F \cong 0.1$. (a) $\alpha L = 0.375$, $\kappa = 0.01$; (b) $\alpha L = 0.75$, $\kappa = 0.02$; (c) $\alpha L = 1.25$, $\kappa = 0.033$.

Spatial hysteresis, associated with dispersive optical bistability and self-lensing due to an intensity dependent index of refraction, arises from the nonuniform switching that gives rise to a switching wave which moves from the area of maximum input intensity toward the beam periphery. When the intensity of a particular radial ring is larger than the switching intensity, that radial ring switches to the upper branch leaving the lower intensity rings on the lower branch. Different radial rings appearing on different branches causes changes in the overall radial profile. The sharpness of the switch is determined by the extent of diffraction or diffusion of the nonlinearity. Such a switching pattern should result in a dramatic change in the bistable loop at different transverse coordinates, as was theoretically predicted by Firth and Galbraith. [67] They show that radial variation of the bistable loop results from a system which considers diffusive coupling. They do not explicitly single out diffusive coupling as the only mechanism leading to this effect.

In the free-space diffraction model, spatial hysteresis of the output beam profile is seen. Figure 21 shows characteristic radial profiles in resonance taken as we adiabatically scan the injected signal strength. Each radial profile is scaled to its maximum to easily compare the transverse structures. The bistable region is marked by the arrows. The parameters used for this figure are an absorption of $\alpha L = 0.75$, a low loss cavity, $\kappa = 0.02$, atomic resonance $\Delta = 0$, and a large Fresnel number $F >> 1$. (See Fig. 14 for the corresponding bistability curve.) We find that the radial profiles of the output field in the lower branch outside of the bistable range remain the same regardless of the initial conditions (profile at $E_{in} = 5$) and similarly with the upper branch outside the bistable range ($E_{in} = 40 - 50$). Within the bistable loop, however, different transverse structures are displayed ($10 < E_{in} < 35$). The radial profile of the lower branch within the bistable range remains similar to the profile at a smaller amplitude of the injected signal. As the injected signal is increased, the profile slowly reshapes itself to appear similar to the profile in the upper branch outside the bistable range. Likewise, as the signal is decreased, the profile slowly reshapes itself to appear like the profile in the lower branch. This gradual change in transverse profile is due to the deformation, slow turn on/off, of the bistable loop.

Atomic detuning is a negative effect in the study of spatial hysteresis. As we increase the detuning, the deformation of the bistable loop increases and we correspondingly lose

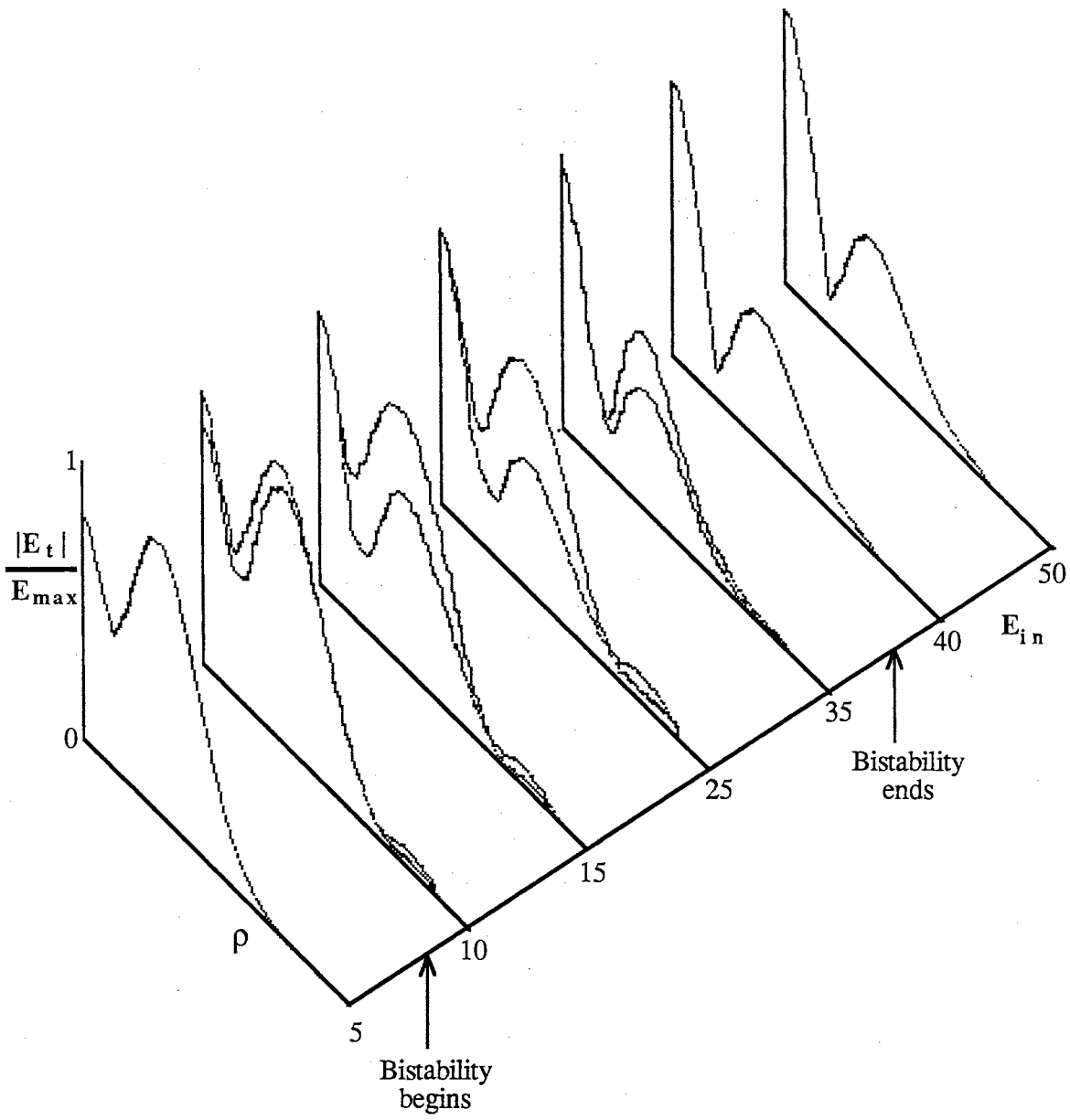

Figure 21. Radial Profiles Display Spatial Hysteresis in the Resonant and Large Fresnel Number Case in the FSD System. Parameters are $\alpha L = 0.75$, $\kappa = 0.02$, $\Delta = 0$, and $F >> 1$. The arrows mark the regions where bistability of the system occurs.

the spatial hysteresis effect. Figure 22 shows how the spatial hysteresis is diminished for an atomic detuning $\Delta = 5$.

Likewise, a small Fresnel number is also a destructive effect when studying spatial hysteresis. Figures 23 and 24 show for small Fresnel number, radial profiles taken as the injected signal is slowly scanned. As we decrease the Fresnel number, we find that spatial hysteresis is less defined, although it still remains measurable.

Spatial hysteresis in the absence of power hysteresis is not seen in the FSD system. This is in contrast to the study by Firth and Wright [50] who consider transverse coupling effects in a plane parallel Fabry-Perot containing a medium exhibiting nonlinear refraction who show that even in systems which do not display power hysteresis, spatial hysteresis can still occur. This was not observed in the FSD system; that is, spatial hysteresis is seen only in the presence of power hysteresis. The absence of a well defined bistable loop eliminates spatial hysteresis in the free-space diffraction model.

Dramatic changes in the bistable loop at different transverse coordinates known as radial variation of the bistable loop is not a strong effect in the FSD system due to the strong deformations of the loop. Figure 25 shows radial variation of the bistable loop in the FSD system. Each bistable loop is scaled to the maximum output field value in order to easily compare the loop structures. Figure 25a is a typical radial profile for this system where we have selected points ρ_1 - ρ_5 along the transverse profile to display bistable loops. Figures 25b - f are the bistable loops taken at radial positions ρ_1 - ρ_5, respectively; only Figs. 25c and f show the only remarkable difference in the bistable loop. In Fig. 25c there exists a double bistable loop and increased instability in the upper branch while Fig. 25f shows an increased instability in the upper branch. The radial variation of the bistability loop of the FSD system pales in comparison to the effect displayed in diffusive systems. The results of the FSD system are unremarkable and support diffusive coupling as a dominant mechanism in the radial variation of the bistable loop.

Discussion

In this chapter we compared the free-space diffraction system to systems which

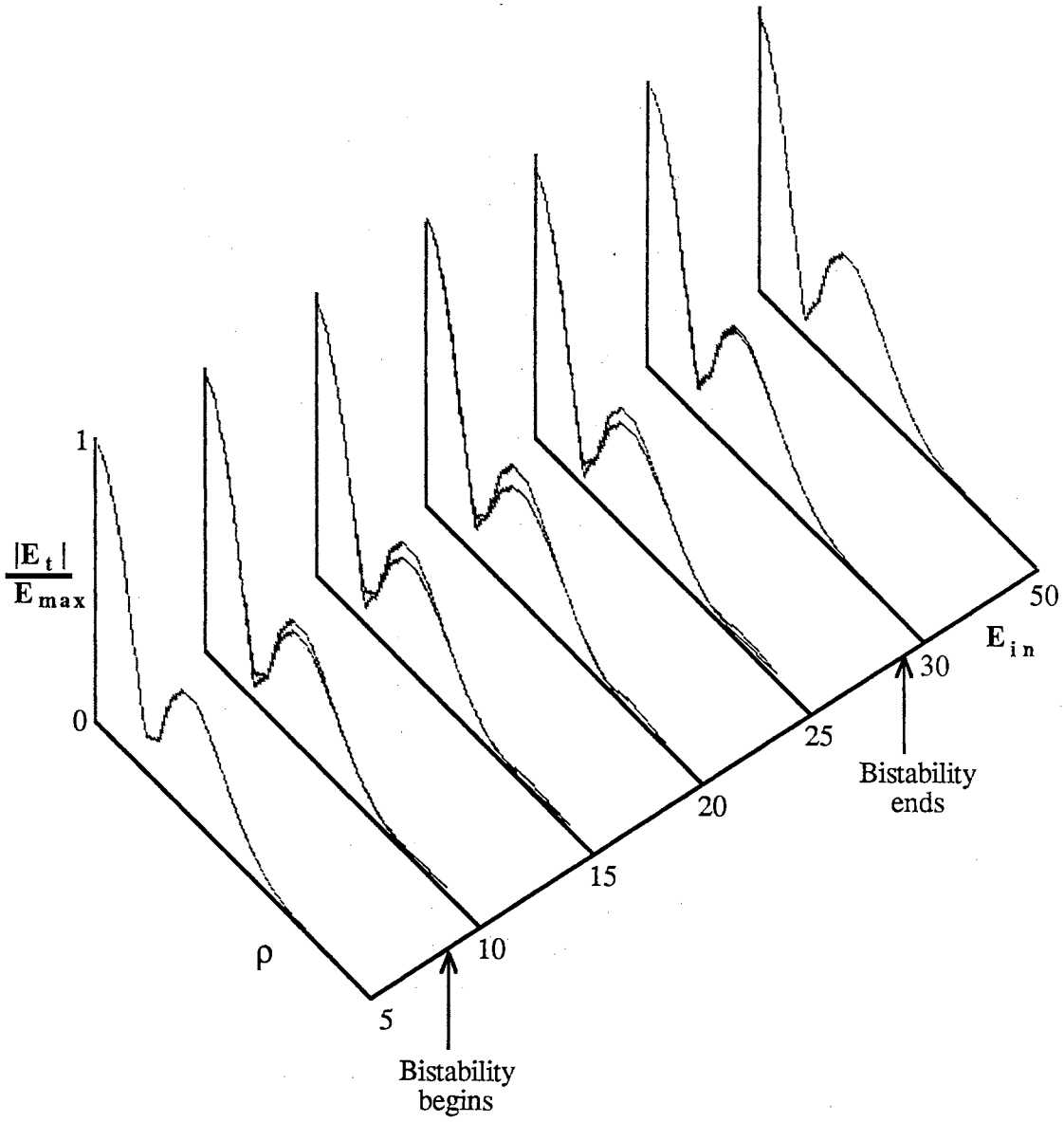

Figure 22. Spatial hysteresis is Washed Out with Positive or Negative Detuning. The parameters are $\alpha L = 0.75$, $\kappa = 0.02$, $\Delta = 5$, and $F >> 1$.

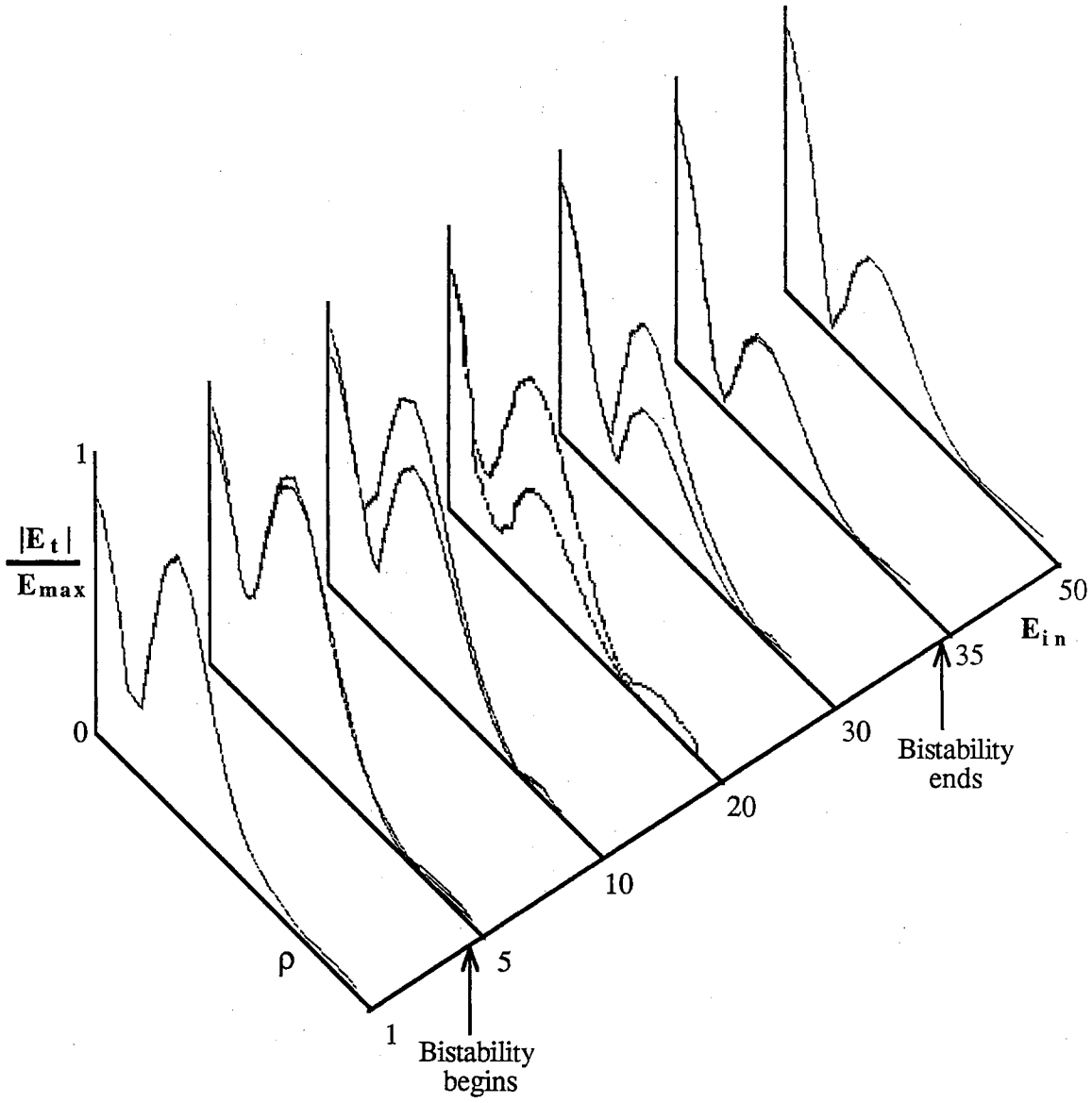

Figure 23. Radial Profiles Display Spatial Hysteresis in the Resonant and Smaller Fresnel Number Cases. $\alpha L = 0.75$, $\kappa = 0.02$, $\Delta = 0$, and $F \cong 0.3$.

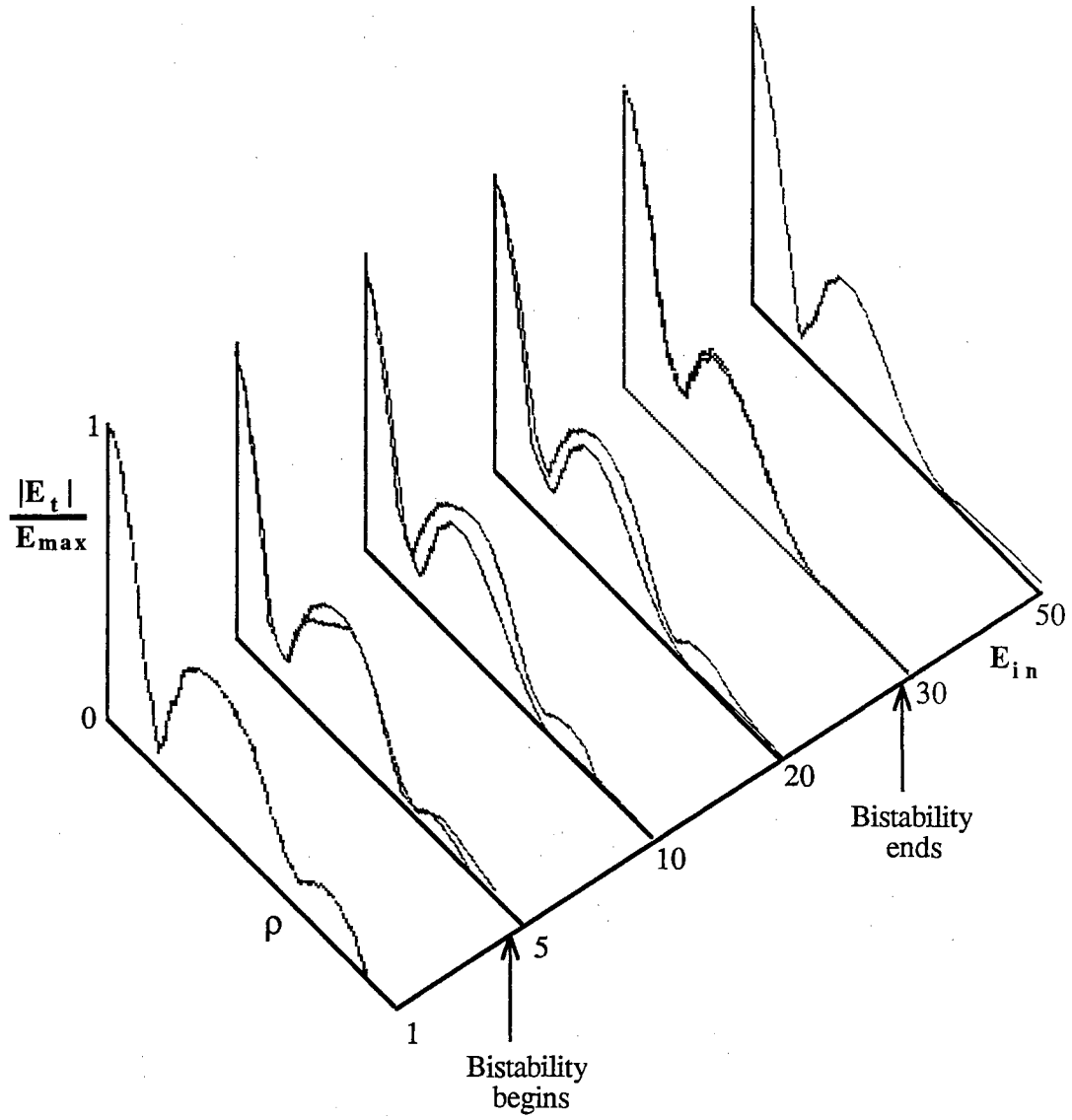

Figure 24. Spatial hysteresis is Less Defined at Small Fresnel Numbers. The parameters are: $\alpha L = 0.75$, $\kappa = 0.02$, $\Delta = 0$ and $F \cong 0.1$.

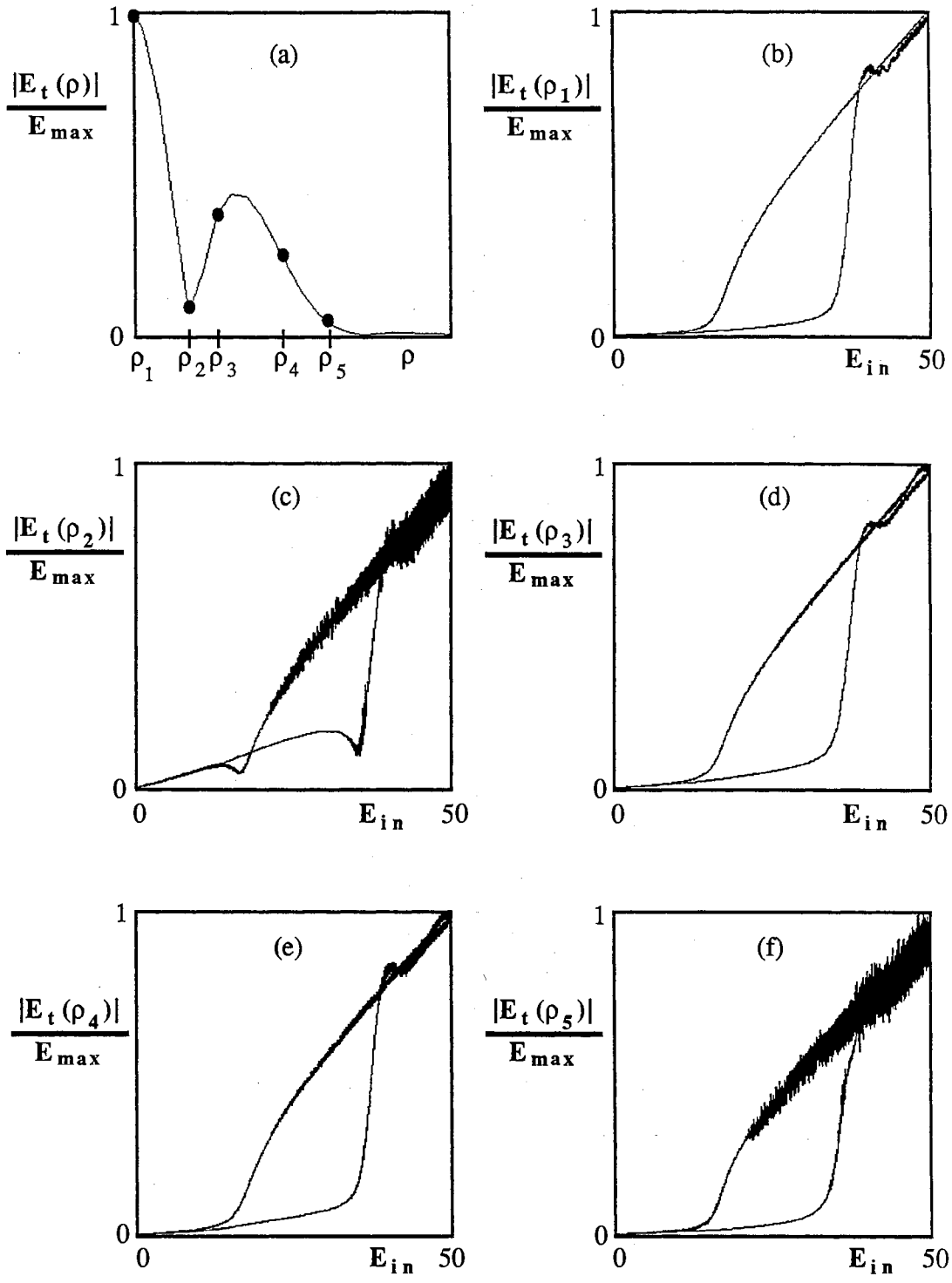

Figure 25. Radial Variation of the Bistable Loop is Demonstrated for the FSD System. (a) A typical radial profile of the FSD System showing the radial coordinates used for the study; (b - f) bistable loops taken at the radial coordinates ρ_1 - ρ_5, respectively.

consider diffractive or diffusive coupling within the medium as the dominant transverse coupling mechanism. We argue that the thin nature of the medium used in the FSD system eliminates/diminishes diffractive or diffusive coupling within the medium which eliminates nonlinear dispersion effects like self-lensing in the usual definition. The only transverse coupling mechanism is free-space diffraction. We find several comparisons between these systems. (1) Models that describe diffractive coupling within the medium in the dispersion limit report switch on powers similar to the PW system. This effect is seen in the FSD system without explicit dispersion dependence. (2) The FSD system resembles transverse effect systems under the influence of self-focusing. We report shifting of the bistable loop as a function of the atomic detuning and Fresnel number. Deformation of the bistable loop is minimal under positive detuning (associated with self-focusing) while negative detuning (associated with self-defocusing) washes out the hysteresis. The DCM systems report deformation of the bistable loop only in the limit of dispersive bistability; they report sharp switch on/off in the absorptive limit. (3) Spatial hysteresis and radial variation of the bistable loop, which are associated with dispersive optical bistability, are observed in the FSD system without explicit dispersion dependence. These effects, shifting, deformation, and radial variation of the bistable loop, and spatial hysteresis can be attributed to a system that considers free-space diffraction in the absence of diffrative effects within the medium.

CHAPTER V

SUMMARY AND CONCLUSIONS

In this thesis, we discuss the free-space diffraction influence in an optically bistable system. This work is the natural extension of work done previously by several authors which studied plane wave effects, diffraction of the field within the medium, and diffusion of the excitation. We argue that the thin nature of the medium eliminates/diminishes transverse coupling within the medium. We make several comparisons between the phenomena displayed in the free-space diffraction system to phenomena reported in other plane wave and diffractive or diffusive systems. We find that the FSD system relates favorably with dispersive systems and relates poorly with absorptive systems. There are several similarities and differences. (1) The atomic and cavity resonant FSD system resembles the plane wave system in the presence of atomic and cavity detuning. (2) Models that describe diffractive coupling within the medium in the dispersion limit report switch on powers similar to the PW system which is seen in the FSD system without explicit dispersion dependence. (3) The FSD system resembles transverse effect systems under the influence of self-focusing. We report shifting of the bistable loop as a function of the atomic detuning and Fresnel number. Deformation of the bistable loop is minimal under positive detuning (associated with self-focusing) while negative detuning (associated with self-defocusing) washes out the hysteresis. The DCM systems report deformation of the bistable loop only in the limit of dispersive bistability; they report sharp switch on/off in the absorptive limit. (4) Spatial hysteresis and radial variation of the bistable loop, which are associated with dispersive optical bistability, are observed in the FSD system without explicit dispersion dependence.

In the plane wave systems and transverse effects systems mentioned, dispersion in a product of large atomic or cavity detunings. However, in the FSD system, there does not exist a clear distinction between absorptive and dispersive bistability. Dispersion is

synonymous with detuning (or phase shift), either atomic or cavity. In the FSD system, dispersion is an inherent, inescapable, part of this system due to the phase shift of the field calculated within the free-space diffraction integral.

The diffraction-induced dispersive behavior reported in this thesis has not been discussed in other transverse effects models to the knowledge of the author. The DCM and DCE models discussed rely on diffractive or diffusive coupling within the medium as the dominant transverse coupling mechanism. Although there is an explicit phase shift of the field in the diffraction term of the DCM model, see Eq. (IV.4), dispersive behavior in the resonant system is not reported. The DCM models adiabatically eliminate the medium variables, both the atomic polarization and population difference, to greatly reduce the complexity of the problem which, in turn, reduces the computation time. This results in a loss of dynamics and information. It is the opinion of this author that if the medium variables had been eliminated from the FSD system, the dispersive phenomena displayed in the resonant case would be greatly diminished or nonexistent consistent with the models that describe diffractive coupling within the medium.

In conclusion, we show spatial hysteresis in the presence of power hysteresis, shifting, deformation and radial variation of the bistable loop and can be attributed to a system that considers free-space diffraction independent of diffusive and diffractive coupling within the medium. The coupling between detuning and free-space diffraction can cause an effect similar to self-focusing and self-defocusing.

LITERATURE CITED

1. S.L. McCall, Phys. Rev. A **9**, 1515 (1974).

2. H. Seidel, U.S. Patent #3610-731 (1971).

3. A. Szoke, V. Daneu, J. Goldhar, and N.A. Kurnit, Appl. Phys. Lett. **15**, 376 (1969).

4. S.L. McCall, H.M. Gibbs, G.G. Churchill, T.N.C. Venkatesan, Bull. Am. Phys. Soc. **20**, 636 (1975); H.M. Gibbs, S.L. McCall, and T.N.C. Venkatesan, Phys. Rev. Lett. **36**, 1135 (1976).

5. R. Bonifacio and L.A. Lugiato, Opt. Comm. **19**, 1972 (1976).

6. R. Bonifacio and L.A. Lugiato, Lett. Nuovo Cimento **21**, 517 (1978).

7. K. Ikeda, Opt. Comm. **30**, 257 (1979).

8. J.Y. Gao, J.M. Yuan, and L.M. Narducci, Opt. Comm. **44**, 201 (1983); J.Y. Gao, L.M. Narducci, H. Sadiky, M. Squicciarini, and J.M. Yuan, Phys. Rev. A **30**, 901 (1984).

9. M. LeBerre, E. Ressayre, A. Tallet, and H.M. Gibbs, Phys. Rev. Lett. **56**, 274 (1986); M. LeBerre, E. Ressayre, A. Tallet, H.M. Gibbs, D.L. Kaplan, and M.H. Rose, Phys. Rev. A **35**, 4020 (1987).

10. P. Meystre and F. Hopf, Opt. Comm. **29**, 235 (1979).

11. V. Benza and L.A. Lugiato, Lett. Nuovo Cimento **26**, 405 (1979); Zeitschrift fur Physik, **B35**, 383 (1979).

12. F. Hopf, P. Meystre, P.D. Drummond, and D.F. Walls, Opt. Comm. **32**, 245 (1979).

13. L.A. Lugiato, M.Milani, and P. Meystre, Opt. Comm. **40**, 307 (1982); L.A. Lugiato, F. Casagrade, and L. Pizzuto, Phys. Rev. A **26**, 3438 (1982); L.A. Lugiato, V. Benza, L.M. Narducci, and J.D. Farina, Zeitschrift fur Physik **B49**, 352 (1982).

14. G.S. Agrawal, L.M. Narducci, R. Gilmore, and D.H. Feng, Phys. Rev. A **18**, 620 (1978); Opt. Lett. 2, **88** (1978); Phys. Rev A **20**, 545 (1979).

15. H.J. Carmichael and D.F. Walls, J. of Phys. B **10**, 685 (1977).

16. F. Casagrande and L.A. Lugiato, Nuovo Cimento **B55**, 173 (1980); F. Casagrande, L.A. Lugiato, and M.L. Asquini, Opt. Comm. **32**, 492 (1980).

17. R. Bonifacio, M. Gronchi, and L.A. Lugiato, Phys. Rev. A **18**, 2266 (1978).

18. F. T. Arecchi and A. Politi, Opt. Comm. **29**, 361 (1979).

19. P.D. Drummond and D.F. Walls, J. Phys. A **13**, 725 (1980); Phys. Rev. A **23**, 2563 (1981).

20. L.A. Lugiato, J. Farina, and L.M. Narducci, Phys. Rev. A **22**, 253 (1980); L.A. Lugiato, F. Casagrande, L. Pizzuto, Phys. Rev. A **26**, 3438 (1982).

21. T.N.C. Venkatesan and S.L. McCall, Appl. Phys. Lett. **30**, 282 (1977).

22. D. Grischkowski, J. Opt. Soc. Am. **68**, 641 (1978).

23. S.L. McCall and H.M. Gibbs, J. Opt. Soc. Am. **68**, 1378 (1978).

24. T. Bishofberger and Y.R. Shen, Appl. Phys. Lett. **32**, 156 (1978).

25. E. Garmire, J.H. Marburger, S.D. Allen, and H.G. Winful, Appl. Phys. Lett. **34**, 374 (1979).

26. D.E. Grant and H.J. Kimble, Opt. Comm. **44**, 415 (1983).

27. W.J. Sandle and A. Gallagher, Phys. Rev. A **24**, 2017 (1981).

28. D.E. Grant and H.J. Kimble, Opt. Lett. **7**, 353 (1982).

29. E. Arimondo, A. Gizzini. L. Lovitch, and E. Pistelli, in Optical Bistability, eds. C.M. Bowden, M. Ciftan, and H. Robl (Plenum Press, 1981).

30. A.T. Rosenberger, L.A. Orozco, and H.J. Kimble, Phys. Rev. A **28**, 2569 (1983).

31. H.M. Gibbs, Optical Bistability - Controlling Light with Light (Academic, New York, 1985).

32. L.A. Lugiato, in Progress in Optics, E. Wolf, ed. **24** (North Holland, Amsterdam, 1984), p. 66.

33. A.T. Rosenberger, L.A. Orozco, and H.J. Kimble, Phys. Rev. A **28**, 2569 (1983); L.A. Orozco, H.J. Kimble, and A.T. Rosenberger, Opt. Comm. **62**, 54 (1987); L.A. Orozco, A.T. Rosenberger, and H.J. Kimble, Phys. Rev. A **36**, 3248 (1988).

34. D.W. McLaughlin, J.V. Moloney, and A.C. Newell, Phys. Rev. Lett. **51**, 75 (1983).

35. V.E. Zakharov and A.B. Shabat, Soviet Phys. JETP **34**, 62 (1972).

36. Y.R. Shen, Prog. Quant. Elect. **4**, 1 (1975).

37. J.H. Marburger, Prog. Quant. Elect. **4**, 35 (1975).

38. A.W. McCord, R.H. Ballagh, and J. Cooper, J. Opt. Soc. Am. B **5**, 1323 (1988).

39. M.D. Feit and J.A. Fleck, Jr., J. Opt. Soc. Am B **5**, 633 (1988).

40. A. Yu. Okulov and A.N. Oraevsky, Sov. J. Quant. Elect. **18**, 233 (1988).

41. T. Karr, J. Morris, D. Chanbers, J. Viecelli, and P. Cramer, J. Opt. Soc. Am. B **7**, 1103 (1990).

42. D.J. Harter and R.W. Boyd, Phys. Rev. A **29**, 739 (1984).

43. H.M. Gibbs, B. Bolger, F.P. Mattar, M.C. Newstein, G. Forster, and P.E. Toschek, Phys. Rev. Lett. **37**, 1743 (1976).

44. M. LeBerre, E. Ressayre, A. Tallet, K. Tai, H.M. Gibbs, M.C. Rushford, and N. Peyghambarian, J. Opt. Soc. Am. B **1**, 591 (1984).

45. R.J. Ballagh, J. Cooper, M.W. Hamilton, W.J. Sandle, and D.M. Warrington, Opt. Comm. **37**, 143 (1981).

46. P.D. Drummond, IEEE J. Quant. Elect. **QE-17**, 301 (1981).

47. W.J. Firth, C.T. Seaton, E.M. Wright, and S.D. Smith, Appl. Phys. B **28**, 131 (1982).

48. M. Dagenais and H.G. Winful, Appl. Phys. Lett. **44**, 574 (1984).

49. A.K. Kar, J.G.H. Mathew, S.D. Smith, B. Davis, and W. Prettl, Appl. Phys. Lett. **42**, 334 (1983).

50. W.J. Firth and E.M. Wright, Opt. Comm. **40**, 233 (1982).

51. W.J. Firth, A. Fitzgerald, and C. Pare, J. Opt. Soc. B **7**, 1087 (1990).

52. H.M. Gibbs S.L. McCall, T.N.C. Gossard, A. Passner, and W. Wiegman, Appl. Phys. Lett. **35**, 451 (1979).

53. D.A.B. Miller, S.D. Smith, and A. Johnston, Appl. Phys. Lett. **35**, 658 (1979).

54. J.V. Moloney, M.R. Belic, and H.M. Gibbs, Opt. Comm. **41**, 379 (1982).

55. N.N. Rozanov and V.E. Semenov, Opt. Comm. **38**, 435 (1981).

56. N.N. Rozanov, V.E. Semenov, and G.V. Khodova, Sov. J. Quant. Elect. **12**, 193 (1982).

57. J.V. Moloney and H.M. Gibbs, Phys. Rev. Lett. **48**, 1607 (1982).

58. Yu. I. Balkarei, M.E. Evtikhov, J.V. Moloney, and Yu. A. Rzhanov, J. Opt. Soc. Am. B **7**, (199).

59. S.C. Sheng and A.E. Siegman, Phys. Rev. A **21**, 599 (1980).

60. D. Weaire, J.P. Kermode, and V.M. Dwyer, Opt. Comm. **55**, 223 (1985).

61. W.J. Firth, I. Galbraith, and E.M. Wright, Optical Bistability III, H.M. Gibbs, P. Mandel, N. Peyghambarian, and S.D. Smith, eds. (Springer-Verlag, Berlin, 1986), p. 197.

62. E.M. Wright, W.J. Firth, and I. Galbraith, J. Opt. Soc. Am. B **2**, 383 (1985).

63. W.J. Firth, I. Galbraith, and E.M. Wright, J. Opt. Soc. Am. B **2**, 1005 (1985).

64. A.V. Grigor'yants and I.N. Dyuzhikhov, J. Opt. Soc. Am. B **7**, 1303 (1990).

65. J. Young, H. Richardson, H.A. Mackenzie, E. Abraham, and D.J. Hagan, J. Opt. Soc. Am. B **5**, 3 (1988).

66. N.N. Rozanov and V.E. Semenov, Opt. Spectrosc. (USSR) **48**, 59 (1980); Sov.

Phys. JETP **53**, 47 (1981).

67. W.J. Firth and I. Galbraith, IEEE J. Quant. Elect. **QE-21**, 1399 (1985).

68. W.J. Firth, Phys. Lett. A **125**, 375 (1987).

69. W.J. Firth, Phys. Rev. Lett. **61**, 329 (1988).

70. Y.A. Rzhanov and Yu. D. Kalafati, Opt. Comm. **70**, 161 (1989).

71. N.N. Rosanov, V.E. Semenov, and G.V. Khodova, Sov. J. Quant. Elect. **12**, 198 (1982).

72. D.W. McLaughlin, J.V. Moloney, and A.C. Newell, Phys. Rev. Lett. **54**, 681 (1985).

73. J.V. Moloney, F.A. Hopf, and H.M. Gibbs, Phys. Rev. A **25**, 3442 (1982).

74. W.J. Firth and E.M. Wright, Phys. Lett. A **92**, 211 (1982).

75. J.V. Moloney, H. Adachihara, D.W. McLaughlin, and A.C. Newell, Chaos, Noise, and Fractals, E.D.R. Pike and L.A. Lugiato, eds. (Hilger, Bristol, UK, 1987), p. 137.

76. J.V. Moloney, in Optical Instabilities, R.W. Boyd, M.G. Raymer, and L.M. Narducci, eds. (Cambridge U. Press, Cambridge, 1986), p. 315.

77. L.A. Lugiato and M. Milani, J. Opt. Soc. Am. B **2**, 15 (1985).

78. L.A. Lugiato and M. Milani, Z. Phys. B **50**, 171 (1983).

79. L.A. Lugiato and Milani, Opt. Comm. **46**, 57 (1983); L.A. Lugiato, R.J. Horowicz, G. Strini, and L.M. Narducci, Phys. Rev. A **30**, 1366 (1984).

80. S. Stuut and M. Sargent III, J. Opt. Soc. Am. B **1**, 95 (1984).

81. D.A. Holm, M. Sargent III, and L.M. Hoffer, Phys. Rev. A **32**, 963 (1985).

82. L.A. Lugiato, R.J. Horowicz, G. Strini, and L.M. Narducci, Philos. Trans. R. Soc. London Ser. A **313**, 291 (1984).

83. L.A. Orozco, A.T. Rosenberger, and H.J. Kimble, Phys. Rev. **53**, 2547 (1984); L.A. Orozco, H.J. Kimble, A.T. Rosenberger, L.A. Lugiato, M.L. Asquini, M. Brambilla, and L.M. Narducci, Phys. Rev. A **39**, 1235 (1989).

84. B. Segard, B. Macke, L.A. Lugiato, F. Prati, and M. Brambilla, Phys. Rev. A **39**, 703 (1989); B. Segard, W. Sergent, B. Macke, and N.B. Abraham, Phys. Rev. A. **39**, 6029 (1989).

85. A.E. Siegman, Lasers, (University Science Books, Mill Valley, CA, 1986).

86. Private communication between Professors Jon Davis and Lorenzo Narducci, 1984.

87. L.M. Narducci, D.K. Bandy, C.A. Pennise, and L.A. Lugiato, Opt. Comm. **44**, 207 (1983).

88. L.A. Lugiato, L.M. Narducci, D.K. Bandy, and C.A. Pennise, Opt. Comm. **43**, 281 (1982).

89. L.A. Lugiato, L.M. Narducci, E.V. Eschenazi, D.K. Bandy, and N.B. Abraham, Phys. Rev. A **32**, 1563 (1985).

90. L.A. Lugiato, Opt. Comm. **33**, 108 (1980).

91. M. Born and E. Wolf, Principles of Optics, (Pergamon Press, Oxford, 1991).

92. O. Svelto, Principles of Lasers, (Plenum Press, New York, 1982), Ch. 4.

93. I.S. Gradshteyn and I.M. Ryzhik, Table of Integrals, Series, and Products, (Academic Press, Inc., Orlando, Florida, 1965.

94. D.K. Bandy, L.W. Hunter, and D.J. Jones, Nonlinear Optics and Materials, ed. C.D. Cantrell and C.M. Bowden, Proc. SPIE **1497** (1991) p. 142.

95. D.K. Bandy, Ph.D. Dissertation, Drexel University (1984).

96. For example, J.V. Moloney, H. Adachihara, R. Indik, C. Lizarraga, R. Northcutt, D.W. McLaughlin, and A.C. Newell, J. Opt. Soc. Am. B **7**, 1039 (1990).

97. N.B. Abraham and W.J. Firth, J. Opt. Soc. Am. B **7**, 951 (1990).

98. J.-J. Zondy, M. Le Berre, E. Ressayre, and A. Tallet, Proceedings of the Optical Bistability IV, W. Firth, N. Peyghambarian, and A. Tallet, eds., (1988) p. 6.

99. M. Le Berre, E. Ressayre, A. Tallet, and J.-J. Zondy, J. Opt. Soc. Am. B **7**, 1346 (1990).

100. W.J. Firth, E. Abraham, E.M. Wright, I. Galbraith, and B.S. Wherrett, Phil. Trans. Roy. Soc. Lond. A **313**, 299 (1984).

101. S.W. Koch, H.E. Schmidt, and H. Haug, Appl. Phys. Lett. **45**, 932 (1984).

102. J.H. Marburger and F.S. Felber, Phys. Rev. A **17**, 335 (1978).

103. M. Scalora and J. W. Haus, J. Opt. Soc. Am. B **6**, 1714 (1989).

104. R. Reinisch and G. Vitrant, J. Appl. Phys. **67**, 6671 (1990).

105. I.C. Khoo, Appl. Phys. Lett. **41**, 909 (1982); I.C. Khoo, P.Y. Yan, T.H. Liu, S. Shepard, and J.Y. Hou, Phys. Rev. A **29**, 2756 (1984).

106. P. Grangier, J.F. Roch, J. Roger, L.A. Lugiato, E.M. Pessina, G. Scandroglio, and P. Galatola, Phys. Rev. A **46**, 2735 (1992).

107. G.P. Agrawal, Nonlinear Fiber Optics, (Academic Press, Inc., San Diego, 1989).

APPENDIX A

BEAM CONFINEMENT CRITERIA FOR A RING CAVITY

Ray optics (geometrical optics without diffraction) is useful in understanding the full diffractive propagation of light waves in optical resonators. Ray matrices (ABCD matrices) are widely used to describe the propagation of geometrical optical rays through paraxial optical elements such as lenses or spherical mirrors. In particular, ray matrices can predict stable and unstable operating conditions of optical resonators. Even though diffraction is not considered, this approach will give us a rough estimate of cavity stability. Another problem that arises is that we are injecting a signal on each round trip of the field. This could cause an instability to occur. Although this would not affect a system based on geometrical optics, it could affect a system which considers diffraction (wave optics).

An empty ring cavity is always stable, provided that the mirrors are planar. However, when any other optical device is placed inside the cavity, the cavity may become unstable. We use matrix optics to do the stability analysis of our empty ring cavity. The empty ring cavity has one planar mirror and two spherical mirrors, see Fig. 27. Here, R_1 and R_2 are the radii of curvature of mirrors 1 and 2 respectively, p_1 and p_2 are the distances between the mirrors and the dashed line (point X), and p_3 is the distance from mirror 2 around the cavity to mirror 1. $\Lambda = p_1 + p_2 + p_3$.

The matrix equation describing propagation in free-space is

$$\begin{bmatrix} r_{out} \\ r'_{out} \end{bmatrix} = \begin{bmatrix} 1 & d \\ 0 & 1 \end{bmatrix} \begin{bmatrix} r_{in} \\ r'_{in} \end{bmatrix} \tag{A.1}$$

while the matrix equation describing a reflection from a perfectly reflecting mirror is

$$\begin{bmatrix} r_{out} \\ r'_{out} \end{bmatrix} = \begin{bmatrix} 1 & 0 \\ -\frac{2}{R} & 1 \end{bmatrix} \begin{bmatrix} r_{in} \\ r'_{in} \end{bmatrix} \tag{A.2}$$

where r_{in} and r_{out} measures the distance from the axis of the ray entering the system and leaving the system, respectively, and r_{in}' and r_{out}' are the slopes of the input and output rays, respectively.

Beginning the stability calculation at point X and using the ray matrices defined above we find the following relation

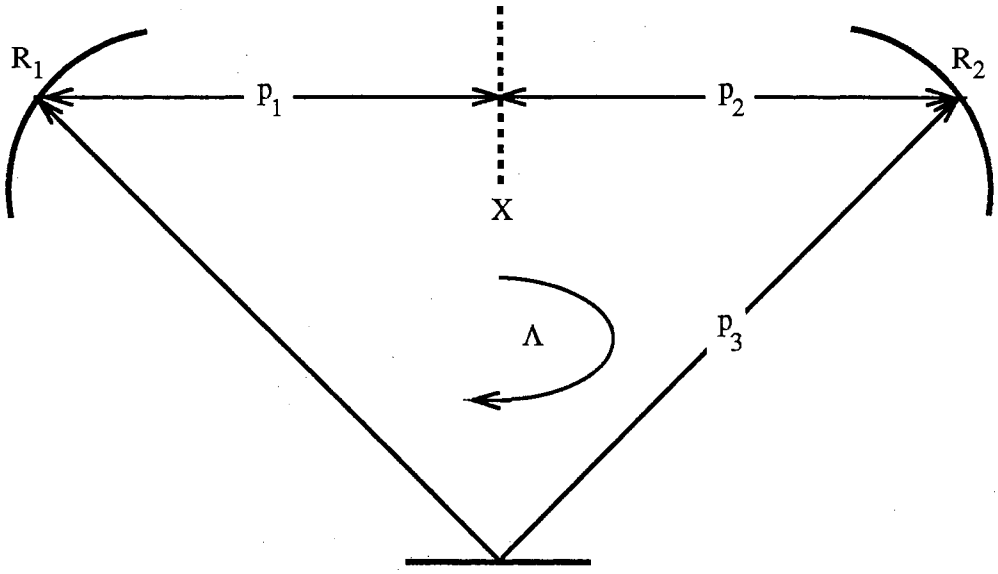

Figure 26. Empty Cavity Schematic

$$\begin{bmatrix} r_{X'} \\ r_{X'}' \end{bmatrix} = \begin{bmatrix} A & B \\ C & D \end{bmatrix} \begin{bmatrix} r_X \\ r_X' \end{bmatrix} \tag{A.3}$$

where X' denotes the same physical point as X after passing around the cavity once. The coefficients in the constant matrix are

$$A = \left(1 - \frac{2p_1}{R_1}\right)\left(1 - \frac{2p_3}{R_2}\right) - \frac{2p_1}{R_2} \tag{A.4a}$$

$$B = \left(p_2 + p_3\left(1 - \frac{2p_2}{R_2}\right)\right)\left(1 - \frac{2p_1}{R_1}\right) + p_1\left(1 - \frac{2p_2}{R_2}\right) \tag{A.4b}$$

$$C = -\frac{2}{R_2} - \frac{2}{R_1}\left(1 - \frac{2p_3}{R_2}\right) \tag{A.4c}$$

$$D = 1 - \frac{2p_2}{R_2} - \frac{2}{R_1}\left(p_2 + p_3\left(1 - \frac{2p_2}{R_2}\right)\right) \tag{A.4d}$$

It is a general property of all the basic optical elements that the ray matrix determinant be equal to one, i.e. AD - BC = 1.

The constant matrix will be independent of the pass through the system, so we can write in general

$$r_{n+1} = Ar_n + Br_n' \tag{A.5a}$$

$$r_{n+1}' = Cr_n + Dr_n' \tag{A.5b}$$

Solving for r_n' in Eq. (A.5a), letting n -> n+1, and substituting into Eq. (A.5b) we find the following difference equation describing the evolution of a geometrical ray in an optical cavity

$$r_{n+2} - (A + D)\, r_{n+1} + (AD - BC)\, r_n = 0 \tag{A.6}$$

Using the fact that AD - BC = 1 and defining 2b = A + D = Tr (constant matrix) we find

$$r_{n+2} - 2br_{n+1} + r_n = 0 \tag{A.7}$$

This difference equation is mathematically equivalent to the differential equation of the form

$$\frac{d^2 r}{dz^2} = - \mathcal{A}^2 r \tag{A.8}$$

where $\mathcal{A}$ is a constant to be found. Eq. (A.8) has solutions of the form $r_{\pm}(z) = \rho_{\pm}$ $\exp(\pm i\mathcal{A}z)$ where ρ is a constant. Therefore, we look for solutions to Eq. (A.7) of the form

$$r_n = \rho\, e^{in\Psi} \tag{A.9}$$

Substituting Eq. (A.9) into Eq. (A.7) and solving for $\exp(i\psi)$ gives

$$e^{i\Psi} = b \pm i\sqrt{1 - b^2} \tag{A.10}$$

but by Euler's theorem

$$\exp(i\psi) = \cos\psi + i \sin\psi \tag{A.11}$$

provided that $|\psi| \leq 1$. Comparing Eq. (A.11) with Eq. (A.10), we have as the necessary and sufficient condition for cavity stability that $|b| \leq 1$, or using the ray matrix elements

$$\frac{|A + D|}{2} \leq 1 \tag{A.12}$$

We can rewrite the stability condition, Eq. (A.12), in terms of the system parameters to give

$$0 \leq 1 - \frac{\Lambda}{2}\left(\frac{1}{R_1} + \frac{1}{R_2}\right) + \frac{p_3(p_1 + p_2)}{R_1 R_2} \leq 1 \tag{A.13}$$

When the system parameters are chosen such that Eq. (A.12) is satisfied, then we have a confined beam. If $|b| > 1$ we no longer have confinement of the beam. This leads to a solution of the form

$$r_n = \rho_1 e^{n\alpha_+} + \rho_2 e^{n\alpha_-} \tag{A.14}$$

where

$$e^{\alpha_{\pm}} = b \pm \sqrt{b^2 - 1}\,. \tag{A.15}$$

Since the magnitude of Eq. (A.14) exceeds unity, the beam radius given by Eq. (A.14) will expand indefinitely as a function of distance, n.

The simplest case of an optical resonator is the case where the system is symmetrical,

i.e. $p_1 + p_2 = p_3 = \Lambda / 2$. This leads to the stability condition

$$0 \leq g_1 g_2 \leq 1 \tag{A.16}$$

where

$$g_i = 1 - \frac{\Lambda}{2R_i} \quad \text{where } i = 1, 2 \tag{A.17}$$

The diagram shown in Fig. 28. is a convenient representation of the confinement condition, Eq. (A.16). The shaded regions where both g_1 and g_2 have the same sign indicate the regions of beam confinement. The $g_1 = g_2$ ($R_1 = R_2 = R$) line indicates the symmetric cavities. The concentric ($R = \Lambda/4$), confocal ($R = \Lambda/2$), and plane-parallel ($R = \infty$) resonators all lie on the confinement boundary. These resonators can become extremely lossy unless great care is taken in the alignment of the mirrors. Most experimental cavities use system parameters lying well within the confinement region along the $g_1 = g_2$ line.

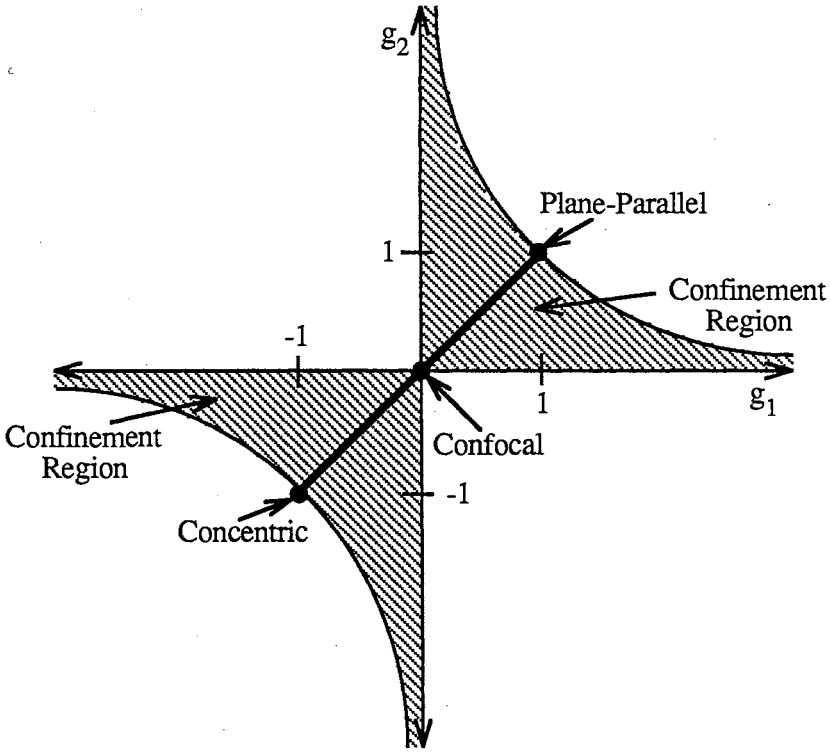

Figure 27. Confinement Regions of the Cavity Resonator.

APPENDIX B

COEFFICIENTS OF THE DESCRETIZED EQUATIONS

$$a_1^r \equiv \alpha \frac{\Delta\tau}{2} (\Delta\tau - 1) \tag{B.1}$$

$$a_1^i \equiv - \alpha \Delta \frac{\Delta\tau^2}{2} \tag{B.2}$$

$$a_2 \equiv - \alpha \frac{\Delta\tau}{2} \tag{B.3}$$

$$a_3 \equiv \alpha \frac{\Delta\tau^2}{2} \tag{B.4}$$

$$b_1^r \equiv 1 + (1 - \Delta^2) \frac{\Delta\tau^2}{2} - \Delta\tau \tag{B.5}$$

$$b_1^i \equiv \Delta (1 - \Delta\tau) \Delta\tau \tag{B.6}$$

$$b_2 \equiv - \frac{\gamma \Delta\tau^2}{4} \tag{B.7}$$

$$b_3^r \equiv \frac{\Delta\tau}{2} \left((1 + \gamma) \Delta\tau - 1 \right) \tag{B.8}$$

$$b_3^i \equiv - \Delta \frac{\Delta\tau^2}{2} \tag{B.9}$$

$$b_4 \equiv - \frac{\Delta\tau}{2} \tag{B.10}$$

$$b_5 \equiv \alpha \frac{\Delta\tau^2}{2} \tag{B.11}$$

$$b_6 \equiv \gamma \frac{\Delta\tau^2}{2} \tag{B.12}$$

$$c_1^r \equiv \gamma \Delta\tau \left(1 - \frac{\Delta\tau}{2} (1 + \gamma) \right) \tag{B.13}$$

$$c_1^i \equiv \gamma \Delta \frac{\Delta\tau^2}{2} \tag{B.14}$$

$$c_2 \equiv \gamma \frac{\Delta\tau}{2} \tag{B.15}$$

$$c_3 \equiv - \alpha \gamma \frac{\Delta\tau^2}{2} \tag{B.16}$$

$$c_4 \equiv - \gamma \frac{\Delta\tau^2}{2} \tag{B.17}$$

$$c_5 \equiv 1 - \gamma \Delta\tau + \gamma^2 \frac{\Delta\tau^2}{2} \tag{B.18}$$

$$c_6 \equiv \gamma \Delta\tau \left(\gamma \frac{\Delta\tau}{2} - 1 \right) \tag{B.19}$$

APPENDIX C

FORTRAN SOURCE CODE FOR THE FREE-SPACE DIFFRACTION MODEL SYSTEM

```
c*****************************TRANSVERSE.F*****************************
c  This program was written by Darlena Jones to solve free-space diffraction effects in an
c  all-optical, passive, driven system.  The Kirchoff diffraction integral and the Maxwell
c  Bloch equations are solved.
c**********************************************************************

      implicit double precision (a-h,o-z)
      real*8 kappa
      dimension x(50),y(50),w(50),bmat(50,50),E1r(50),E1i(50)
      dimension time(20000),Emodt(50),E5r(50),E5i(50),Emod(20000),Dmod(20000)
      dimension radial(50),Estorr(50,200),Estori(50,200),Er(50)
      dimension A(0:2,50),B(0:2,50),P(0:2,50),Q(0:2,50),D(0:2,50)
      character*8 rfile

c  This program solves for laser with injected signal (LIS), optical bistability (OB), and the
c  free running laser.

      type*,'-------------------------------Menu-----------------------------------------'
      type*,'For LIS ..........................................................  enter 1'
      type*,'For OB ...........................................................  enter 2'
      type*,'For Free Running Laser ...........................................  enter 3'
      type*,'--------------------------------------------------------------------------'
      accept*, iLOB

c*********************************INITIALIZE*****************************
      iteg2 = 2
      icount = 1
      iwidth = 48
      iplot = 0
      kk = 0
      Ndiv = 200
      M = 48
      u = 1.0
      s = 0.0
      if(iLOB .ne. 2) sigma = -1.0d0
      if(iLOB .eq. 2) sigma = 1.0d0
      sodlen = 1.0d0/dble(Ndiv)
      beta = 2.0

c  This calls the arrays x and w that contain the Gauss-Lagurre values.
      call absic(x,w)

c  This sets up the initial conditions for the medium.
      do 1 j=1,M
            Err = dexp(-x(j))
            A(s,j) = 0.001*Err
            B(s,j) = 0.001*Err
            P(s,j) = .001d0*Err
            Q(s,j) = .001d0*Err
            D(s,j) = -sigma*Err
1     continue

c  This initializes the roundtrip field to zero.
      do 3 i=1,Ndiv-1
            do 2 j=1,M
```

```
                    Estorr(j,i) = 0.0
                    Estori(j,i) = 0.0
2               continue
3           continue
            Ntrips = 1

c************************DATA ENTRY*********************************
c  alpha - absorption, delta - atomic detuning, gamma - medium decay rate, and kappa -
c  cavity decay rate.
4           type*,'enter alpha, delta, gamma, and kappa'
            accept*,alpha,delta,gamma,kappa

c  T - mirror transmittivity and R - mirror reflectivity.
            T = kappa/beta
            R = 1.0d0 - T
            TT = dsqrt(T)
            RR = dsqrt(R)

            if(iLOB .ne. 3) then
                type*,'enter Ein and delta0'
                accept*,Ein,delta0
                type*,'enter aperature width in units of half widths'
                accept*,iwidth
                width = float(iwidth)*dsqrt(dlog(2.0d0))
                do 5 i=1,M
                    if(width .le. dsqrt(x(i))) then
                        iwidth = i-1
                        goto 6
                    endif
5               continue
              else
                Ein = 0.0d0
                delta0 = 0.0d0
            endif
6           pha = dcos(delta0)
            phb = dsin(delta0)
            inum = Ntrips
            type*,'enter number of roundtrips'
            accept*,newtrp
            type*,'Number of points = ',newtrp*200,'  enter skip'
            accept*,jskip
            Ntrips = Ntrips + newtrp
            itrip = Ntrips

c**********************************INITIALIZE*****************************c
This sets the injected signal.  "iwidth" is the aperature width.
            do 8 i=1,M
                if(i .le. iwidth) Er(i) = TT*Ein*dexp(-x(i))
                if(i .gt. iwidth) Er(i) = 0.0d0
                y(i) = x(i)
                radial(i) = dsqrt(x(i))
8           continue

c  These are the Risken-Nummendal coefficients.
            deleta = sodlen
```

```
      deltat = deleta/beta
      delsq = deltat**2
      delsq2 = delsq/2.0d0
      del2 = deltat/2.0d0
      a1r = alpha*delsq2 - alpha*del2
      a1i = -alpha*delta*delsq2
      a2  = -alpha*del2
      a3  = alpha*delsq2
      b1r = 1.0d0 + (1.0d0 - delta**2)*delsq2 - deltat
      b1i = -delta*delsq2 + delta*deltat
      b2  = -delsq2*gamma/2.0d0
      b3r = -del2 + (1.0d0 + gamma)*delsq2
      b3i = -delta*delsq2
      b4  = -del2
      b5  = a3
      b6  = alpha*sigma*delsq2
      c1r = 2.0*(gamma*del2 - (gamma/2.0d0)*(1.0d0 + gamma)*delsq2)
      c1i = gamma*delta*delsq2
      c3 = gamma*del2
      c5 = -alpha*gamma*delsq2
      c6 = -gamma*delsq2
      c7 = 1.0d0 - gamma*deltat + gamma**2*delsq2
      c8 = gamma*sigma*deltat*(-1.0d0 + gamma*del2)

c  These are the cavity parameters scaled to the cavity length.  etaf - focal length, etazr -
c  Rayleigh range, eta - distance from mirror to medium, eta3 - feedback distance.  Amatx,
c  Bmatx, Dmatx - coefficients of the ABCD matrix.
      etaf = .5d0
      etazr = 0.25d0
      eta = 1.0d0/4.0d0 - sodlen/2.0
      eta3 = 0.5d0
      Aaf = 1.0 - eta/etaf
      Adf = 1.0 - eta3/etaf
      Amatx = Aaf*Adf - eta/etaf
      Bmatx = eta*Aaf*Adf - eta**2/etaf + eta3*Aaf + eta
      Dmatx = -eta*(1.0/etaf + Adf/etaf) + 1.0 - eta3/etaf
      xciB = etazr/Bmatx

c  Matrix is a subroutine that calculates the Bij matrix.
      call Matrix(xciB,x,y,w,M,bmat)

      con1 = Amatx*xciB
      con2 = Dmatx*xciB

9     type*,' '
      type*,'Calculating.....'

c*********************************************************************
      do 13 k=inum,Ntrips
            do 12 N = 1,Ndiv-1
                  do 10 j=1,M

c  Boundary conditions.
                        A0 = Er(j)+Estorr(j,N)*pha-Estori(j,N)*phb
                        B0 = Estori(j,N)*pha + Estorr(j,N)*phb
```

```
c Maxwell-Bloch equations describing the medium. A and B are real and imaginary
c fields. P and Q are real and imaginery polarizations. D is the population difference.
c The medium is only one unit in thickness.
                        A(u,j) = A0 + a1r*P(s,j) - a1i*Q(s,j)+ a3*D(s,j)*A(s,j)

                        B(u,j) = B0 + a1i*P(s,j) + a1r*Q(s,j)+ a3*D(s,j)*B(s,j)

                        P(u,j) =b1r*P(s,j)-b1i*Q(s,j)+ 2.0*b2*(A(s,j)**2*P(s,j)
     1                  - A(s,j)*B(s,j)*Q(s,j))+ D(s,j)*(b3r*A(s,j)- b3i*B(s,j)
     2                  +b4*A0 + b5*P(s,j)) + b6*A(s,j)

                        Q(u,j) = b1r*Q(s,j)+b1i*P(s,j)+2.0*b2*(A(s,j)**2*Q(s,j)
     1                  +A(s,j)*B(s,j)*P(s,j)) +D(s,j)*(b3r*B(s,j) + b3i*A(s,j)
     2                  + b4*B0 + b5*Q(s,j)) + b6*B(s,j)

                        D(u,j) = c1r*(P(s,j)*A(s,j)+Q(s,j)*B(s,j))+
     1                  c1i*(P(s,j)*B(s,j) - Q(s,j)*A(s,j)) +
     2                  c3*(P(s,j)*A0 + Q(s,j)*B0) +
     3                  c5*(P(s,j)**2 + Q(s,j)**2) +
     4                  c6*D(s,j)*(A(s,j)**2 + B(s,j)**2)+c7*D(s,j)+c8

                        E5r(j) = A(u,j)
                        E5i(j) = B(u,j)
                        E1r(j)=E5r(j)*dcos(con1*y(j))-E5i(j)*dsin(con1*y(j))
                        E1i(j)=E5i(j)*dcos(con1*y(j))+E5r(j)*dsin(con1*y(j))
10                  continue

c The toggle switch between matrices in the Risken-Nummendal calculation.
                    u = dabs(u - 1)
                    s = dabs(s - 1)

c Calculate the diffraction integral using the "integ" subroutine.
                    call integ(E1r,E1i,x,y,w,xciB,con2,E5r,E5i,bmat,iteg2)

c Place the feedback field into storage, Estorr and Estori. This is also a boundary
c condition.
                    do 11 i=1,M
                        Estorr(i,N) = R*E5r(i)
                        Estori(i,N) = R*E5i(i)
11                  continue

c Selecting every jplot point to store for later use.
                    jplot = jplot + 1
                    if(jplot .eq. jskip) then
                        jplot = 0
                        kk = kk + 1
                        Emod(kk) = TT*dsqrt(E5r(1)**2 + E5i(1)**2)
                        Dmod(kk) = Q(s,1)
                        time(kk) = dble(kk)
                    endif
12              continue
                if(k/icount .eq. 25) then
                    icount = icount + 1
                    field = TT*dsqrt(E5r(1)**2 + E5i(1)**2)
```

```
                type*,'iteration number',k,'  field = ',field
            endif
13      continue
c*************************************************************************
        Em1 = dsqrt(E5r(1)**2 + E5i(1)**2)
        Em2 = dsqrt(E5r(2)**2 + E5i(2)**2)
        coef = dlog(Em1/Em2)/(x(2)-x(1))
        E5m = TT*Em1/dexp(-coef*x(1))
        type*, char(7)
        type*, char(7)
14      type*,' '
        type*,'------------------------------Menu-------------------------------------------'
        type*,'To create radial profile file ..... enter 1'
        type*,'To create final conditions file ..... enter 2'
        type*,'To create amplitude of Etrans vs roundtrips ..... enter 3'
        type*,'To continue the present run ..... enter 4'
        type*,'To view the given parameters..... enter 5'
        type*,'To increase a parameter..... enter 6'
        type*,'To plot ..... enter 8'
        type*,'To exit program ..... enter 9'
        type*,'-----------------------------------------------------------------------------'
        accept*,ians

c  Here you can save the radial points for later use.
        if(ians .eq. 1) then
            type*,'enter name of data file for radial profile'
            accept '(a)',rfile
            open(22,file=rfile,status='new')
            write(22,*) M
            do 15 i=1,M
                Emodt(i) = TT*dsqrt(E5r(i)**2 + E5i(i)**2)
                if(Emodt(i) .lt. 1.0d-90) Emodt(i) = 0.0d0
                write(22,*) radial(i),Emodt(i)
15          continue
            write(22,*) 0.0,E5m
            type*,'file creation completed'
            goto 14
        endif

c  Here we can save the final conditions of the run.
        if(ians .eq. 2) then
            type*,'enter name of data file for final conditions'
            accept '(a)',rfile
            open(12,file=rfile,status='new')
            do 17 N = 1,Ndiv-1
                do 16 i=1,M
                    if(dabs(Estorr(i,N)) .lt. 1.0d-90) Estorr(i,N) = 0.0d0
                    if(dabs(Estori(i,N)) .lt. 1.0d-90) Estori(i,N) = 0.0d0
                    write(12,*) Estorr(i,N),Estori(i,N)
16              continue
17          continue
            do 19 i=1,mmax
                do 18 j=1,M
                    write(12,*) A(s,j),B(s,j)
                    write(12,*) P(s,j),Q(s,j)
```

```
                        write(12,*) D(s,j)
18                  continue
19              continue
                type*,'file creation completed'
                goto 14
        endif

c We can save the amplitude versus the roundtrips in a file.
        if(ians .eq. 3) then
                type*,'enter name of data file for amp vs. roundtrips'
                accept '(a)',rfile
                open(13,file=rfile,status='new')
                type*,'is this file for spec?.....enter 1 for yes'
                accept*,ispec
                if(ispec .ne. 1) then
                        itrmin = 1
                        itrmax = kk
                        type*,'do you want the entire run saved?....enter 1 for yes'
                        accept*,ians
                        if(ians .ne. 1) then
                                type*,'enter beginning and ending times'
                                accept*,itrmin,itrmax
                        endif
                        write(13,*) itrmax - itrmin + 1
                        do 20 i=itrmin,itrmax
                                write(13,*) time(i),Emod(i)
20                      continue
                        write(13,*) 1.0d0,Emod(1)
                endif
                if(ispec .eq. 1) then
                        type*,'enter the number of points to be saved'
                        accept*,numpts
                        write(13,*) numpts,jskip,deltat
                        itrmin = kk + 1 - numpts
                        itrmax = kk
                        do 21 i = itrmin,itrmax
                                write(13,*) Emod(i)
21              continue
                endif
                type*,'file creation completed'
                goto 14
        endif

c We can increase the number of roundtrips.
        if(ians .eq. 4) then
                inum = Ntrips
                type*,'enter the number of roundtrips and skip'
                accept*,newtrp,jskip
                Ntrips = Ntrips + newtrp
                goto 9
        endif

c This allows you to see what the current parameters are set at.
        if (ians .eq. 5) then
                type*,' '
```

```
                type*,'Echoing  input.....'
                type*,'delta = ',delta
                type*,'gamma = ',gamma
                type*,'alpha = ',alpha
                type*,' etaf = ',etaf
                type*,'delta0= ',delta0
                type*,'  Ein = ',Ein
                goto 14
        endif

c To increase a parameter, adiabatically, use this.
        if(ians .eq. 6) goto 4

c This is the plotting menu.
        if(ians .eq. 8) then
22      type*,' '

        type*,'------------------------------Menu-----------------------------------------------'
        type*,'Please specify what to plot.....                                               '
        type*,'Temporal .....                                                  enter 1'
        type*,'Radial profile .....                                            enter 2'
        type*,'To quit plot routine .....                                      enter 3'
        type*,'To plot in phase space .....                                    enter 4'
        type*,'Temporal pop. diff .....                                        enter 5'
        type*,'--------------------------------------------------------------------------------'
        accept*,iplt
        if(iplt .eq. 1 .or. iplt .eq. 4 .or. iplt .eq. 5) then
                itrmin = 1
                itrmax = kk
                type*,'do you want the entire run plotted?...enter 1 for yes'
                accept*,ians
                if(ians .ne. 1) then
                        type*,'enter beginning and ending times'
                        accept*,itrmin,itrmax
                endif
                coefin = Ein

c The plotting subroutine is called "plottran".
                if(iplt .eq. 1)call plottran(iplt,itrmin,itrmax,0.0,time,Emod)
                if(iplt .eq. 4)call plottran(iplt,itrmin,itrmax,0.0,Emod,Emod)
                if(iplt .eq. 5)call plottran(iplt,itrmin,itrmax,0.0,time,Dmod)
                goto 22
        endif
        if(iplt .eq. 2) then
                coeff = E5m
                do 23 i=1,M
                        Emodt(i) = TT*dsqrt(E5r(i)**2 + E5i(i)**2)
                        if(Emodt(i) .lt. 1.0d-90) Emodt(i) = 0.0d0
23              continue
                call plottran(iplt,1,M,coeff,radial,Emodt)
                goto 22
        endif
        if(iplt .le. 1 .or. iplt .eq. 3 .or. iplt .ge. 5) goto 14
        endif
```

```
      if(ians .eq. 9) then
            type*,'do you really want to quit?....enter 1 for yes'
            accept*,ians
            if(ians .ne. 1) goto 14
      endif

      if(ians .le. 0 .or. ians .ge. 10 .or. ians .eq. 7) goto 14

      stop
      end

c*************************************************************************c
 SUBROUTINE INTEG
c  This subroutine calculates the diffraction integral by multipling the two
c  dimensional matrix A (which is called Bij in my notes) by the field vector,
c  Er (real) and Ei (imaginery).

      subroutine integ(Er,Ei,x,y,w,xci,cc,Ehatr,Ehati,A,iteg)
      implicit double precision (a-h,o-z)
      dimension A(50,50), Ehatr(50), y(50), x(50), w(50)
      dimension Er(50), Ei(50), Ehati(50),Emod(50),N(50)
      M = 48
      Emax=0.0d0
      iff = 0
      inum = 48
      num = 0
      cofmax = 0.0
      do 2 i=1,M
            sumr = 0.0d0
            sumi = 0.0d0
            do 1 j=1,M
                  sumr = sumr + A(i,j)*Er(j)
                  sumi = sumi + A(i,j)*Ei(j)
1           continue
            const = cc*y(i)
            Ehatr(i) = xci*(sumr*dsin(const)+sumi*dcos(const))
            Ehati(i) = xci*(-sumr*dcos(const)+sumi*dsin(const))
            Emod(i) = dsqrt(Ehatr(i)**2 + Ehati(i)**2)
            if(Emod(i) .ge. Emax .and. i .lt. 20) then
                  Emax = Emod(i)
                  num = num + 1
                  N(num) = i
            endif
            if(i .ge. 20) then
                  diff = Emod(i) - Emod(i-1)
                  if(diff.ge.0.0d0 .and. iff.eq.0) then
                        inum = i
                        iff = 1
                  endif
            endif
2     continue

c  This section is the data smoothing required to keep the aliasing from getting out of
c  hand.
      do 3 i=1,num
```

```
                coef = dlog(Emod(N(i))/Emod(N(i)+1))/(x(N(i)+1)-x(N(i)))
                if(coef .gt. cofmax) cofmax = coef
3       continue
        j = inum - iteg
        do 4 i=j,M
                Ehatr(i)=Ehatr(i-1)*dexp(-cofmax*(x(i)-x(i-1)))
                Ehati(i)=Ehati(i-1)*dexp(-cofmax*(x(i)-x(i-1)))
4       continue
        return
        end


c*************************************************************************c
SUBROUTINE MATRIX
c  This calculates the A matrix (called the Bij matrix in my notes) by first
c  calling "laguer" to get the Lagurre values then summing by using the "summ"
c  subroutine.
        subroutine Matrix(xci,x,y, w,M,A)
        implicit double precision (a-h,o-z)
        dimension x(50), y(50), w(50), A(50,50), alag(50)
        do 2 i=1,M
                argue = xci*y(i)
                call laguer(argue, M, alag)
                do 1 j = 1,M
                        argue = xci*x(j)
                        call summ(argue, M, alag, answer)
                        A(i,j) = dexp(-(xci-1.0d0)*x(j))*answer*w(j)
1               continue
2       continue
        return
        end

c*************************************************************************c
SUBROUTINE LAGUER
c  This calculates the Lagurre polynomials given the value of the arguement.
        subroutine laguer(x,M,al)
        implicit double precision (a-h,o-z)
        dimension al(50)
        al(1) = 1.0d0
        al(2) = 1.0d0 - x
        do 1 i=3,M
                k = i-1
                al(i) = (2.0d0-(x+1.0d0)/k)*al(i-1) - (1.0d0-1.0d0/k)*al(i-2)
1       continue
        return
        end
c*************************************************************************c
SUBROUTINE SUMM
        subroutine summ(x,M,al,answer)
        implicit double precision (a-h,o-z)
        dimension al(50)
        a = 1.0d0
        answer = al(1)
        do 1 i=2,M
                k = i-1
```

```
                a = a*x/dble(k)
                answer = answer + a*al(i)
1       continue
        return
        end

c*****************************************************************c
SUBROUTINE PLOTTRAN
c  This is the plotting package used to plot both temporal and spatial values.

        subroutine plottran(inum,istart,idone,coeff,w,z)
        implicit double precision(a-h,o-z)
        real*4 xmin,xmax,ymin,ymax,xx,yy
        dimension x(20000),y(20000),z(20000),w(20000)

        do 1 i=istart,idone
                y(i) = z(i)
                x(i) = w(i)
1       continue
        xminp = 100000.0
        yminp = 100000.0
        xmaxp = -100000.0
        ymaxp = -100000.0
        xx = istart
        yy = coeff
        if(inum .eq. 2) xx = 0.0
        do 2 i=istart,idone
                if(x(i) .lt. xminp) xminp = x(i)
                if(y(i) .lt. yminp) yminp = y(i)
                if(x(i) .gt. xmaxp) xmaxp = x(i)
                if(y(i) .gt. ymaxp) ymaxp = y(i)
2       continue
        type*,'Do you want to scale the field? enter 1 for yes'
        accept*,iscale
        if(iscale .eq. 1) then
                scalex = xmaxp
                scaley = ymaxp
                if(inum .eq. 1) scalex = 1.0d0
                type*,'the scaling values are: '
                type*,'scale in x = ',scalex,'scale in y = ',scaley
                do 3 i=istart,idone
                        x(i) = x(i)/scalex
                        y(i) = y(i)/scaley
3               continue
                xx = xx/scalex
                yy = yy/scaley
                xmaxp = xmaxp/scalex
                xminp = xminp/scalex
                ymaxp = ymaxp/scaley
                yminp = yminp/scaley
        endif
4       type*,' '
        type*,'enter xmin, hint:min of x=',xminp
        accept*,xmin
        type*,'enter xmax, hint:max of x=',xmaxp
```

```
      accept*,xmax
      type*,'enter nx'
      accept*,nx
      type*,'enter ymin, hint:min of y=',yminp
      accept*,ymin
      if(iEin .eq. 1) ymaxp = coef2
      type*,'enter ymax, hint:max of y=',ymaxp
      accept*,ymax
      type*,'enter ny'
      accept*,ny
      type*,'to change parameters.....enter 1'
      accept*,ians
      if(ians .eq. 1) goto 4
      call lnstp
      call lnplt1(xmin,xmax,ymin,ymax,nx,ny)
      call movea(xx,yy)
      do 5 i=istart,idone
            if(inum .ne. 4) call drawa(sngl(x(i)),sngl(y(i)))
            if(inum .eq. 4) call drawa(sngl(x(i-1)),sngl(y(i)))
5     continue
      call lnendp
      type*,' '
      type*,'plot is finished.....'
      return
      end

c**************************************************************************c
SUBROUTINE ABSIC
c  This subroutine merely stores the absiscas and weigths in the Gauss-Laguerre
c  integration routine.

      subroutine absic(x,w)
      implicit double precision (a-h,o-z)
      dimension x(50), w(50)
      x(1) = .298112358299601d-1
      x(2) = .157107990617896
      x(3) = .386265037576455
      x(4) = .717574694116972
      x(5) = 1.15139383402643
      x(6) = 1.68818582341904
      x(7) = 2.32852700665322
      x(8) = 3.07311086165263
      x(9) = 3.92275241304648
      x(10)= 4.87839335592134
      x(11)= 5.94110805462455
      x(12)= 7.11211053589074
      x(13)= 8.39276759909122
      x(14)= 9.78458318468732
      x(15)= 11.2892591680095
      x(16)= 12.9086577782855
      x(17)= 14.6448408832097
      x(18)= 16.5000814289645
      x(19)= 18.4768823868741
      x(20)= 20.5779986340222
      x(21)= 22.8064622905213
```

x(22)= 25.1656121564391
x(23)= 27.6591280444805
x(24)= 30.2910710010085
x(25)= 33.0659306624987
x(26)= 35.9886813274789
x(27)= 39.0648487641977
x(28)= 42.3005903629030
x(29)= 45.7027920385114
x(30)= 49.2791863828367
x(31)= 53.0384980878166
x(32)= 56.9906848148044
x(33)= 61.1468647861402
x(34)= 65.5202069290186
x(35)= 70.1247062361131
x(36)= 74.9809775189113
x(37)= 80.1068573503243
x(38)= 85.5283111160321
x(39)= 91.2757079936680
x(40)= 97.3866677135915
x(41)= 103.908833357176
x(42)= 110.904220884976
x(43)= 118.456425046283
x(44)= 126.683425768885
x(45)= 135.762589577864
x(46)= 145.986432709463
x(47)= 157.915612022977
x(48)= 172.996328148563
w(1) = .7426200582802624d-1
w(2) = .1522719498093528
w(3) = .1904090882639114
w(4) = .1866330594848059
w(5) = .1534242001575782
w(6) = .1087796928074902
w(7) = .6746073860921946d-1
w(8) = .3688119411582121d-1
w(9) = .1785684426915671d-1
w(10)= .767716514497608d-2
w(11)= .2935785903739463d-2
w(12)= .9990655378158858d-3
w(13)= .3025980169922584d-3
w(14)= .8153871180355413d-4
w(15)= .1953158715728072d-4
w(16)= .4154182945052174d-5
w(17)= .7833700380277587d-6
w(18)= .1307394774920602d-6
w(19)= .1927071408017028d-7
w(20)= .2502638937126341d-8
w(21)= .2855785508771622d-9
w(22)= .2854622412059155d-10
w(23)= .2491010684937224d-11
w(24)= .1890336606971544d-12
w(25)= .1242162685949152d-13
w(26)= .7034231520212617d-15
w(27)= .3414549148591887d-16
w(28)= .1412315414895739d-17

```
w(29)= .4944218008097474d-19
w(30)= .1453952481367899d-20
w(31)= .3561068365004085d-22
w(32)= .7194055996494724d-24
w(33)= .1185537228350586d-25
w(34)= .1573491357075602d-27
w(35)= .1657285440919482d-29
w(36)= .1361434162716342d-31
w(37)= .8546155813963136d-34
w(38)= .4000090532481346d-36
w(39)= .1355019991102997d-38
w(40)= .3201636795354913d-41
w(41)= .5035869166061095d-44
w(42)= .4962487540702732d-47
w(43)= .2823510716120112d-50
w(44)= .8268446069505063d-54
w(45)= .1049064847821271d-57
w(46)= .4346574422738856d-62
w(47)= .3434736438396578d-67
w(48)= .1319066088398016d-73
return
end
```

VITA

Darlena J. Jones

Candidate for the Degree of

Doctor of Philosophy

Thesis: FREE-SPACE DIFFRACTION EFFECTS IN AN ALL OPTICAL PASSIVE DRIVEN SYSTEM

Major Field: Physics

Biographical:

Personal Data: Born in Kansas City, Missouri, July 1, 1965, the daughter of Wendell and Ernestine Jones.

Education: Graduated from Bolivar Senior High School, Bolivar, Missouri, in May 1983; received Bachelor of Science Degree in Mathematics and Engineering Physics from Southwest Missouri State University in May, 1987; completed requirements for the Doctor of Philosophy degree at Oklahoma State University in December, 1993.

Professional Experience: Teaching Assistant, Department of Mathematics, Southwest Missouri State University, August 1985 to May 1986; Research Assistant, Department of Physics, Southwest Missouri State University, January 1986 to May 1987; Teaching Assistant, Department of Physics, Oklahoma State University, August 1987 to May 1993; Research Assistant, Department of Physics, Oklahoma State University, August 1989 to August 1993.